

MODELLING OF GEOBAGS FOR RIVER BANK PROTECTION

Aysha Akter

Submitted for the degree of Doctor of Philosophy

Heriot-Watt University

School of the Built Environment

May 2011

The copyright in this thesis is owned by the author. Any quotation from the thesis or use of any of the information contained in it must acknowledge this thesis as the source of the quotation or information.

ABSTRACT

In recent years, sand filled geotextile bags (geobags) have been used as a means of long term riverbank protection. However, despite their deployment in a significant number of locations the failure modes of such structures are not well understood. The aim of this research is to influence future design guidelines for geobag riverbank protection work. To achieve this it is necessary to enhance the fundamental knowledge of the performance of geobags in a revetment subject to flowing water. To achieve this quasi-physical model studies have been carried out considering two cases: a fixed bed and mobile sediment bed. To further help understand the forces acting on geobags the quasi-physical model observations have been used to validate numerical model simulations using a commercial 3D Discrete Element Model (DEM) software EDEM[®] coupled with a 3D water velocity field.

From the quasi-physical modeling it was known that there are types of geobag revetment failure common to both fixed bed and mobile beds. However, in mobile bed case toe scouring including the bed formation at different water depths has a significant influence on geobag performance. The aspect of the work reported is the use of two analytical techniques, the Conveyance Estimation System (CES) and the membrane analogy method developed by Chow to predict hydraulic shear stress on the geobag surface. It is concluded that both methods produce acceptable predictions, although the CES is recommended for further use because of its ease computational effort.

Then the third part of the research deals with the Discrete Element Modelling (DEM) simulation. The CES results were used for preparing a mapped velocity field for a DEM simulation. The validated DEM model could identify well the critical bag location in varying water depths and with varying bed formations. Toe scour, one of the major instability factors in revetments, and its influence on bottom most layer of the bags were reasonably represented in this DEM model. Finally, it is envisaged that the usage of DEM model will provide more details on geobag revetment in riverbank.

Finally, through an intensive review on available guidelines or recommendation on geobag protection work an application of DEM model for guideline setup has proposed. The main recommendation of this research is that with proper measured data from field can enhance the applicability of the DEM model for predicting the geobag performance in riverbank protection.

ACKNOWLEDGEMENT

First of all I would like to acknowledge Heriot Watt University for providing funding for this study through the James Watt Scholarship. The additional supports from DEM Solutions Limited and NAUE GmbH & Co., are also gratefully appreciated.

My deep gratitude goes to Professor Gareth Pender for selecting me as the recipient of the scholarship and providing me an excellent opportunity to work in the rewarding working environment of the School of Built Environment. Here I was fortunate to work with not one but three inspiring supervisors. Without proper guidance, advice and suggestions from Professor Gareth Pender, Dr. Grant Wright and Dr. Martin Crapper, this research would have never been completed.

I wish to offer my gratitude to Dr. Alex. Fotheringham; for graciously allowing me to use the facility of the School of Textiles and Design, Heriot Watt University, to prepare more than 700 model geobags. I would also like to thank Dr. B.T. Linfoot for the technical supports during my work in the Hydraulic laboratory, Heriot Watt University. In the same lab the logistic supports I received from the school staffs; namely, Mr. Hodder William, Mr. Tom Stenhouse, Mr. David Murray, Mr. James Maguire and Mr. Alastair Macfarlane, are highly appreciated.

I thank Mr. Mark Cook and Dr. Wai Sam Wong from DEM Solutions Limited. Without their help on model setup it would have been impossible to setup the EDEM[®] model for geobag revetment successfully, as this is the first time EDEM[®] has been used to explore the geobag revetment performances. I am also grateful for the logistic helps received from Mr. Steve Kirkaldy, Mr. Stuart Telford and Mr. Stephen Hawkin from Heriot Watt University, and Mr. Michael Gordon from the University of Edinburgh.

I thank all my friends from both Heriot Watt University and the University of Edinburgh. Their love and compassion are the most valuable treasures in my life.

Thanks to Chittagong University of Engineering and Technology (CUET) for approving a study leave for pursuing my PhD study.

Last but most definitely not the least, I would like to thank my parents and husband, Mr. G. M. Sadiql Islam, for their unconditional love and support during my study. Islam has always inspired me, kept me motivated and his strong support helped me to overcome crucial moments not only during this PhD journey but also in my life.

ACADEMIC REGISTRY
Research Thesis Submission



Name:	AYSHA AKTER		
School/PGI:	School of Built Environment		
Version: (<i>i.e. First, Resubmission, Final</i>)	Final	Degree Sought (Award and Subject area)	PhD

Declaration

In accordance with the appropriate regulations I hereby submit my thesis and I declare that:

- 1) the thesis embodies the results of my own work and has been composed by myself
- 2) where appropriate, I have made acknowledgement of the work of others and have made reference to work carried out in collaboration with other persons
- 3) the thesis is the correct version of the thesis for submission and is the same version as any electronic versions submitted*.
- 4) my thesis for the award referred to, deposited in the Heriot-Watt University Library, should be made available for loan or photocopying and be available via the Institutional Repository, subject to such conditions as the Librarian may require
- 5) I understand that as a student of the University I am required to abide by the Regulations of the University and to conform to its discipline.

* *Please note that it is the responsibility of the candidate to ensure that the correct version of the thesis is submitted.*

Signature of Candidate:		Date:	12 May 2011
-------------------------	--	-------	-------------

Submission

Submitted By (<i>name in capitals</i>):	AYSHA AKTER
Signature of Individual Submitting:	
Date Submitted:	12 May 2011

For Completion in the Student Service Centre (SSC)

Received in the SSC by (<i>name in capitals</i>):			
Method of Submission (<i>Handed in to SSC; posted through internal/external mail</i>):			
E-thesis Submitted (mandatory for final theses)			
Signature:		Date:	

TABLE OF CONTENTS

Lists of tables	i
Lists of figures	ii
Glossary of terms	iv
List of publications	v
Chapter 1	1
Introduction	1
1.1 General context.....	1
1.1.1 Geobag coastal structures	3
1.1.2 Geobag riverbank protection	15
1.1.3 Summary of the previous studies.....	21
1.2 Aims and objectives	22
1.3 Thesis outline	22
Chapter 2	25
Quasi–Physical Model Study	25
2.1 Quasi–physical model scale	26
2.2 Geobag–geobag interaction.....	27
2.2.1 Dry tests	27
2.2.2 Results.....	32
2.3 Hydrodynamic forces	33
2.3.1 Experimental setup	33
2.3.2 Methodology.....	37
2.3.3 Results.....	41
2.4 Hydrodynamic forces and riverbank toe scour.....	55
2.4.1 Experimental setup	55
2.4.2 Methodology.....	57
2.4.3 Results.....	60
2.5 Analysis of quasi–physical model result.....	75
Chapter 3	76
Analytical Approach	76
3.1 Active shear stresses on geobag	77
3.1.1 Conveyance Estimation System (CES)	77
3.1.2 Chow (1959) method	80

3.2	Results	83
3.2.1	Conveyance Estimation System	83
3.2.2	Chow (1959) method	88
3.3	Summary outcomes of the CES and Chow (1959) method.....	90
3.4	Application of CES	91
3.4.1	Geobag–water flow interaction.....	91
3.4.2	Geobag–water flow–mobile sandbed interaction	93
3.4.3	Mapped water velocity field preparation	98
3.5	Conclusions	98
Chapter 4	99
Numerical Model Study		99
4.1	General	100
4.2	Hypothesis	100
4.3	EDEM [®] model.....	100
4.4	Geobag-geobag interaction.....	104
4.4.1	Model setup.....	104
4.4.2	Validation process.....	106
4.5	Geobag – water flow interaction	108
4.5.1	DEM couple model.....	108
4.6	DEM model for the geobag – water flow interaction.....	110
4.6.1	Mapped velocity field	111
4.6.2	DEM model results	112
4.7	DEM model for the geobag - water flow- mobile bed interactions.....	117
4.7.1	DEM model results	120
4.8	Analysis of numerical model results	125
4.9	Conclusion.....	126
Chapter 5	127
Practical Application.....		127
5.1	Published geobag guidelines	128
5.2	Lessons from JMREM project	131
5.2.1	Bag design specification	131
5.2.2	Construction specification	131
5.2.3	Maintenance and inspection.....	132
5.2.4	Hydraulic parameters.....	132
5.3	Application of this thesis in design guideline	133
5.3.1	Quasi–physical model study	133
5.3.2	Analytical approach	134

5.3.3	DEM model.....	134
5.4	DEM model application in design guideline.....	135
5.4.1	Bag design specification.....	135
5.4.2	Construction specification.....	136
5.4.3	Maintenance and inspection.....	136
5.5	Summary.....	137
Chapter 6	138
Conclusions	138
6.1	Conclusions.....	140
6.2	Further research recommendations.....	142
Appendix A	150
Appendix B	153
Appendix C	158

LISTS OF TABLES

1.1	Published bag size in field practice.....	5
1.2	Velocity against the performance of costal geobag structures.....	10
1.3	Coefficient of drag and lift forces due to wave induced flow on geobag.....	10
1.4	Findings on costal geobag structures.....	11
1.5	Published failure mode observation in physical modelling.....	13
1.6	Published failure location observation in physical modelling.....	14
1.7	Published physical modelling study on geobag riverbank protection work.....	17
2.1	Scale ratio for the experimental setup.....	26
2.2	Experimental outcomes with different revetment construction method.....	53
2.3	Summary of bed formation and associate failure modes in geobag revetment.....	65
2.4	Summary of the bed changes in terms of total area.....	70
3.1	Summary of the CES prediction against experimental measured value.....	84
3.2	Comparative shear stress estimation on geobags.....	89
3.3	CES predicted hydraulic parameters of flow over mobile bed.....	95
4.1	Required material and interaction properties for the geobag model...	105
4.2	Required material and interaction properties for the EDEM® geobag model.....	111
5.1	Published geobag guideline obtained for both coastal and riverbank..	129

LISTS OF FIGURES

1.1	Failure in geobag revetment (Jamuna River, 2009).....	2
1.2	Published filling ratio under laboratory experiments and field experience.....	6
1.3	Published sandbag structure slope.....	7
1.4	Published geobag–geobag friction angle.....	9
1.5	Geobag displacement, Jamuna River (Field study, 2009).....	18-20
1.6	Flow chart of the research outline.....	24
2.1	Initial experimental setup on test rig.....	28-29
2.2	Dry test on wooden test rig.....	30-31
2.3	Experimental setup in flume.....	35-36
2.4	Water depth conditions (fixed bed).....	38-39
2.5	Observed failure modes in the RM1 – jack on jack.....	45-46
2.6	Observed failure modes in the RM2 – running bond.....	47-48
2.7	Observed failure modes in the RM3 – half basket weave.....	49-50
2.8	Different types of the failure zones in the geobag revetment.....	51-52
2.9	Failure map of geobag revetment due to geobag–flow interaction..	54
2.10	Experimental setup in flume (mobile bed).....	56
2.11	Water depth conditions (mobile sediment bed).....	58-59
2.12	Different failure modes in geobag revetment.....	62-63
2.13	Bed formation under different water level and model run time.....	64
2.14	Classification of bed forms (based on Figure 6.3 of Raudkivi, 1998).	68
2.15	Outline of bed changes after experiment.....	69
2.16	Changing bed under four different conditions.....	71-74
3.1	Geobag revetment section in experimental setup.....	79
3.2	Shear force in terms of $\gamma_h S$ (based on Chow, 1959).....	81
3.3	Active forces on (a) washed away geobag, and (b) sediment particle on trapezoidal channel surface.....	82
3.4	Comparison of the laboratory measured with CES simulated velocity.....	85-87
3.5	Geobag failure diagram due to geobag– flow interaction using CES.	92
3.6	Rating curves based on measure and CES predicted data.....	93
3.7	Classification of bed formation using CES prediction.....	96

LISTS OF FIGURES (CONT'D)

3.8	CES predicted high resolution water velocity data on geobag surface.....	97
4.1	Laboratory model geobag representation in EDEM.....	101
4.2	Model setup for the dry test on wooden test rig.....	104
4.3	Comparison between laboratory and EDEM [®] prediction.....	107
4.4	Model setup for the geobag revetment in flume.....	110
4.5	Visual validation of the DEM simulation against laboratory.....	113-116
4.6	Bed change (a) laboratory measures and (b) DEM representation..	118
4.7	Initial setup of geobag revetment using EDEM [®]	119
4.8	Comparison of laboratory observation and DEM outcome.....	121-124

GLOSSARY OF TERMS

ADV	Acoustic Doppler Velocimete
CES	Conveyance Estimation System
DEM	Discrete Element Method
JMREM	Jamuna–Meghna River Erosion Mitigation

LIST OF PUBLICATIONS

JOURNAL PAPERS

1. Akter A, Pender G, Wright G, Crapper M, Predicting the hydrodynamic forces on geobag revetments. *Journal of Flood Risk Management*, 2010, manuscript number: JFRM-0063-10, (*Under review*).
2. Akter A, Pender G, Wright G, Crapper M, The performance of a geobag revetment, I: Quasi-physical modelling, *Water Resources Management*, manuscript number: WARM2321 (*Under review*).
3. Akter A, Crapper M, Pender G, Wright G, Wong W S, The performance of a geobag revetment, II: Numerical modelling, *Water Resources Management*, manuscript number: WARM2322 (*Under review*).
4. Akter A, Crapper M, Pender G, Wright G, Wong W S, Modelling the failure modes in geobag revetments, manuscript number: IWA-7451 (*Under review*).

CONFERENCE PAPERS

1. Akter A, Wright G, Crapper M, Pender G, Failure Mechanisms in Geobag Structures. Recent Advances in Water Resources, Hydraulics and Hydrology, Proceedings of the 4th IASME/WSEAS International Conference on Water Resources, Hydraulics and Hydrology (WHH'09), Cambridge, Published by WSEAS Press, ISBN: 978-960-474-057-4, ISSN: 1790-2769, United Kingdom 2009, pp 25- 30.
2. Akter A, Pender G, Wright G, Crapper M, Modelling the hydrodynamic forces on geobag revetments using CES. Proceedings First European Congress of the IAHR, Edinburgh, United Kingdom 2010 (*CD publication*).
3. Akter A, Crapper M, Pender G, Wright G, Wong W S, Failure modes observed in geobag revetment using EDEM, 12th IWA UK National Young Water Professionals Conference, University of Edinburgh, pp 24-28.

BEST POSTER AWARDS

1. Heriot-Watt Postgraduate Research Conference (June 2008), in Heriot Watt University, Edinburgh, UK.
2. Second EDEM User Conference 2009 (August 2009), organized by DEM Solutions, Edinburgh, UK.
3. ERPem Industry Evening Seminars and PG Student Poster (October 2009), in the University of Edinburgh, Edinburgh, UK.

Chapter 1

Introduction

1.1 General context

In this thesis the term geobag is reserved for sand filled geotextile bag, whereas the term sandbag is used to describe bags manufactured from any materials including geotextile, nylon, polyester, jute. Geobags are a common geotextile product used for the construction of low cost coastal and river bank protection.

Geobags have been used in river protection structures for more than 10 years (JMREM, 2006 a, b). In addition to their use as groynes, geobags have also been used to prevent erosion and scour in bulkheads and revetments in coastal, island and bridge abutment applications (Gutman, 1979; Gadd, 1988; Korkut *et al.*, 2007). Similarly, geobag protection has been employed to prevent erosion in the Changjiang River in China (Zhu *et al.* 2004), Yangtze River in China (Yang *et al.*, 2008) and in the Jamuna and Meghna Rivers in Bangladesh (JMREM, 2006 a). Geobag revetment performance has been evaluated using both laboratory and field observation in the Jamuna River context (nhc 2004, 2006; JMREM, 2006 a). These investigations have identified pullout/dislodgement, sliding, slumping and physical damage as potential failure mechanisms for geobag in revetments (Figure 1.1).



1: Pullout ; 2: Slump; 3: Dislodgement of the top bag; 4: Slide; 5: Physically damaged

Figure 1.1: Failure in geobag revetment (Jamuna River, 2009)

So far the technical information available in the literature is based on the geobag performance in coastal protection works i.e. mostly wave action on geobag structure. On the other hand, only the scale model experiments of Zhu *et al.* (2004), nhc (2006), Korkut *et al.* (2007) and Yang *et al.* (2008) have investigated the performance for geobag protection works in rivers. The next two subsections review the laboratory, field and numerical model studies previously undertaken on geobag performance in a coastal and riverbank context.

1.1.1 Geobag coastal structures

Several attempts have been made to understand the performance of sandbags (Venis, 1968; Porraz *et al.*, 1979; Kobayashi and Jacobs, 1985) and geobags (Bezuijen *et al.*, 2004; Recio and Oumeraci, 2009 a, b) in coastal applications. Findings from physical modelling (Venis, 1968; Porraz *et al.*, 1979; Kobayashi and Jacobs, 1985; Gadd, 1988; Grüne *et al.*, 2006; Krahn *et al.*, 2007; Mori *et al.*, 2008b, Recio and Oumeraci, 2009 a,b; Dassanayake and Oumeraci, 2010), field studies (Heerten *et al.*, 2000 a, b; Pilarczyk, 2000; Bezuijen *et al.*, 2004; Corbet, 2005; Saathoff *et al.*, 2007; Heerten *et al.*, 2008; Mori *et al.*, 2008 a), analytical approaches (Breteler *et al.*, 1998) and numerical modelling (Recio and Oumeraci, 2009 a) are tabulated in Table 1.4. This presents a summary of the contribution to the body of knowledge from these researches on the (i) bag design specification, (ii) geobag structure construction specification, (iii) the mechanical properties of bag, and (iv) the active hydraulic forces on the structure.

The bag design specification includes the physical properties of the bag materials i.e. sand and fabric. Saathoff *et al.* (2007) mentioned the sand d_{50} was in a range between 15 to 25 mm for the protection work in field. From field test, Bezuijen *et al.* (2004) concluded that the use of dry and clean sand as a fill material can reduce the risk of tearing the bag fabric geotextile through absorbing a significant part of the fall energy while dropping the bag as practiced during revetment construction. The thickness of the fabric is also an issue, Restall *et al.* (2002) noted down the thickness of the geotextile employed for bag preparation in this case 5.3 mm (Stockton beach revetment) to 5.5 mm (North Kirra groyne). Table 1.1 summarizes the bag size used in different protection works in the field. The length of these bags was in a range of 1.22 to 2 times of its width (Table 1.1). The empty bag size is expressed normally by the length and breadth, as the thickness might vary with the fill ratio. The sand filling ratio got priority due to its influence on geobag performance towards the whole structure performance. Studies in the laboratory and the field suggest that the most acceptable filling ratio is 80% of the actual volume of a geobag (Figure 1.2). Presently more research is carrying

out by Dassanayake and Oumeraci (2010) to summarize the influence of fill ratio on geobag structure performance.

Construction specification for geobag structures mostly addresses protection work thickness, bag placement (with respect to coast/bank line) and the slope of the structure. In the Stockton beach revetment, the double layer bag thickness and the running bond bag setup (the geobags are laid longitudinally, in a typical brick wall pattern, with the geobag joints laying in the middle of the bags in the layers directly above and below) was innovative as there was no guidelines for bag placement available at this time (Saathoff *et al.*, 2007). The most effective bag placement relative to the coast/bank line is found to be parallel to the flow direction (Table 1.4). Apart from the geotechnical features in the field, the geobag structure slope is controlled by the extent of bag overlapping employed and the optimum overlapping has been found to be 50% (Table 1.4). From the available literatures the most commonly used slope is between 1V: 1H to 1V: 2H although slopes as flat as 1V: 10H have also been employed (Figure 1.3). In field the selection of slope is normally based on the design wave height and the pattern of erosion or scour hole (Heibaum, 1999), so it will be variable based on location. To achieve the design bag layer, bond, placement and finally the slope, there is often a need for mechanical device. Manually bag drop introduces quality control issues and there is therefore uncertainty involved in the final position achieved. To overcome this issue, there is a well known computer software the GeoCoPS (2.0) which is used for predicting the theoretical shape of geobag on the seabed after placement from a mechanical device (Hornsey *et al.*, 2003).

Table 1.1: Published bag size in field practice

Geobag structure	Bag size			Year	References
	Length (m)	Width w (m)	Thickness (m)		
Stockton beach revetment	1.5 (1.36w)	1.1	0.4 (0.36 w)	2002	Restall <i>et al.</i>
Stockton beach revetment	1.5 (1.25w)	1.2	0.45 (0.38 w)	2007	Saathoff <i>et al.</i>
Maroochy groynes	2.2 (1.22w)	1.8	0.7 (0.39 w)		
Jumaira beach revetment	2.2 (1.22 b)	1.8	0.7 (0.39 w)		
Eider storm surge barrier	2.7 (2 w)	1.35	–		
Marina di Ronchi (submerged groin)	2.5 (1.67w)	1.5	0.5 (0.33 w)	2008a	Mori <i>et al.</i>

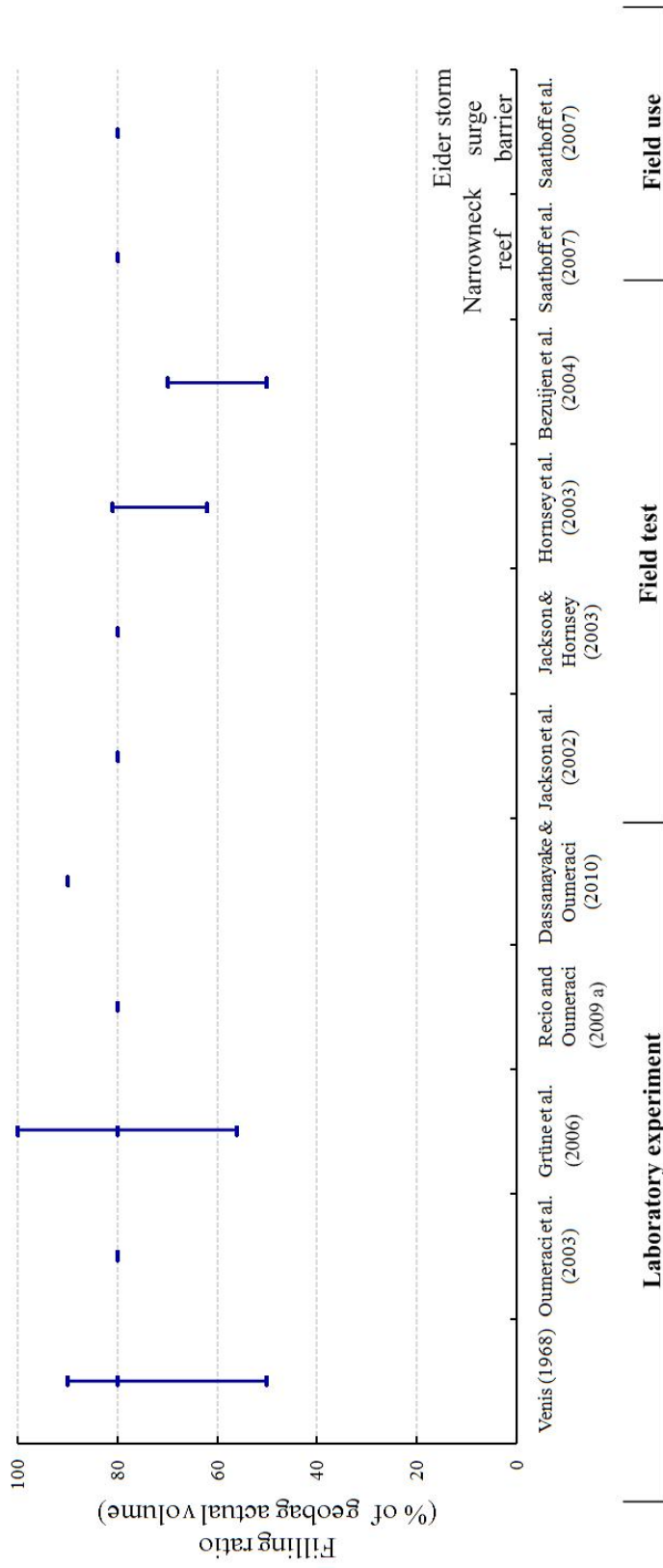


Figure 1.2: Published filling ratio under laboratory experiments and field experience

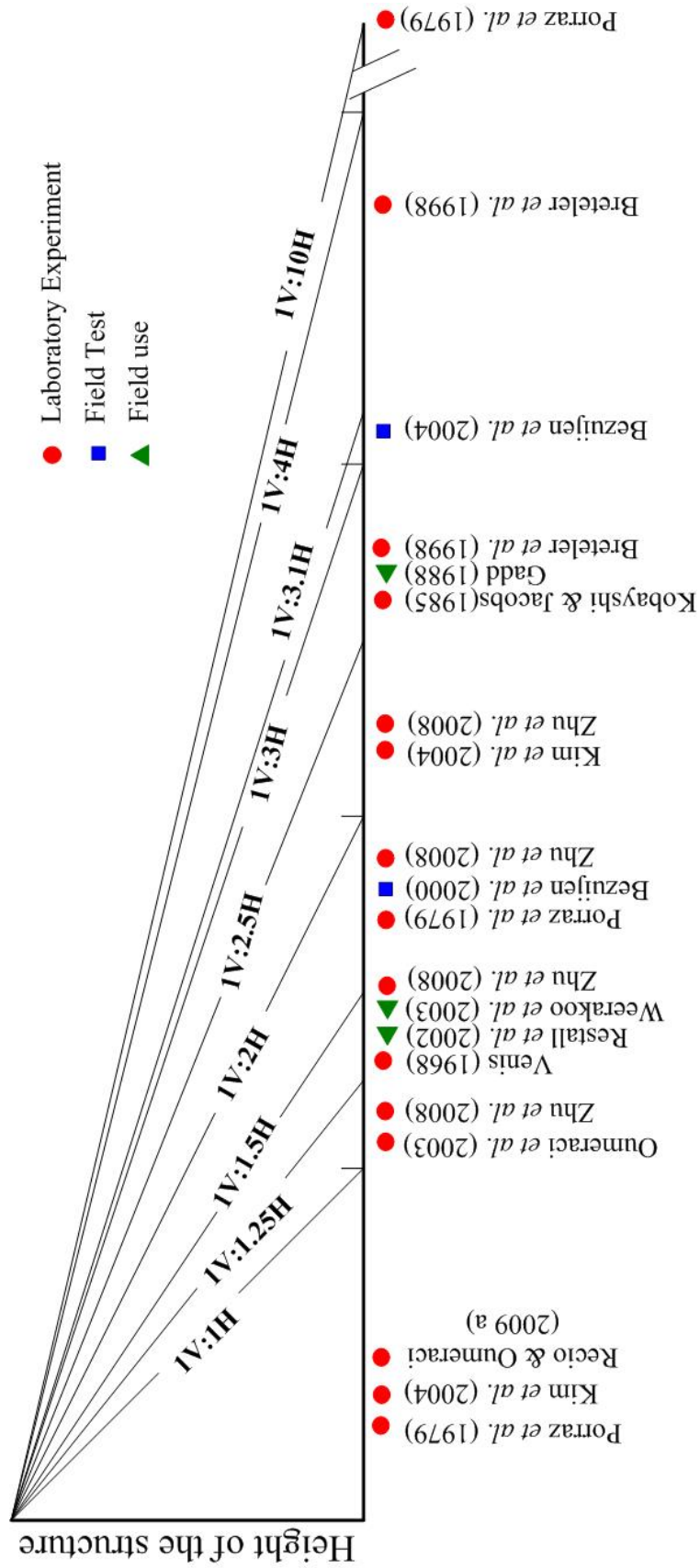


Figure 1.3: Published sandbag structure slope

Chapter 1: Introduction

The life expectancy of geobag structure in coastal protection work is normally 20 to 25 years (Jackson and Hornsey, 2003; Saathoff *et al.*, 2007; Heerten *et al.*, 2008).

Mechanical properties of bags, that are the core properties to ensure the stability of a geobag construction, are the internal friction, permeability and deformation of the bag. Recio and Oumeraci (2007) intensively studied the permeability and deformation of bags and the effect of these properties on the structure (Table 1.4). Among the available literature, Kim *et al.* (2004) and Krahn *et al.* (2007) only carried out experiments using a large shear box to obtain estimates of friction angle under different loads. The average friction angle between geobags is found to be 30° (Figure 1.4).

The hydraulic loading causing instability in a structure are only noted by Pilarczyk (2000) for incipient velocity (Table 1.2) and Recio and Oumeraci (2009 a) for hydrodynamic forces (drag and lift) (Table 1.3). The term ‘incipient velocity’ was explained by Pilarczyk (2000) in terms of active intensive flow on the bag fabric and this causes counter movement of bag infill sand. Also highlighting on the same concept, Recio and Oumeraci (2009 b) represented numerically the wave induced velocity causing uplift in a bag and the outer velocity of the bag was found as 0.9 m/s. On the other hand, Kim *et al.* (2004) defined the allowable value for a specific size of model bags while the whole structure collapses, as these bags are placed using artificial connection units. Among these three available studies the acquired velocities are dependent on the bag size and wave type; so, exactly there is no information on the incipient velocity ranges which could initiate individual geobag movement from a coastal structure. It should be noted that the definition of ‘incipient velocity’ within the study reported hereien is the velocity required to cause movement of geobags from the revetment structure; it may therefore be considered ‘geobag incipient velocity’.

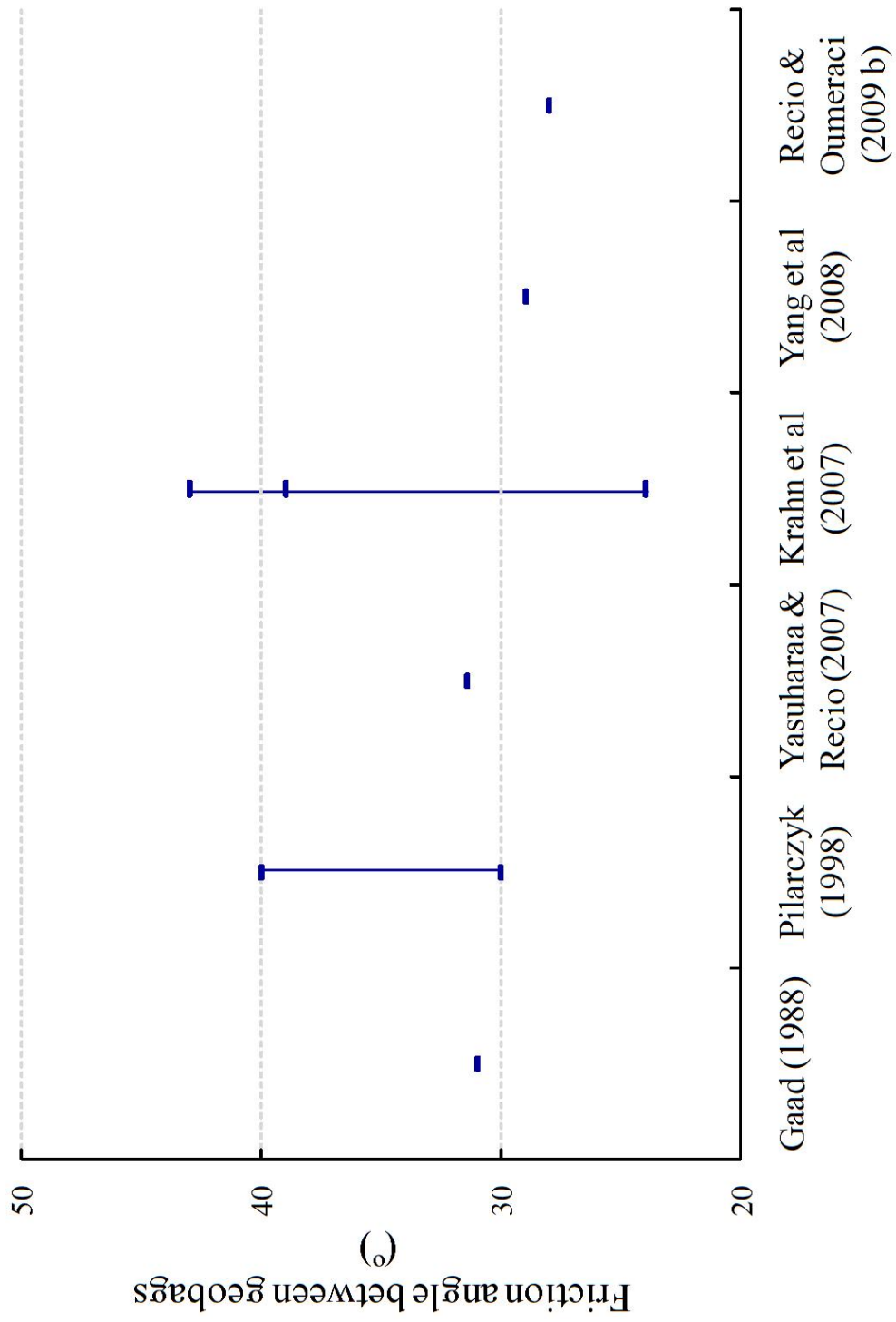


Figure 1.4: Published geobag-geobag friction angle

Table 1.2: Velocity against the performance of costal geobag structures

Year	Reference	Velocity value	Remark
2000	Pilarczyk	1.5 m/s	Velocity above 1.5 m/s increases internal sand movement results in instability.
2004	Kim <i>et al.</i>	1–3 m/s	Applicable experimental velocity on different bag size while they are placed on connection unit.
2009b	Recio and Oumeraci	Wave induced velocity outside of bag = $20 \times$ average velocity inside the bag (Numerical model outcome)	The flow through structure is governed by the voids between geobags.

Table 1.3: Coefficient of drag and lift forces due to wave induced flow on geobag

Year	Reference	Cd	Cl	Re	Comment	
2000	Bezuijen <i>et al.</i>	1	–	–	Field test	
2004	Kim <i>et al.</i>	1	–	–	Laboratory test	
2009a	Recio and Oumeraci	0.5–3	0.3–1.2	$8 \times 10^4 - 1.8 \times 10^5$	Bottom most bag	Laboratory test
		2.5–9	0.3–1.2		Middle bag	
		4–15	0.3–1.2	$8 \times 10^4 - 2 \times 10^5$	Topmost bag	

Table 1.4: Findings on costal geobag structures

Parameters		Findings
Physical property	Fabric	Nonwoven needle – punched geotextile (Brand and Pang, 1991; Heerten <i>et al.</i> , 2000b; Corbet, 2005; Heerten <i>et al.</i> , 2008).
	Seam strength	Should be at least 80 – 90% of the tensile strength of the fabric (Gadd, 1988; Saathoff <i>et al.</i> , 2007).
	Sand filling ratio	To avoid ‘interlocking’ problem among bags, the fill ratio of approximately 80% is defined as an optimum stability of the elements (Figure 1.2).
	Saturation of the fill	The degree of saturation influences the geobag weight and the falling velocity during dropping. A low degree of saturation (i.e. dry sand fill) increases the capacity of the sand to absorb energy during impact on the bottom of the bag (Bezuijen <i>et al.</i> , 2004).
Revetment construction	Slope steepness	With experience from different type layer-to-layer over lapping, such as – face to face (Venis, 1968), 50% overlapping (Porraz <i>et al.</i> , 1979; Kobayashi and Jacobs, 1985; Gadd, 1988; Recio and Oumeraci, 2009 a); the optimum setup can be achieve from 50% overlapping.
	Drop test	Irrespective of the initial orientation, laboratory experiments showed geobags sink under water with the largest axis towards stream wise direction if a sufficient water depth is available (Dassanayake and Oumeraci, 2010).
	Geobag launching	In the field, bag placement with its longest axis as a function of water depth between 15 m to 22 m, and a standard deviation of less than 1 m can be achieved in launching accuracy if the water depth is limited to 10 m (Bezuijen <i>et al.</i> , 2004).
Mechanical property	Interface Friction	The average friction angle between geobags found to be 30° (Figure 1.4).
	Permeability	The total forces and moments for geobag displacement in a structure depend on the wave pressure propagation inside the internal gaps between bags (Recio and Oumeraci, 2007).
	Deformation	The infill sand accumulates at the seaward end and leads to the deformation of the latter part of the bag. This reduces the contact areas with the neighbouring bags (Recio and Oumeraci, 2007). Then internal movements of the sand are activated by an incremental horizontal displacement of the geobags. Pilarczyk (2000) reported bag rolling initiation due to internal sand movement caused by surrounding flow velocity more than 1.5 m/s.
Hydraulics	Incipient velocity	Geobag becomes unstable above a flow velocity of 1.5 m/s (Pilarczyk , 2000).
	Forces	In wave flume experiments, the coefficient of drag and lift forces found as a function of Reynolds numbers and the roughness of geobags (if $10^4 > Re > 10^6$) (Recio and Oumeraci, 2009 a).

Chapter 1: Introduction

Among the major parameters, the physical properties and revetment construction methods have already been intensively studied and only few recent studies covered the mechanical and hydraulic properties. Although the importance of exploring the local scale failure modes in wave flume started in 1979 by Porraz *et al.*, in last three decades only few studies have explored this aspect in more detail (Table 1.5). Failure modes in geobag structures can be categorised using the observations from physical models noted in Table 1.5 and as per location in the structure (Table 1.6). The main reasons for failures are friction, inertia, drag and lift forces. To date acquisition of the coefficient of friction for force calculations is from a direct shear test (Kim *et al.*, 2004; Krahn *et al.*, 2007), as there is no available standard for determining this value when considering the whole structure. Recio and Oumeraci (2009 a, b) introduced physical modelling on inertia, drag and lift forces in a wave flume. As this experimental study concentrated on wave loading and did not link failure mode to underlying hydraulic loading, it can be deduced that there is current lack of knowledge on the performance of geobag revetments in riverbank protection works.

Table 1.5: Published failure mode observation in physical modelling

Year	Authors	Failure modes	Failure reason
1979	Porraz <i>et al.</i>	Slide	○ Friction.
		Push	○ Thrust force due to waves.
		Pullout	○ Uplift pressure and wave current.
1985	Kobayashi and Jacobs	Plugging, collapsing and surging	○ Combined effect of slope angle, wave steepness and wave period.
1988	Gadd	Dislodgement	○ Wave impact and physical property.
2004	Kim <i>et al.</i>	Slide, overturn and pullout	○ Friction.
2006	Jackson <i>et al.</i>	Pullout/ dislodgement	○ Physical property of bags; and ○ Geobag–geobag friction.
2007	Saathoff <i>et al.</i>	Overtopping	○ Wave run–up and freeboard.
		Uplift	○ Wave run–down.
2009b	Recio and Oumeraci	Slide	○ Bag submerged weight and lift force; ○ Friction.
		Pullout effect	○ Several wave cycles on the structure; ○ Relatively longer experimental time.
		Uplifting/ overturn	○ Drag and inertia force.

Table 1.6: Published failure location observation in physical modelling

Year	Authors	Failure locations	Failure reason
2008b	Mori <i>et al.</i>	Whole structure fail	○ Hydraulic stresses in bags due to wave load.
		Top bags in structure	○ Wave height; and ○ Wave period.
2009b	Recio and Oumeraci	Top bags in structure	○ Wave uprush induces landward uplift and overturning of bag; ○ Uplift, deformation of bag and wave down rush results in seaward overturning; and ○ Sliding.
		Slope bags in structure (bags located just below and below the surface water level)	○ Large wave height; and ○ Sliding.

Field monitoring of coastal geobag structures indicated that overtopping, sliding, puncturing, pullout/dislodgement and toe scour are the most common failure modes (Mori *et al.*, 2008 a; Jackson *et al.*, 2006; Oumeraci, 2003). Details on these failure mechanisms are not available.

To date the only published numerical model study (Recio and Oumeraci, 2009b) simulated the effect of frictional forces on the stability of geobag structures. In their work, a 2 D representation of a geobag was adopted to represent the resultant force and displacement due to wave action. They used the ‘COBRAS – UDEC’ model to represent the displacement of the geobags with three different friction angles i.e., 8°, 18° and 28°, and their findings showed the smaller friction angle resulted in larger displacement. Thus the coefficient of friction was assumed a priori and local scale failure in the geobag structure due to friction was not modelled. There is no available published study detailing the impact of hydrodynamic forces on revetment erosion and toe scour on geobag revetment performance. Therefore, numerical modelling remains unexplored to fully evaluate the geobag structure performance.

1.1.2 Geobag riverbank protection

To better understand the issues surrounding geobag placement for revetment structures in Jamuna – Meghna River erosion protection scheme, nhc (2006) used 1:20 scale models in four categories of test (drop, launch, incipient motion, mega container). The majority of these were designed to investigate a range of launching and placement methods (Table 1.7). Some findings are, however, a very important contribution to hydraulic performance investigation. For example,

- at a slope of 1V: 2H 126 kg bags were the most stable compared to bags of lower weight under high water velocities up to 4.5 m/s; and
- in an incipient motion test (incipient motion was defined by the point at which 10 geobags are displaced), it was found that failure initiated at a prototype velocity of 2.9 m/s at a side slope of 1V: 2H.

Drop tests (bag were released at the water surface in the direction of stream flow) and incipient motions tests were also carried out by Zhu *et al.* (2004), to investigate bag settling distance and the critical velocity for geobag incipient motion. They described the hydrodynamic forces (drag and lift) subjected to bag drops based on data from both physical models and field observations. Application of geobags against scour protection is described by Korkut *et al.* (2007) in the context of abutment scour protection and by Yang *et al.* (2008) on riverbank toe scour. The details of the findings from these physical model studies are tabulated in Table 1.7.

Regarding failure modes, sliding/slip and slumping are recorded by nhc (2006) as a result of inadequate bag coverage and toe scour or protected river bed mobility. On the other hand, the effects of geobag sliding and alternatives to reduce the sliding has described by Korkut *et al.* (2007). The conclusion that can be drawn from all of these four available studies is that more information is required on local scale failure modes and failure zones in geobag structures.

Chapter 1: Introduction

Observations and field experience of geobag revetments in the Jamuna River showed failure zones due to hydraulic loading, including toe scouring and management, as follows:

- (i) with hydraulic loading: the loss of hydrostatic counterforce during the rapid drawdown at the end of the flood season can result in failure due to slump or/ and pullout and sliding, Figure 1.5 a;
- (ii) hydraulic loading and toe scour failure when a combination of the retarded scour and drawdown, here both crest bags and slope bags are displaced by a slip circle formation (Individual Consultants, 2003), Figure 1.5 b;
- (iii) management depends on human involvement in implementation and maintenance levels, for example, poor maintenance can result in inadequate thickness at the revetment top, Figure 1.5 c.

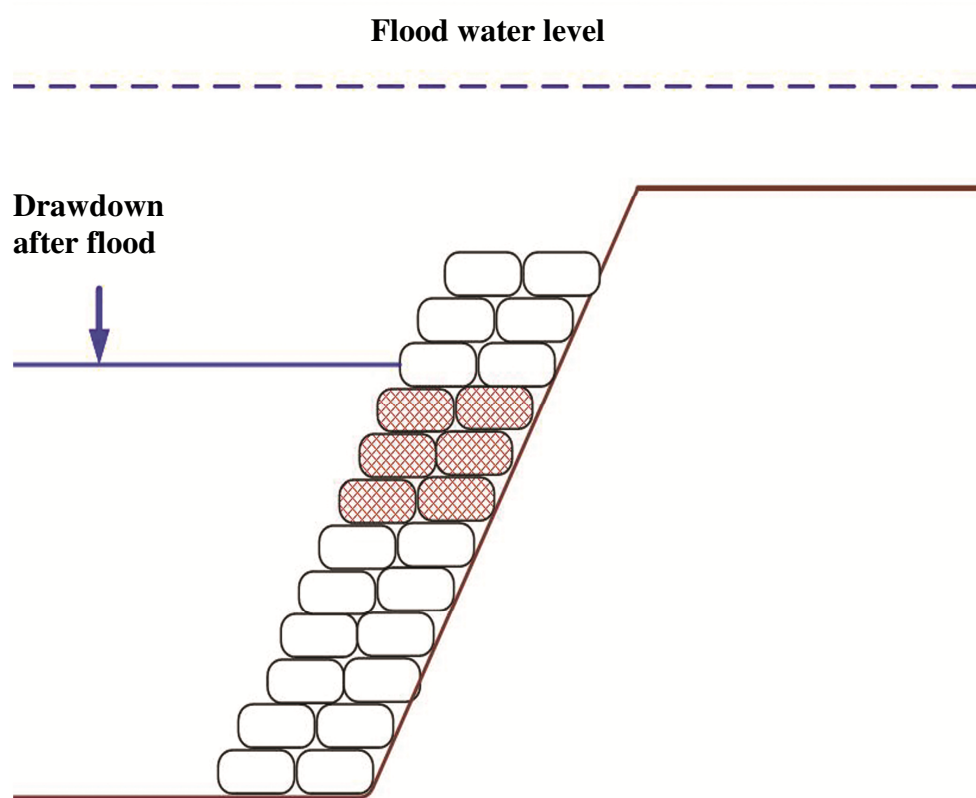
In general these failure zones progresses following basic local geotechnical failures. So, from the river engineering point of view both of the hydraulic loading and toe scouring effects on revetment need further investigation at the local scale.

Table 1.7: Published physical modelling study on geobag riverbank protection work

Test name	Study Mode	Findings
Bag drop test	Laboratory	<ul style="list-style-type: none"> • When dropped, wet bags travel shorter distances before settling on the bed than dry bags, due primarily to their greater weight (nhc, 2006).
Bag launching	Laboratory	<ul style="list-style-type: none"> • When launched, mixed size geobags produce slightly steeper revetment slopes than the typical 1V:2H slopes found with single 126 kg size bags. The same test also concluded that bags of 126 kg are more stable compared to bags of lower weight under high flow velocities (up to 4.5 m/s); • 60% of bags settled onto the channel bed with the longest axis in the streamwise direction (Zhu <i>et al.</i>, 2004) same as (Dassanayake and Oumeraci, 2010 in Table 1.4). • The geobag structure of slope 1V:2H and by at least two thickness of bag was recommended for better toe scour protection work (Korkut <i>et al.</i>, 2007).
	Field test (Jamuna)	<ul style="list-style-type: none"> • The bag launched slopes are of steeper than 1V: 2H could result in slumping of the entire protected rivebank (Individual Consultants, 2003).
Internal friction	-	<ul style="list-style-type: none"> • The friction angle between geobags is 29° (Yang <i>et al.</i>, 2008).
Incipient velocity	Laboratory	<ul style="list-style-type: none"> • The bag movement is initiated at a prototype velocity of 2.9 m/s; • Zhu <i>et al.</i> (2004) investigated bags settling distance and the critical velocity for the geobag incipient motion.
Scour protection	Laboratory	<ul style="list-style-type: none"> • The mega container tests, involving large geobags (25 m long, 8 m wide, 3 m high), indicate that mega containers provide good support against toe scour by their constant “reshaping” as scour progresses. However, due to practical difficulties in mega container handling, geobags of this size are not commonly used in the Jamuna. • Without proper placement of the additional bags, mega container may slide and can fail to offer the desire protection against scour (Korkut <i>et al.</i>, 2007).



(a 1) Displacement due to rapid drawdown

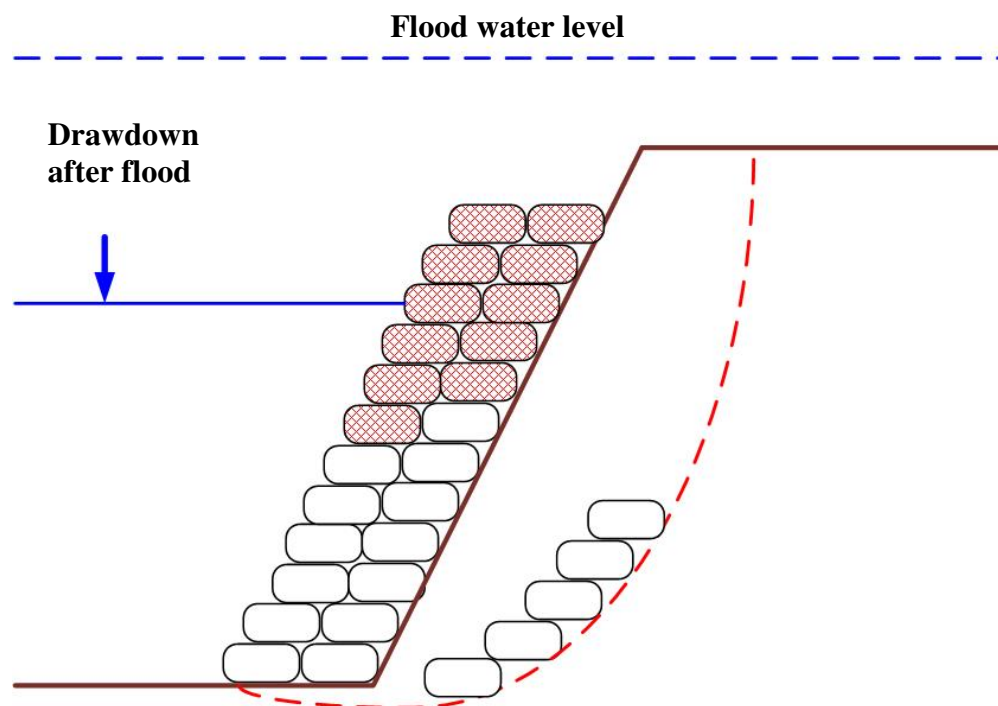


(a 2) Schematic of displacement due to rapid drawdown

Figure 1.5 a: Geobag displacement, Jamuna River (Field study, 2009) (Cont'd)



(b 1) Bag displacement due to combined effect of retarded scour and drawdown

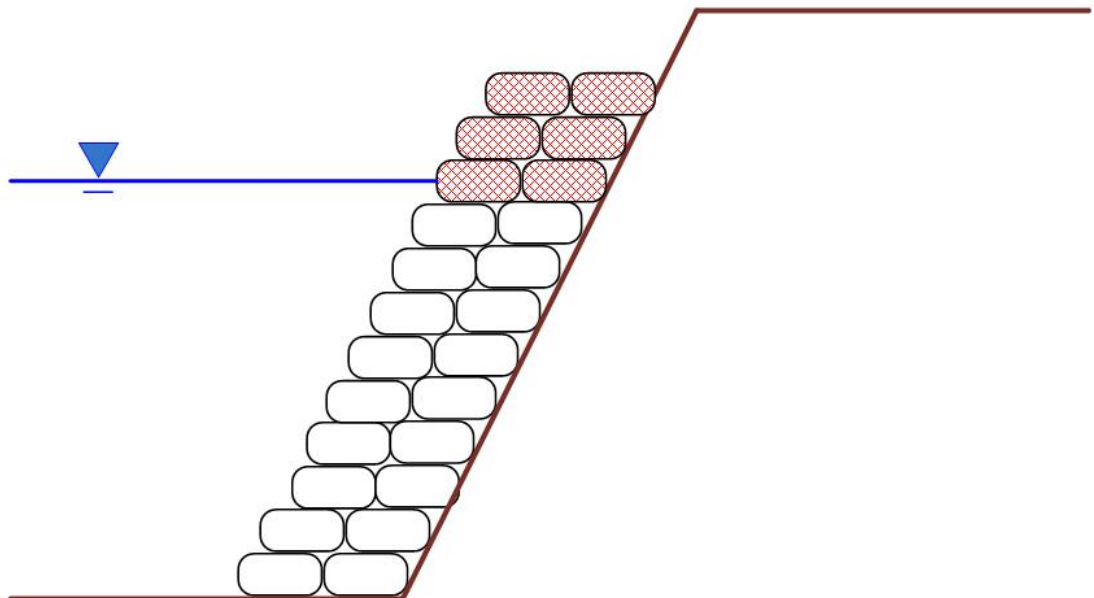


(b 2) Schematic of the combined effect of retarded scour and drawdown

Figure 1.5 b: Geobag displacement, Jamuna River (Field study, 2009) (Cont'd)



(c 1) Inadequate thickness of geobag revetment



(c 2) Schematic of bags prone to displacement due to inadequate thickness of revetment

Figure 1.5 c: Geobag displacement, Jamuna River (Field study, 2009)

1.1.3 Summary of the previous studies

Previous laboratory studies have shown that physical properties (i.e., filling ratio, fabric), mechanical properties (friction between geobags, overlapping of geobags), hydraulic properties (i.e., flow acting on the revetment, water depth variations), and revetment construction (i.e. the steepness of the slope, orientation of the bag with respect to flow) are the important influencing factors for geobag revetment performance.

To date, only a few parameters have been explored with relation to geobag revetment performance in a riverbank protection context, however, these studies do not consider the hydrodynamic forces associated with varying water depth and geobag protected riverbank toe stability. As a result, details of the local failure process in the riverbank protection context remain unknown. This emphasises the need for further laboratory experiments on geobag revetment performance at the local scale. As physical model results are influenced by scale effects and experimental limitations (e.g. accuracy and coverage of laboratory measurements), additional numerical models are required to determine the hydraulic loading and movement of each individual/discrete geobag in a revetment.

The discrete element method can track the motion of each individual particle (geobag), and its interaction with other particles (geobag to geobag) and boundary surfaces (geobag to riverbank material) using Newton's law of motion and contact laws. The discrete element method (DEM) or distinct element method is the numerical technique applied for modelling the movement and interaction of rigid or deformable bodies, particles, or arbitrary shapes that have been subjected to external stresses or forces (Crapper *et al.*, 2005; Mustoe and Miyata, 2001). DEM has been extensively used in different fields such as rock mechanics, mining, pharmaceutical, chemical, agricultural, advanced materials and food (Bertrand *et al.*, 2005). Despite the widespread use of commercial DEM codes, referred to as EDEM[®] in some engineering applications, it has not been used previously to model the failure mechanisms in a geobag structure.

1.2 Aims and objectives

The main aim of this study is to influence the future guidelines on the design of geobag riverbank protection works through both quasi-physical and numerical model studies. To achieve this specific aim the project objectives were:

- i. to undertake a quasi-physical model study to develop an improved understanding of geobag stability under frictional, horizontal (hydrodynamic) and vertical (riverbank toe scour) loadings and provide data for numerical model validation;
- ii. to determine the applicability of an analytical approach to extend the quasi-physical model measurements and observations; and
- iii. to assess the suitability of the existing EDEM[®] numerical model to simulate the performance of a geobag revetment under hydrodynamic forces alone and combined with the riverbank toe scour.

These studies are conducted considering the most expected possibilities of the particular conditions in the context of large sandbed riverbank protected geobag revetment.

1.3 Thesis outline

The methodology adopted in this study is briefly illustrated in a conceptual chart (Figure 1.6).

In Chapter 2, an intensive quasi-physical model studies were presented on the major issues affecting the geobag performance i.e. friction and the hydrodynamic forces and riverbank toe scour. The features investigated the geobag revetment are: (i) failure modes, (ii) hydraulic parameters of the flow, (iii) mobile bed formation, (iv) age of bag since first immersion, and (v) settling distance of bag displaced from revetment.

Chapter 1: Introduction

In Chapter 3, an attempt has also made to extend the quasi-physical model measurements by means of an analytical approach as it is not practical to measure fluid shear stress on the geobag. The purpose of this approach is to use the measured depth-average velocity to estimate the applied fluid shear stress on the geobags in the revetment. The Conveyance Estimation System (CES) was used to calculate the variation in velocity and shear stress with water depth. In addition, an analytical method (Membrane Analogy) was also employed to determine the depth averaged parameters.

In Chapter 4, the CES results are used to prepare a mapped velocity field for a Discrete Element Model (DEM). Using a drag model for non-spherical particles (Hölzer and Sommerfeld, 2008), and a separate lift model (Yin *et al.*, 2003), a one-way coupling is employed to link the mapped velocity field to the DEM calculation. A commercial DEM model is calibrated to represent the quasi-physical model features.

Chapter 5 influences future design guidelines for geobag riverbank protection works using the knowledge gained from the quasi-physical model studies, the analytical study and the numerical modelling. The observations and findings obtained throughout Chapter 2, 3 and 4 are discussed, in view of the particular context to which this study is meant to apply, i.e., riverbank geobag revetment performance. Comments on this thesis applicability on the revetment design guideline preparation in riverbank are finally made.

Final conclusions are drawn in Chapter 6, including further research recommendations are made.

Appendices A to C are concerned with relevant issues along with the main text.

The use of footnotes in the thesis indicated by numbers in superscript positioned in left side of the concerned text.

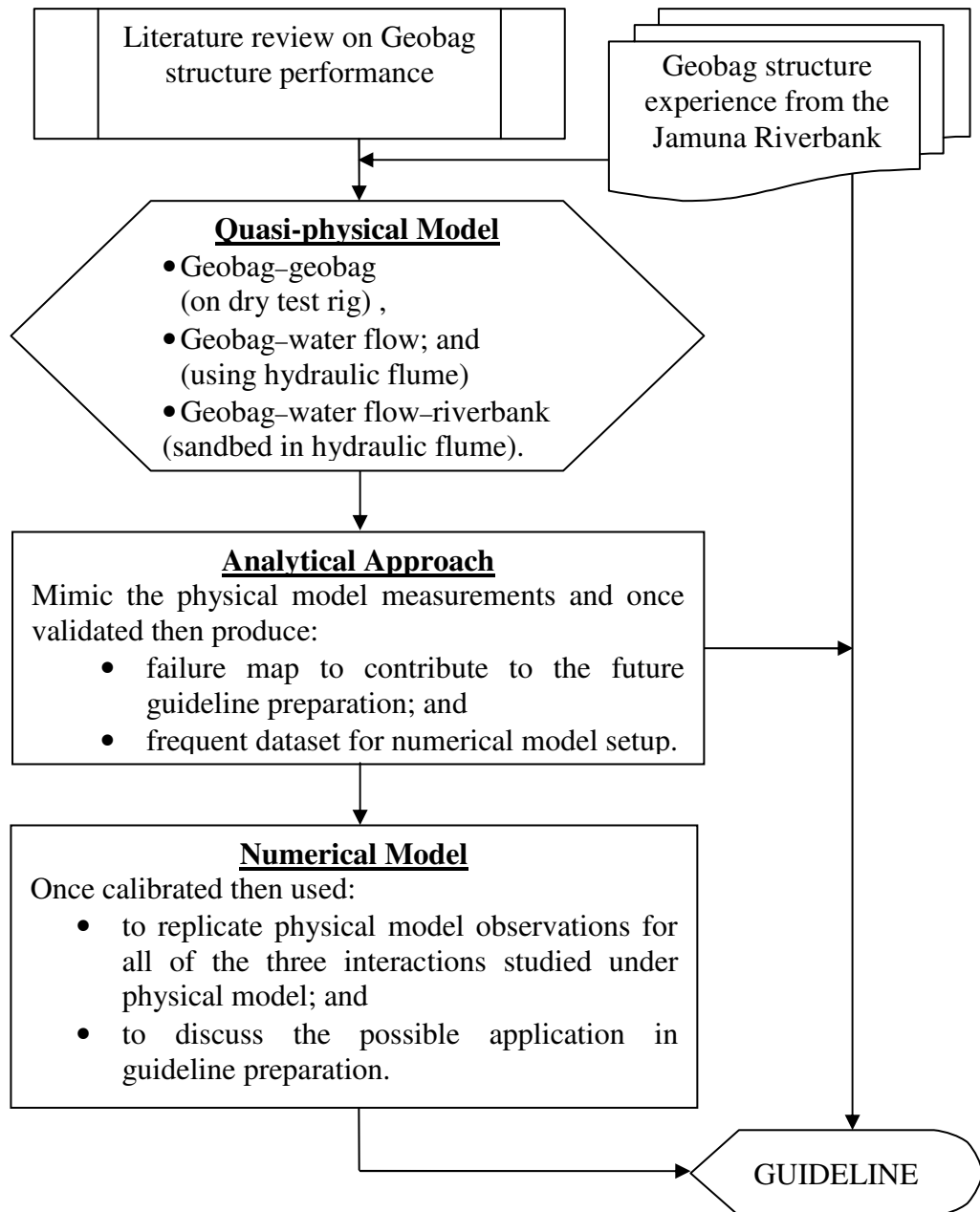


Figure 1.6: Flow chart of the research outline

Chapter 2

Quasi–Physical Model Study

The processes involved in the failure of geobag revetments have been experimentally investigated by means of several quasi–physical model runs.

Firstly, along with the quasi–physical model scale setup this chapter describes a dry test to develop a basic understanding of the failures due to friction alone, additionally the effect of bag wetness is noted.

Secondly, the chapter is concerned with estimating the active hydrodynamic forces. The features investigated for the geobag revetment are: (i) failure modes, (ii) hydraulic parameters of the flow, (iii) age of geobag since first immersion, and (iv) settling distance of displaced geobags from the revetment. The relationships among different water levels and geobag failure in revetment are presented.

Finally, a set of experimental runs with a sandbed underneath the geobag revetment is reported. The studied features are: (a) failure modes in geobag revetment, (b) hydraulic parameters, and (c) bed formation. The influence of revetment toe scour along with varying water depth on the failure of initiation in geobag revetment is detailed.

The reader is advised that although individual results are provided for each part, a general result analysis of this Chapter is included. Final conclusions are presented in Chapter 6.

2.1 Quasi-physical model scale

For this study, a scale of 1:10 (L) has been selected based on the Froude scaling law. As it was not possible to manufacture a scaled down model of the constituent materials within the geobags (geotextile and sand), some material distortion exists in the study. From the Froude criteria, the velocity scale relates to the geometric scale in terms of $L^{1/2}$, so the relevant scale ratio was 3.17. Thus, other relevant scales were computed as shown in Table 2.1.

Nonwoven geotextile Secutex[®] 451 GRK 5 C was used for bag preparation and sand with a Fineness Modulus of 1.72 and a dry density of 1.83 was used for bag filling. As described in Chapter 1, the 126 kg geobag offered the best performance in Jamuna riverbank protection work, the quasi-physical model study considered this size to be scaled down for the laboratory experiments. An 80% filling ratio for each bag was used to achieve the bag size of 103 mm by 70 mm of 0.126 kg to replicate the 1.03 m by 0.70 m bag of 126 kg used in field. The density of the dry geobag was found as 1596 kg/m³. A revetment slope of 1V: 2H was maintained through this study as Korkut *et al.* (2007) noted it as the maximum acceptable slope using geobags and also to replicate the previous laboratory work undertaken by nhc (2006).

Table 2.1: Scale ratio for the experimental setup

Quantity	Dimension	Scale Ratio
Length, Breadth	L	1 : 10
Bag Volume/ Weight	L^3	1 : 1000
Velocity	$L^{1/2}$	1 : 3.17
Discharge	$L^{3/2}$	1 : 316

2.2 Geobag–geobag interaction

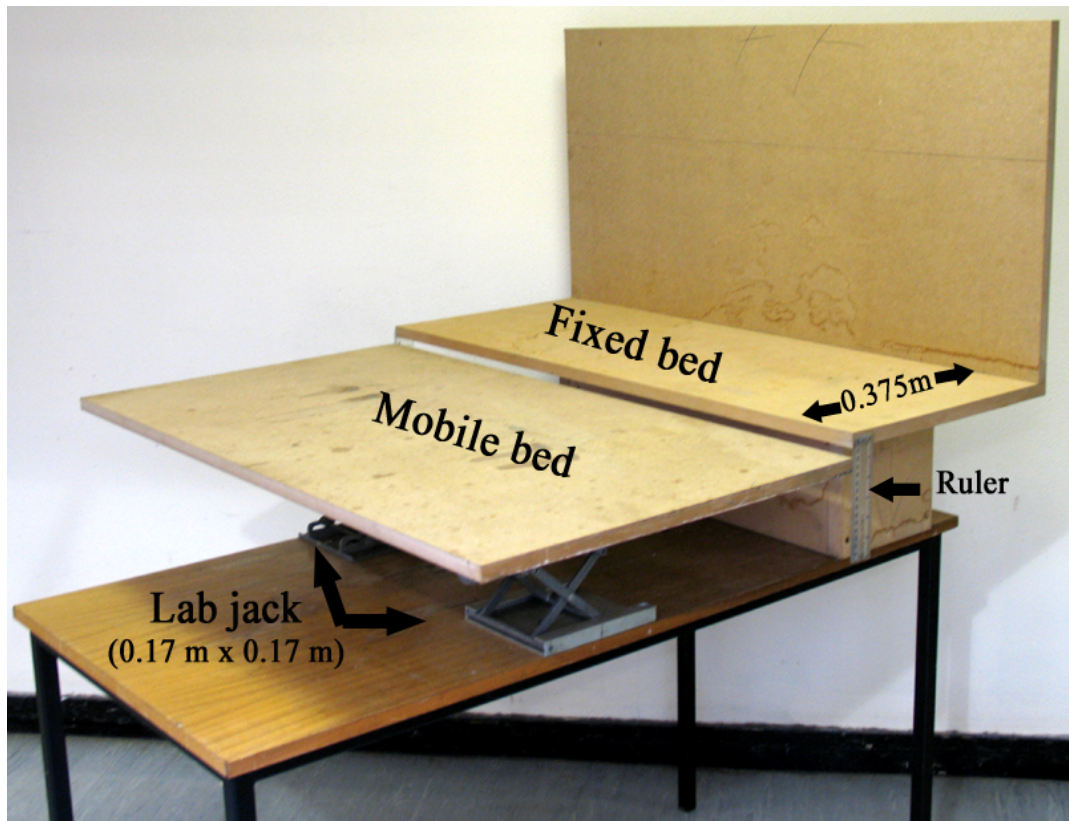
As friction has little influence on the outcome of simulations it is given a conservative value (constant roughness coefficient = 0.6 [Gadd, 1988]), or neglected in most of the hydrodynamic behaviour studies of geobags (Zhu *et al.*, 2004; Oberhagemann and Kamal, 2004; Korkut *et al.*, 2007). The available standard method for friction angle measurement between geotextile–sand interfaces is based on a direct shear stress experiment ¹(BS 6906 – 8:1991). Different studies suggested the average friction angle for geobag–geobag interaction is 30° (Recio and Oumeraci, 2009 b; Yang *et al.*, 2008; Chapter 1).

To understand the active friction force on failure initiation in geobag revetment, a number of model runs were conducted on a wooden test rig.

2.2.1 Dry tests

The test rig was constructed to represent the features of geobag – geobag movement due to river bed scour and geobag self weight. Medium Density Fiberboard (MDF) was used to construct the test rig which was 1.0 m long, 0.96 m wide and 0.50 m deep (Figure 2.1 a). A section of fixed bed 0.375 m wide and the mobile portion was fixed on two lab jacks (individual size 0.17 m × 0.17 m × 0.17 m) and clockwise rotations of the lab jacks allowed downward movement of the mobile bed by up to 0.10 m; this movement represents the scour of the river bank during a flood event.

¹ A test had performed using the direct shear test to achieve the initial idea on coefficient of friction for an individual geobag (applied in numerical model Chapter 4).

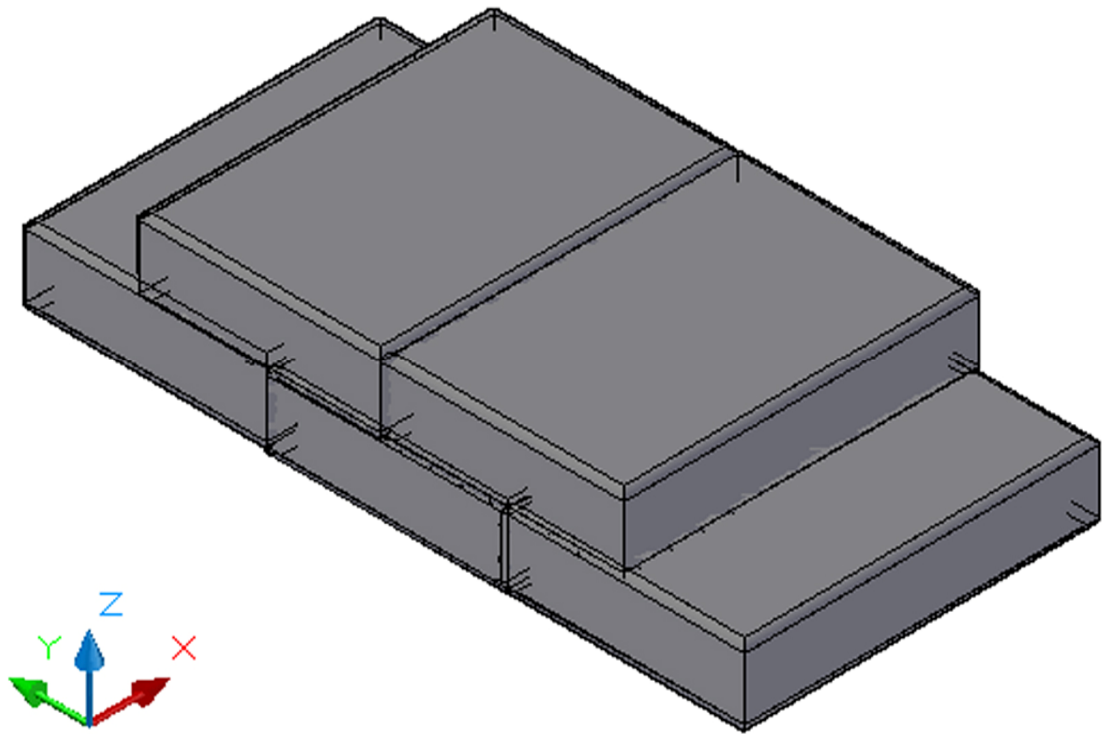


(a) Test rig



(b) Geobag
(103mm×70 mm; 0.126 kg)

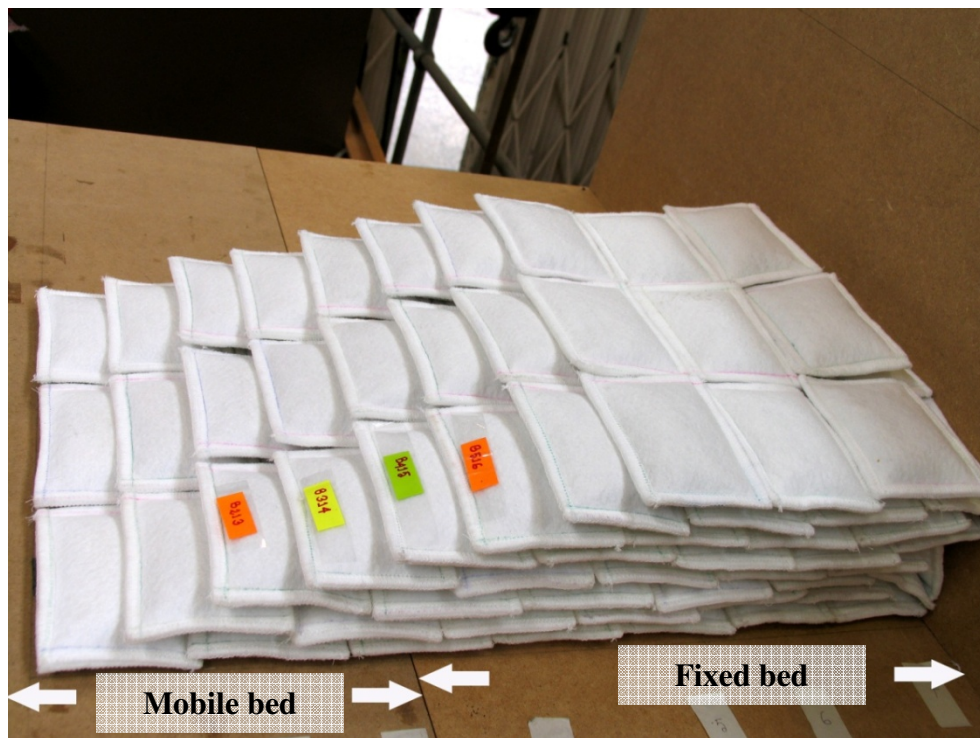
Figure 2.1 (a to c): Initial experimental setup on Test rig (Cont'd)



(c) Layer to layer setup

Figure 2.1(a to c): Initial experimental setup on Test rig

The geobag revetment constructed using the prescribed overlapping (i.e., 50% layer-to-layer overlapping in Figure 2.1c). Two broad categories of experiments were carried out using (a) dry geobags and (b) 24 h soaked geobags. The length ($y = 0.333$ m in Figure 2.1 a) and width ($x = 0.57$ m) of the revetment remained the same for all categories; note that the width is the sum of the fixed and mobile portions.



(a) Initial geobag revetment in wooden test rig



(b) Failure mode at 0.10 m scour depth in wooden test rig using dry bags

Figure 2.2 (a to c): Dry test on wooden test rig. (Cont'd)



(c) Failure mode at 0.10 m scour depth in wooden test rig using Soaked bags

Figure 2.2 (a to c): Dry test on wooden test rig

Chapter 2: Physical Model Study

The following observations were noted for dry bag and soaked bag experiments on wooden test rig (Figure 2.2):

- Dry bags
 - Sliding starts at 0.06 m scour depth;
 - Failure initiation was observed at 0.07 m scour depth; and
 - At 0.0982 m scour depth the bottom series bags on the joint stand perpendicular to the mobile bed. Two bags, from the middle and one at the far end have dropped.
- Soaked bags
 - Failure initiation observed at 0.08 m scour depth; and
 - The structure height decreases by 2.43% (i.e., 5 mm) from dry condition.

2.2.2 Results

The dry test run were performed with dry and soaked bags on wooden test rig (Figure 2.2). Details on this model run can be found in Appendix A. The key findings were:

- The difference between dry and soaked bags showed the effect of the friction coefficient on the fixed bed giving about 10% (i.e. 10 mm) of scour difference. Comparisons of horizontal and vertical displacements show soaked bags are more stable (Figure 2.2 b and c); and
- The structure height decreases by approximately 2.5% of the dry condition in the model (Figure 2.2 c); Krahn *et al.* (2004) observed a 5% difference in the height of a sand bag dike due to densification by wetting in large scale experiment.

2.3 Hydrodynamic forces

The driving formula for geobag incipient motion was based on a critical depth–average flow velocity, flow depth and geobag dimensions by considering a constant coefficient of drag and lift for flow around the bag (Zhu *et al.*, 2004). Recio and Oumeraci (2009 a) derived a geobag drag coefficient inversely proportional to the Reynolds number of the flow in a wave flume and a lift coefficient proportional to it (Chapter 1). Achenbach (1971, 1972) derived that drag coefficients for flow around a long cylinder and a sphere remain constant in a range of Reynolds number of the flow of around 1.5×10^4 to 2×10^5 . So, the active hydrodynamic forces on the geobag revetment under different water level are unknown.

In this study, using different revetment construction methods and water depth variations, laboratory experiments on hydrodynamic forces were performed to obtain (i) observations of failure initiation, (ii) velocity measurements of flow, (iii) effect of geobag wetness and (iv) the settling distance of the displaced geobags.

2.3.1 Experimental setup

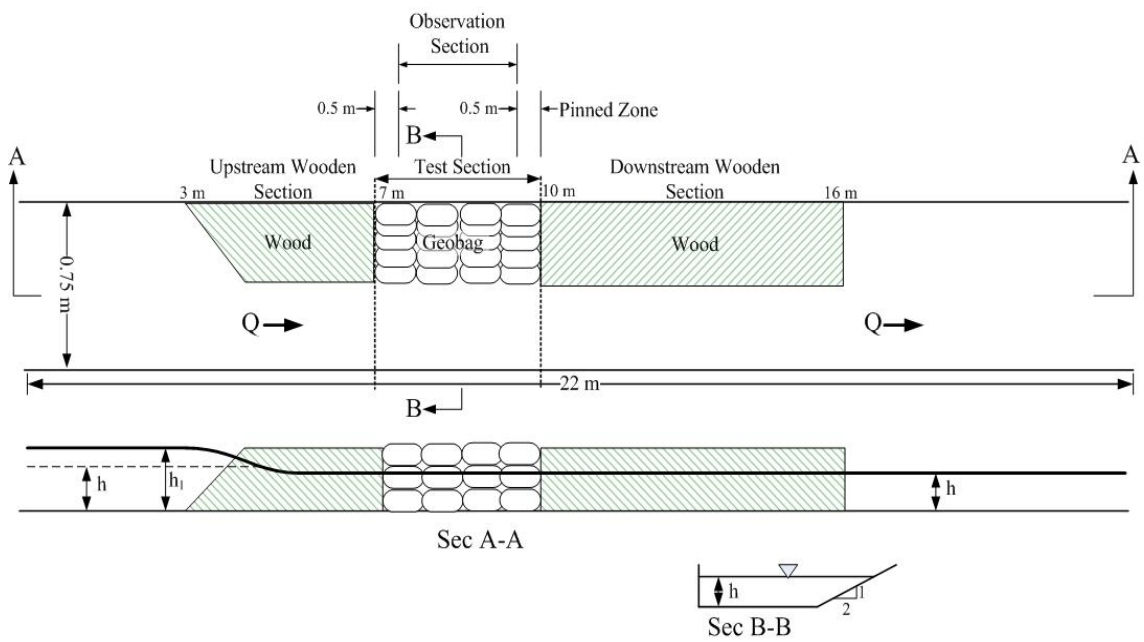
The laboratory experimental tests were undertaken in an open channel hydraulic flume (22 m long, 0.75 m wide, 0.50 m deep). The bed slope of the flume was set to 5.5×10^{-3} , which is approximately the same as the bed slope of the Jamuna River where the present geobag revetment exists. At the upstream end of the flume, two pumps are engaged for flow generation, each of them has a maximum pumping rate of 75 l/s. Within the flume, a test section was built with 600 model geobags (103 mm long, 70 mm wide, 0.126 kg weight), using a 50% layer–to–layer overlapping structure (Figure 2.3 c) with a transverse slope of 0.5; this gave overall revetment dimensions of 0.375 m width and 0.18 m depth.

As it was not feasible to construct the revetment along the whole length of the flume, a 3 m long geobag test section was located within the quasi–uniform flow zone within the

flume (Figure 2.3 a). To avoid artificially induced “end effects”, due to the sudden flow contraction and expansion occurring at either end of the test section, tapered wooden sections were located immediately upstream and downstream of the test section. However, despite this configuration, preliminary observations indicated that the end effects within the experimental setup were inducing geobag failure, i.e. failures occurred at the interface between the wooden sections and the geobag structure. To overcome this deficiency, the surface at geobags either end of the test section were pinned down for a distance of 0.5 m (Figure 2.3 a), hence allowing water flow conditions to stabilise before the mobile test section.

To understand the influence of geobag to geobag bond, three different revetment construction methods were tested, namely: RM1 – jack on jack (Figure 2.3 b), RM2-running bond (Figure 2.3 c), and RM3 – half basket weave (Figure 2.3 d). In the RM1 bond, the geobags are laid with their longer axis parallel to the flow direction in individual “columns”, with each bag being placed directly on top of another. In RM2, the geobags are again laid longitudinally, in a typical brick wall pattern, with the geobag joints lying in the middle of the bags in the layers directly above and below. The RM3 bond comprises of alternate layers of bags aligned with their longer and shorter axis parallel to the flow direction. In practice in a river such as the Jamuna, bag placement is normally performed manually; above the water level, placement is relatively easy, whereas under water placement necessitates dropping the bags from a “dumping” pontoon and can result in a combination of all of the 3 geobag bonds within any particular revetment. In reality, the dropped bags normally settle on the riverbed with their longest axis parallel to the streamwise direction (Chapter 1). So, the bottom layer of the geobag test section was constructed with the longest axis in the streamwise direction for all three revetment construction methods (Figure 2.3 b, c, d).

Chapter 2: Physical Model Study



(a) Schematic of fixed flume bed experiment setup

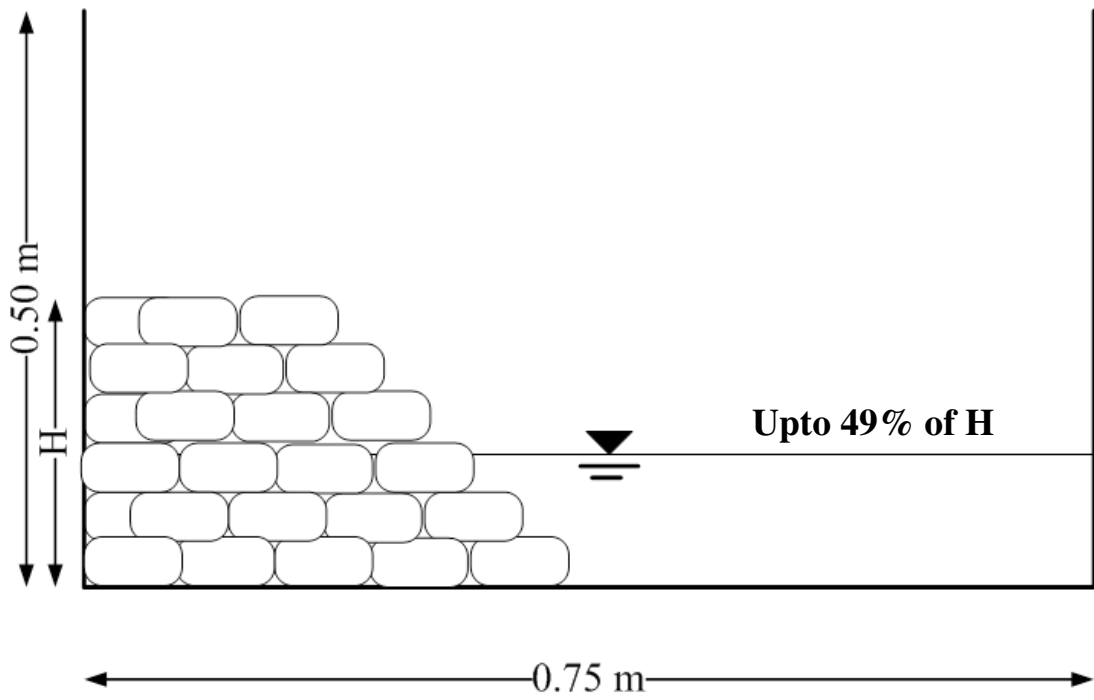


(b) RM1: Jack on jack

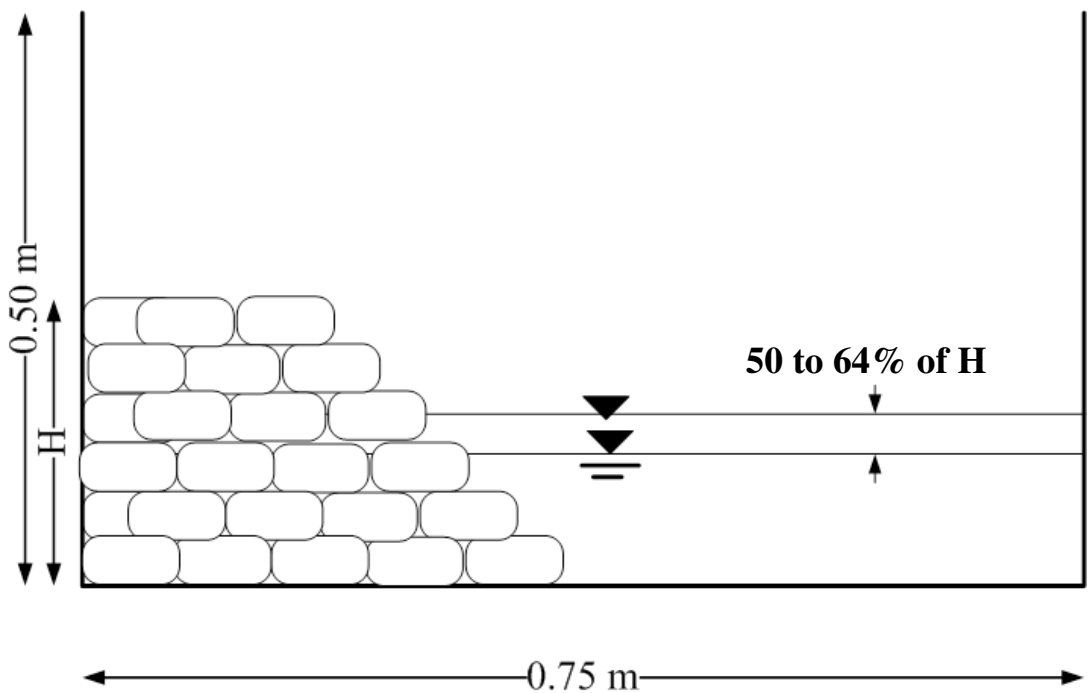
Figure 2.3 (a to d): Experimental setup in flume (Cont'd)

2.3.2 Methodology

Prior to commencement of each experimental test, the weights of the individual surface geobags were recorded, to provide benchmark data for washed away bags. Each experiment was run for 4.5 hours, which was sufficient for all processes to occur and replicated the time used in previous similar studies (nhc, 2006). From preliminary model runs it was determined that specific failures tended to occur in four distinct water depth ranges. Consequently, experimental tests were run at the following depth ranges: (A) up to 49%, (B) 50 to 64%, (C) 65 to 84%, and (D) 85% to 100% of the geobag revetment height (Figure 2.4).

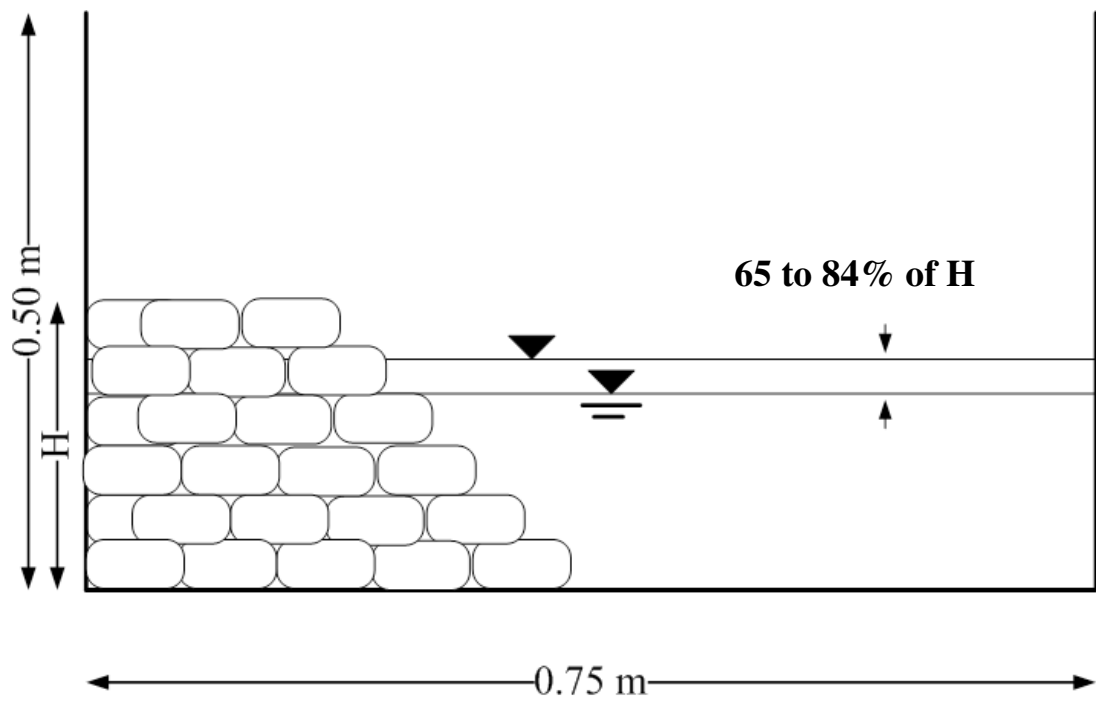


(a) Condition A

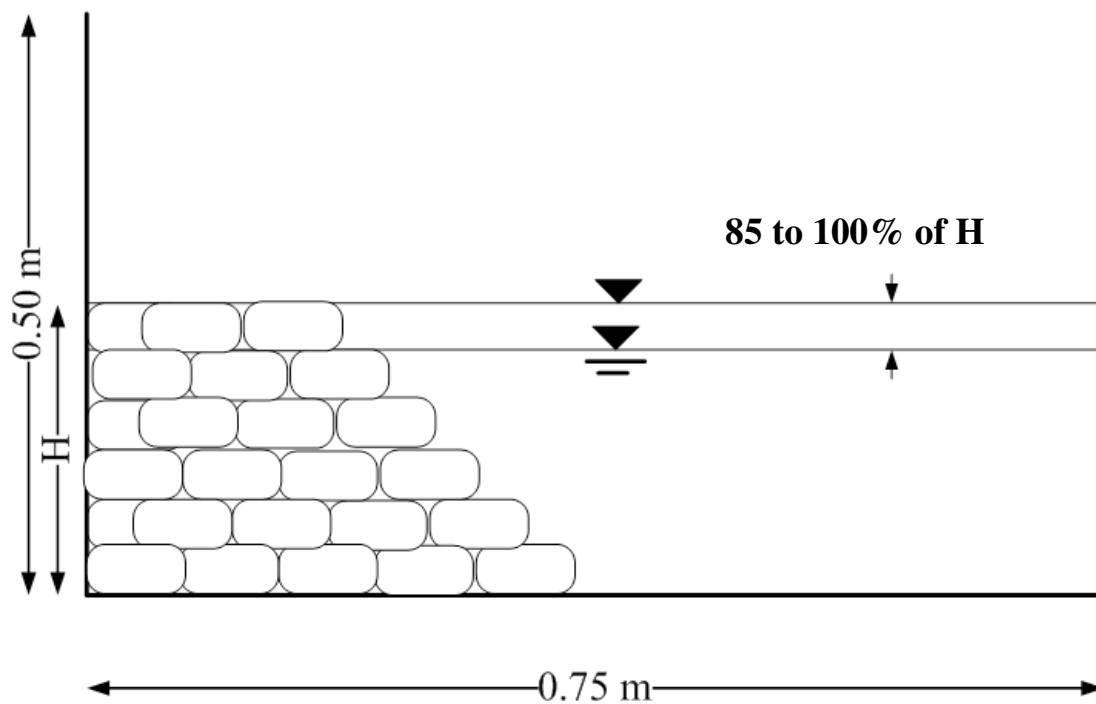


(b) Condition B

Figure 2.4 (a to d): Water depth conditions (fixed bed) (Cont'd)



(c) Condition C



(d) Condition D

Figure 2.4 (a to d): Water depth conditions (fixed bed)

Chapter 2: Physical Model Study

Each model run was recorded by a video camera, and velocity measurements were taken using a side looking Acoustic Doppler Velocimeter (ADV). A right angle V– notch was used to provide flow measurements to validate the ADV– measurements against. Using the ADV, the velocity was measured at 0.10 m intervals in the streamwise direction, and at 0.2, 0.4, 0.6 and 0.8 of the water depth. The mean velocity for each water level condition was calculated following the traditional three–point method (BS EN ISO 748:2007), i.e. the average of the values at 0.2, 0.6 and 0.8 of the flow depth (Table B.1, Appendix B). The ADV data enabled the velocity at the top surface of each (exposed) bag to be determined.

Each set of the acquired ADV measurements was despiked using WinADV32-version 2.027 software. For this study the Phase–space threshold despiking (provided by Goring and Nikora, 2002 and modified by Wahl, 2002) was adopted. Then the flow in the flume was estimated using the velocity–area method. The flow Q of the channel was estimated by means of measuring velocities, v_i , representative for the part ΔA_i of the area A ; while the width Δb_i ($= 0.15$ m) of the total width of B ($= 0.75$ m). The method is as follows:

$$Q = \int_A v_i \cdot dA \approx \sum_{i=1}^n v_i \cdot \Delta A_i \quad 2.1$$

With the ADV measured data, the exact velocity in front of the bag (except the bottom most layer) and the frequent bag surface velocity (against 0.10 m interval ADV measurement) are unknown. So, to replicate the ADV measured streamwise velocity data the Conveyance Estimation System (CES) is employed to predict average velocities for the geobags in revetment (described in Chapter 3).

For the bags washed away from the test section, the streamwise horizontal travel distance and final bag weight were recorded. The validated CES was then applied to calculate the active shear stress on the washed away bag and compared against Chow (1959) method (details in Chapter 3).

2.3.3 Results

The failure modes and zone observations were noted previously. While the hydrodynamic forces evaluated using the laboratory measurements are tabulated in Table 2.2. The summary results are provided at the end of this subsection.

In the RM1 – jack on jack, the observed failure initiates due to the passage of turbulent eddies at the revetment face causing pressure fluctuations between the main flow and revetment void flow, resulting in the geobag being displaced while the flow depth is low to moderate (Figure 2.5 a). So, in low flow the geobags move because of pressure differences between the main flow and void flow. The increased flow depth causes uplifting of the geobags and the extreme condition of flow depth results normally in pullout of the geobag and others (Figure 2.5 b, c, d). In all of the incipient failure progression and sliding seemed to occur (Video clips on these failures are attached in the submitted thesis CD).

The RM2 – running bond showed the observed failure initiates due to pressure differences between the main flow and void flow associated with sliding while the flow depth is low to moderate (Figure 2.6 a). Also in the increased flow depth sliding persists with the geobags uplifting and pullout occurring (Figure 2.6 b, c). At the extreme flow depth, there is uplifting observed in places along with other forms of failure initiation (Figure 2.6 d). Video clips on these failures are attached in the submitted thesis CD.

In the RM3 – half basket weave, pressure differences between the main flow and void flow associated with sliding initiated failures in low to moderate water depth (Figure 2.7 a, b, d). In the increased flow depth sliding accompanies with the geobags uplifting as a basis of incipient failure in geobag revetment (Figure 2.7 c, d). Video clips on these failures are attached in the submitted thesis CD.

So, bag displacement due to pressure differences between the main flow and void flow was observed at relatively shallow depths (Condition A, i.e. water levels less than 49% of the revetment height), (Figure 2.5 a; Figure 2.6 a; Figure 2.7 a, b, c), whilst uplifting

Chapter 2: Physical Model Study

(Figure 2.5 a, b,c; Figure 2.6 b, c; Figure 2.7 d) was typically observed in moderate water levels (i.e. water levels more than 50% of the revetment height), and followed by a similar process to that described for coastal revetments (Recio and Oumeraci, 2009 a, b; Chapter 1). Uplifting can be associated with local vortices or pullout processes depending on the flow conditions and the initial physical state of the geobags (dry or saturated). At the end of experiments, the observed failure modes are the slide, pullout and slump (Figure 2.8). Similar failure modes have also been observed in the field (JMREM, 2006 a).

The hydrodynamic forces on the geobag revetment were evaluated through ten individual experimental runs for each of the water level condition and construction method combinations. Whilst four water level conditions were used for both the jack on jack and running bond construction methods, only two water level conditions (B and D) were tested with the half basket weave construction method (Table 2.2). Bag failure initiation was observed in all three different construction methods, along with velocity measurements and the effect of bag wetness (evaluated through change in weight and travel distance).

In the laboratory revetment, with relatively dry geobags, higher streamwise velocities influenced the bag pullout processes. Internal sliding, combined with other modes, characterized the failure process in almost all cases, but most prominently in the lower to moderate water level condition (Figure 2.5, 2.6, 2.7). The measured velocities are given in Table 2.2.

The results from the fixed bed experiments can be summarized as follows:

- The failure modes were normally initiated with an anticlockwise movement with respect to the streamwise direction, regardless of water depth;

Chapter 2: Physical Model Study

- The initial failure modes for each water level condition were:
 - Condition A (up to 49% of the geobag revetment height): geobag displacement due to pressure differences between the main flow and void flow with internal sliding;
 - Condition B (50 to 64% of the geobag revetment height): pressure differences between the main flow and void flow, sliding of the bag;
 - Condition C (65 to 84% of the geobag revetment height): uplifting, sliding or/and pullout of the bag; and
 - Condition D (85% to 100% of the geobag revetment height): overtopping washing away or pulls geobags from the revetment.

Using these results a failure map can be prepared for geobag–water flow interaction as shown in Figure 2.9.

- The maximum velocity at the initiation of bag failure was 1.1 to 1.3 m/s, representing a field velocity of 3.5 to 4 m/s (calculated using Table 2.1), which is of the same magnitude to that previously reported for revetments with similar side slopes of 1V:2H (nhc, 2006; Chapter 1);
- The experimental data indicate that the mean transverse and vertical velocities were about 2.4% and 0.5% of the mean streamwise velocity respectively (Table 2.2);
- The Froude and Reynolds numbers confirm that the flow in the flume was supercritical and turbulent in nature (Table 2.2);
- The initial physical state of the geobags played an important role in determining settling distance as a result of shear force on the bag. In the extreme case (saturated bags used in overtopping condition i.e. the highest water level condition) 89 bags out of a total 600 (15%) were displaced from the test section. This does not compare to the results of similar experimental studies (nhc, 2006), where 22 bags were displaced from the test section, and the maximum recorded settling distance was

Chapter 2: Physical Model Study

6 m; it should be noted that these experimental studies were undertaken at a scale of 1:20 and included an unspecified number of bags; and

- Individual experiments with initially dry bags showed that the majority of the dry bags displaced from the revetment travelled further than the saturated bags. The observed failure mechanisms were the same as described in *nhc (2006) launching test*, dry bags remain lighter at the start of the experiments. Although they absorbed water, by the time they were washed away from the test section. The additional weight absorbing percentage for half of the total dry bags used in the experimental work was 30% to 40% [i.e. self weight of bag + (30% to 40% of self weight)]. Comparatively the saturated bags remain stable as 70% of the total bags used in experiment absorbed only 0 to 10% additional weight [i.e. self weight of bag + (0% to 10% of self weight)]. As a result the saturated bags normally travel less distance than the dry bags.



(a) Displacement due to (i) pressure differences between the main and void flow and (ii) uplift



(b) Partial uplifting and sliding

Figure 2.5 (a to d): Observed failure modes in the RM1 – jack on jack (Cont'd)

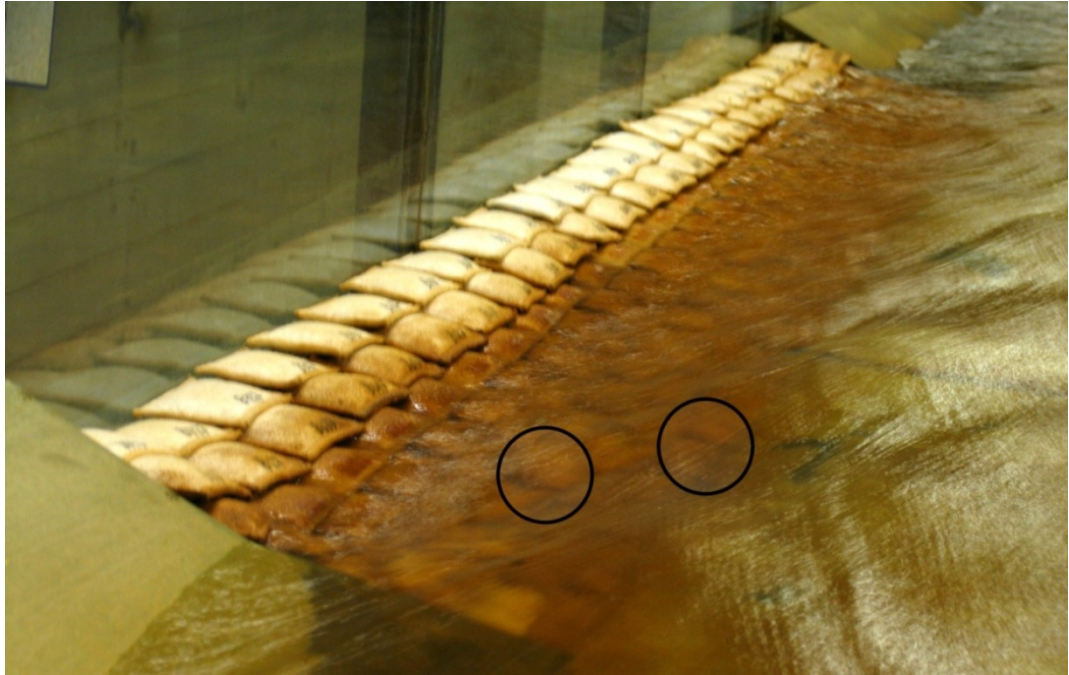


(c) Full uplifting



(d) Overtopping

Figure 2.5 (a to d): Observed failure modes in the RM1 – jack on jack

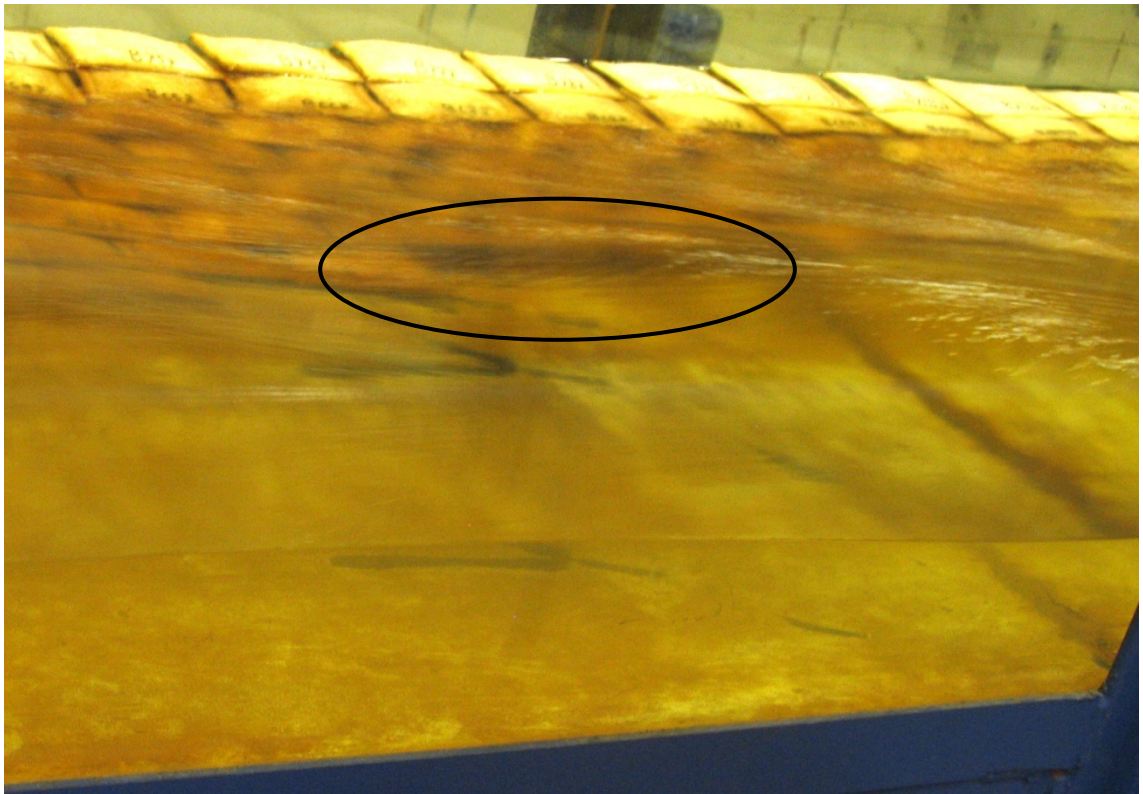


(a) Displacement due to (i) pressure differences between the main and void flow and (ii) sliding

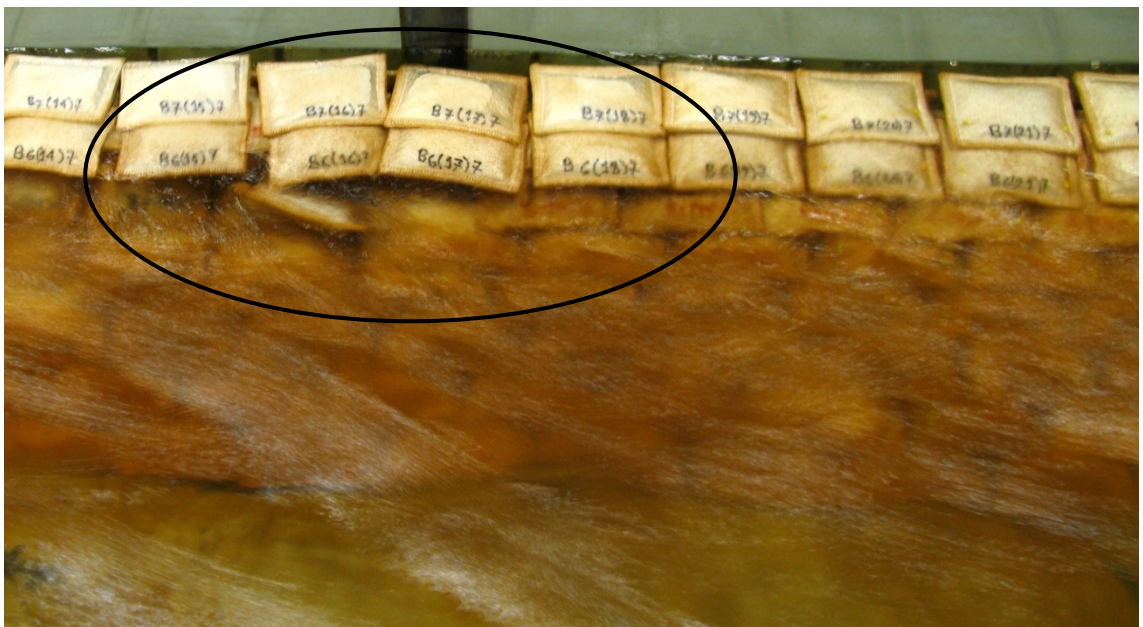


(b) Sliding, partial uplift and pullout

Figure 2.6 (a to d): Observed failure modes in the RM2 – running bond (Cont'd)



(c) Full uplift



(d) Overtopping

Figure 2.6 (a to d): Observed failure modes in the RM2 – running bond



(a) Pressure differences between the main flow and void flow

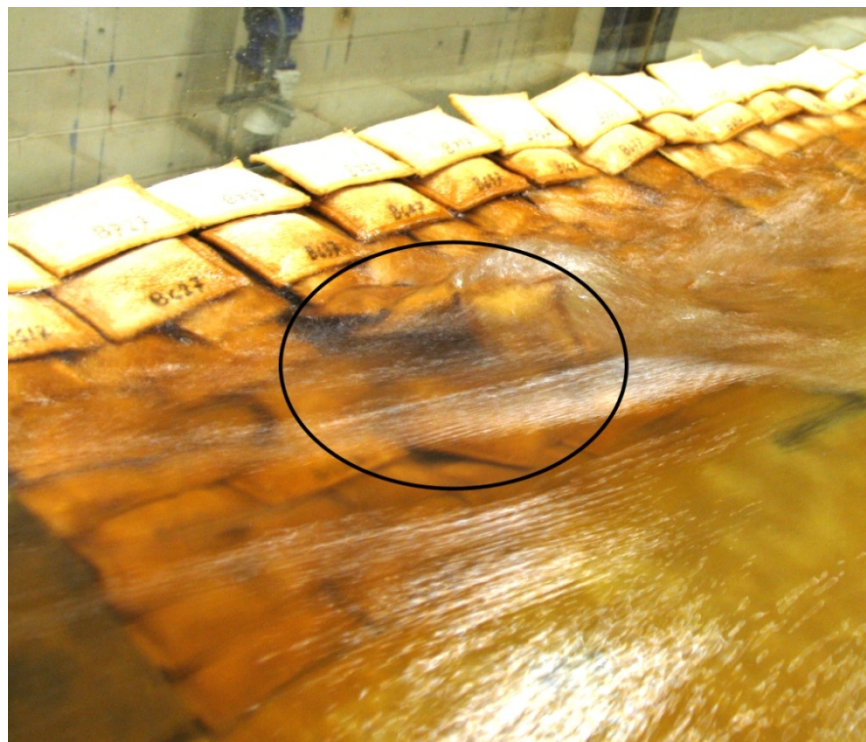


(b) Displacement due to (i) pressure differences between the main and void flow and (ii) sliding

Figure 2.7 (a to d): Observed failure modes in the RM3 – half basket weave(Cont'd)

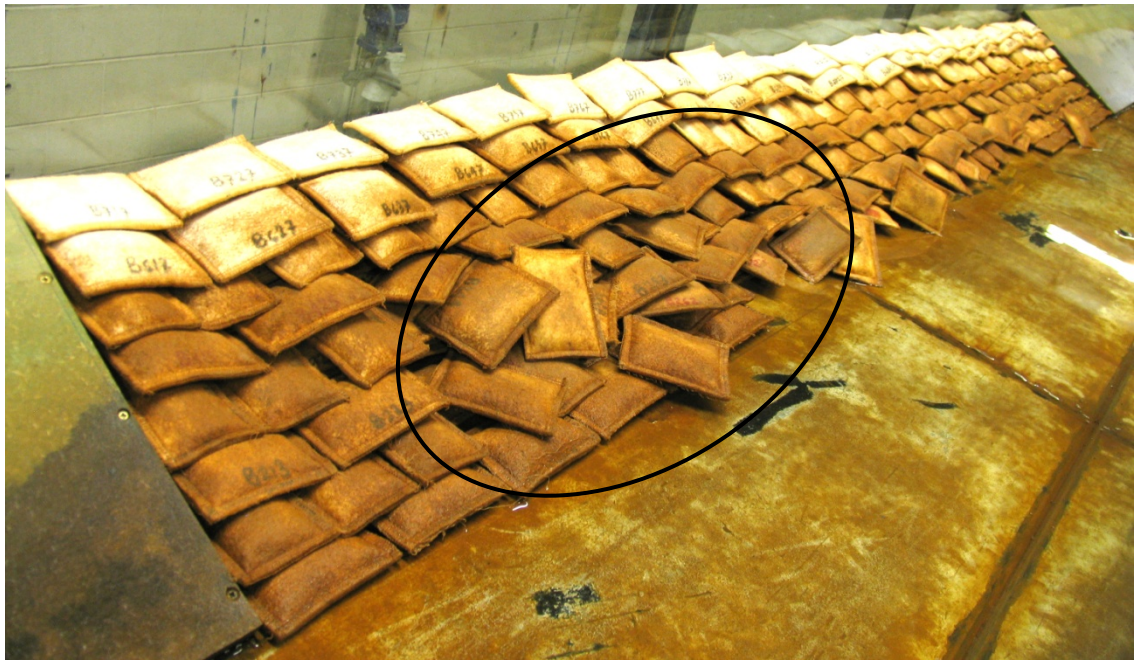


(c) Displacement due to (i) pressure differences between the main and void flow and (ii) sliding



(d) Full uplift and sliding

Figure 2.7 (a to d): Observed failure modes in the RM3 – half basket weave

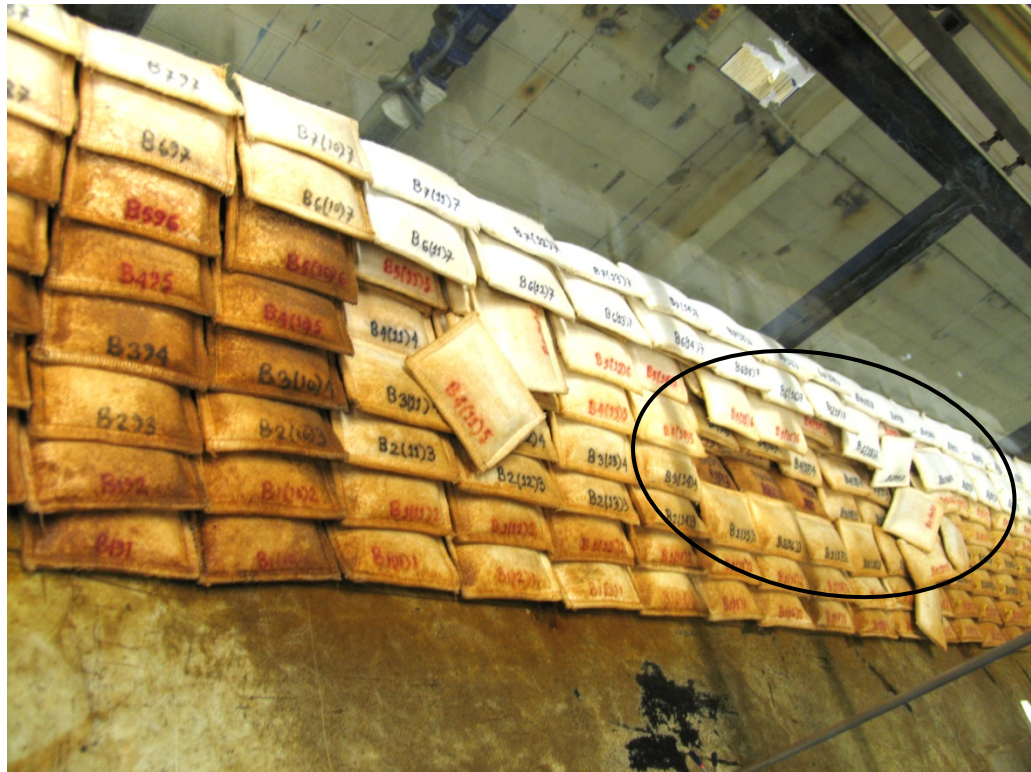


(a) Sliding zone

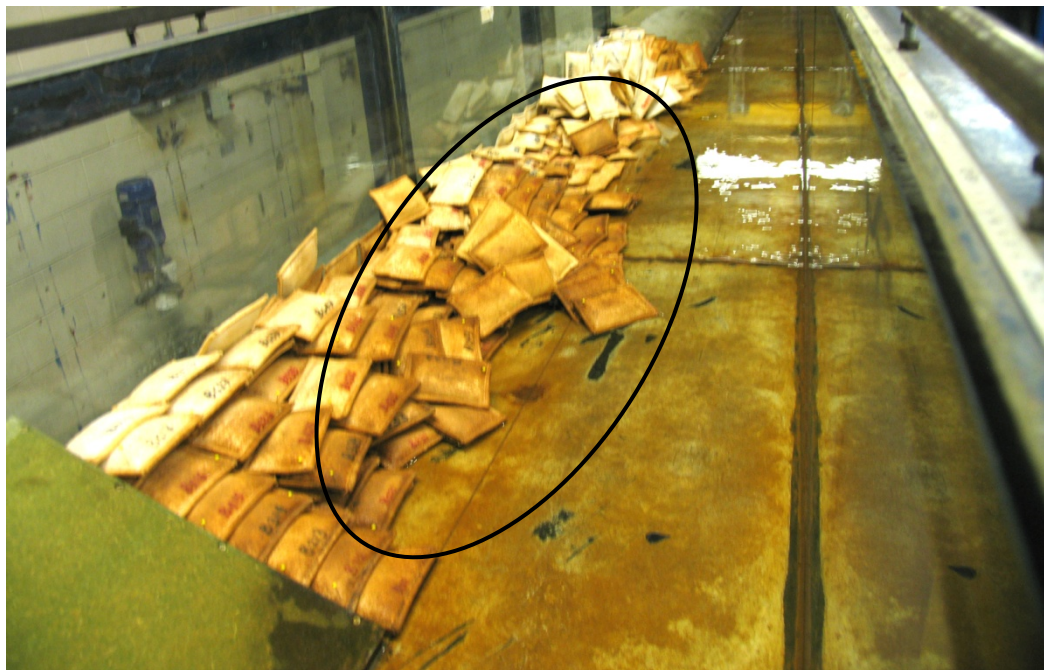


(b) Sliding zone (with slumps)

Figure 2.8 (a to d): Different types of the failure zones in the geobag revetment (Cont'd)






(c) Plug zone



(d) Plug, slump and slide zones

Figure 2.8 (a to d): Different types of the failure zones in the revetment

Table 2.2: Experimental outcomes with different revetment construction method

Model Setup	² Condition	Model run no.	Mean water level (m)	Mean near bank velocity (m/s)	Transverse	Vertical	Flow rate (cumec)	³ Froude No.	Reynolds No.	Initial Failure type
					% of the mean stream wise velocity					
(RM1) Jack on jack										
	A	1	0.051	1.09	2.38	1.20	0.024	1.54	55,369	Pressure difference
	B	2	0.065	1.13	2.54	2.23	0.033	1.42	73,157	
	C	3	0.095	1.27	2.24	0.86	0.055	1.32	120,169	⁴ Uplift
	D	4	0.110	1.30	2.28	0.69	0.070	1.25	142,430	Uplift
(RM2) Running bond										
	A	5	0.054	1.13	2.48	0.33	0.027	1.55	60,777	Pressure difference
	B	6	0.072	1.18	2.54	0.06	0.039	1.40	84,622	
	C	7	0.098	1.28	2.25	0.26	0.058	1.31	124,940	⁴ Uplift
	D	8	0.112	1.30	2.35	0.98	0.071	1.24	145,020	Uplift
(RM3) Half basket weave										
	B	9	0.079	1.21	2.57	0.56	0.043	1.38	95,209	Pressure difference
	D	10	0.115	1.36	2.14	0.16	0.071	1.28	155,777	Uplift

² The water level conditions had classified for 0.13 m revetment height.

³ Froude Number, $F = \frac{V}{\sqrt{gL}}$, L= Characteristic length, i.e., hydraulic depth, h (for open channel)

⁴ Partial or full uplifting

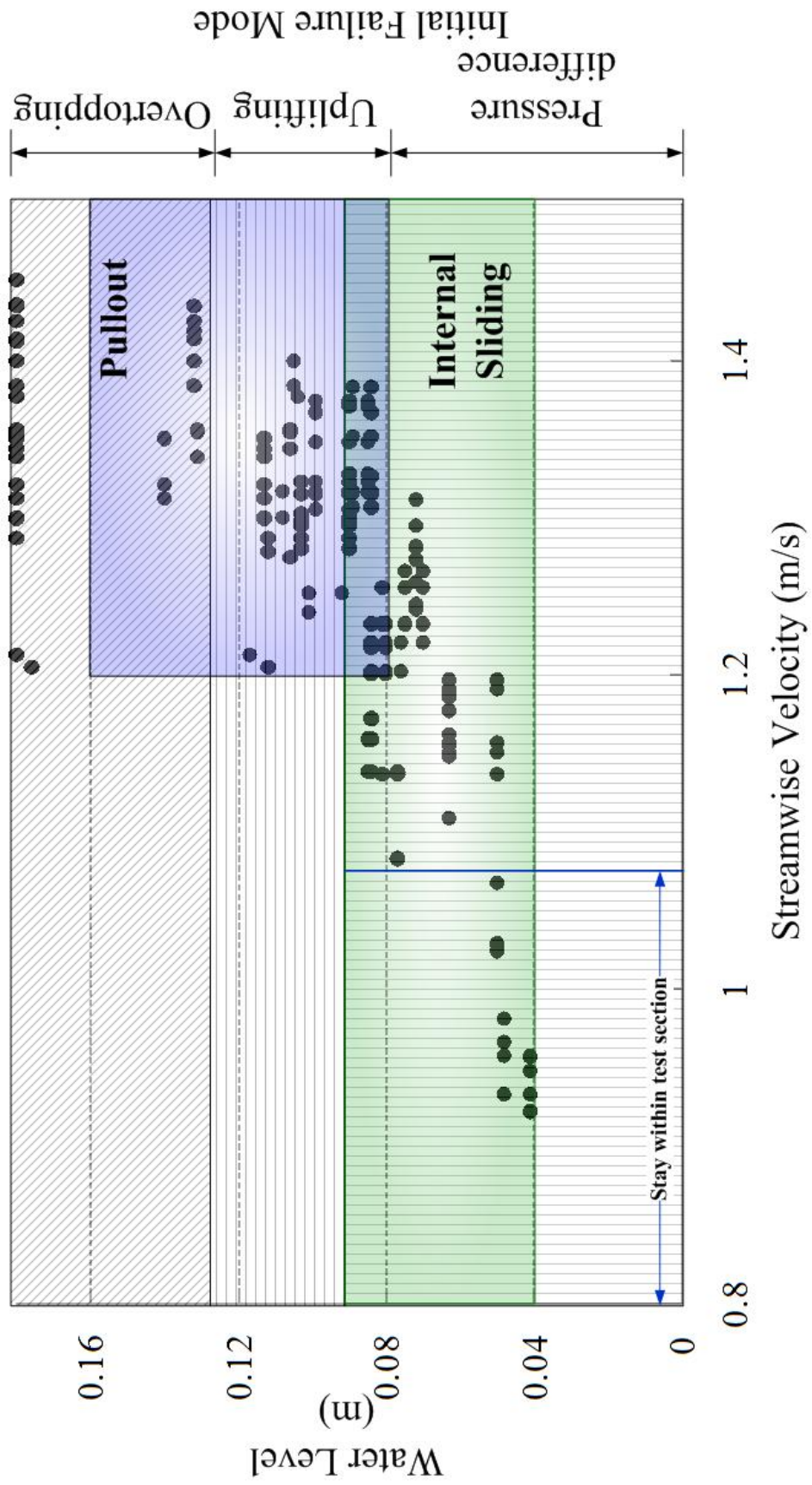


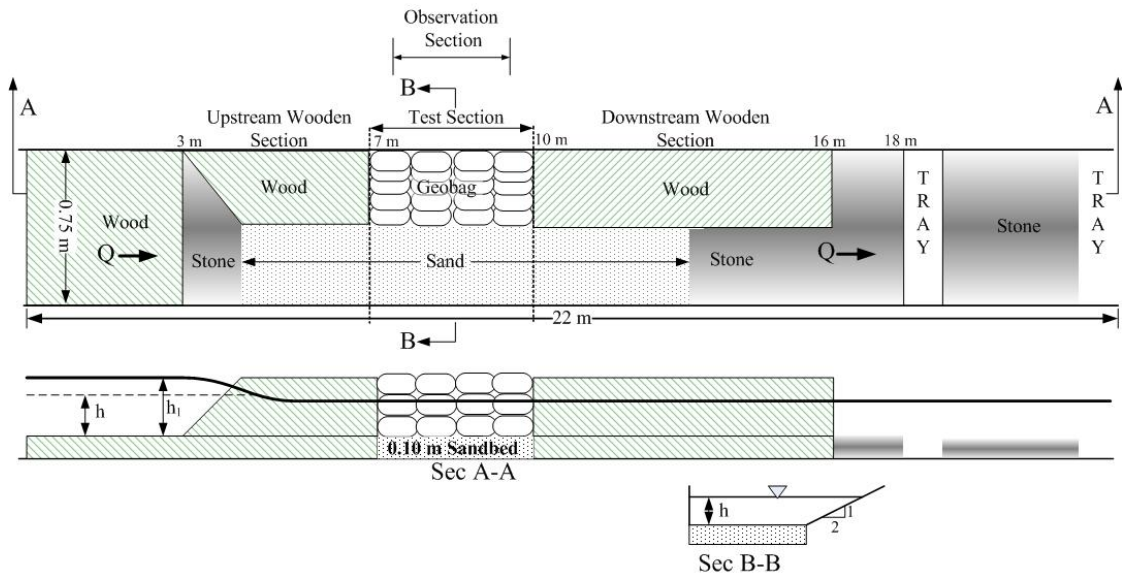
Figure 2.9: Failure map of geobag revetment due to geobag-flow interaction (using measured data)

2.4 Hydrodynamic forces and riverbank toe scour

Using a sandbed underneath the geobag revetment, the aim of these experiments was to obtain failure initiation observation and bed formation in varying water depth under known flow rate in the flume.

2.4.1 Experimental setup

The quasi-physical model for the mobile bed setup consisted of a 0.10 m sand bed ($d_{50} = 0.2$ mm) underneath the geobag test section (Figure 2.10 a, b). As this essentially raised the test section by 0.10 m, it was also necessary to elevate the bed level immediately upstream and downstream of the test section by 0.10 m to minimise experimental setup factors; this was again achieved through the use of wooden sections (Figure 2.10 b). Stone was placed between the wood fixed bed and sand bed section to minimize the roughness differences. From the experimental tests with a fixed bed, it was identified that the bag incipient velocity was not dependent on specific geobag bond configuration; consequently, only the jack on jack revetment construction was tested with the mobile bed (Figure 2.10 b).



(a) Schematic of mobile flume bed experiment setup

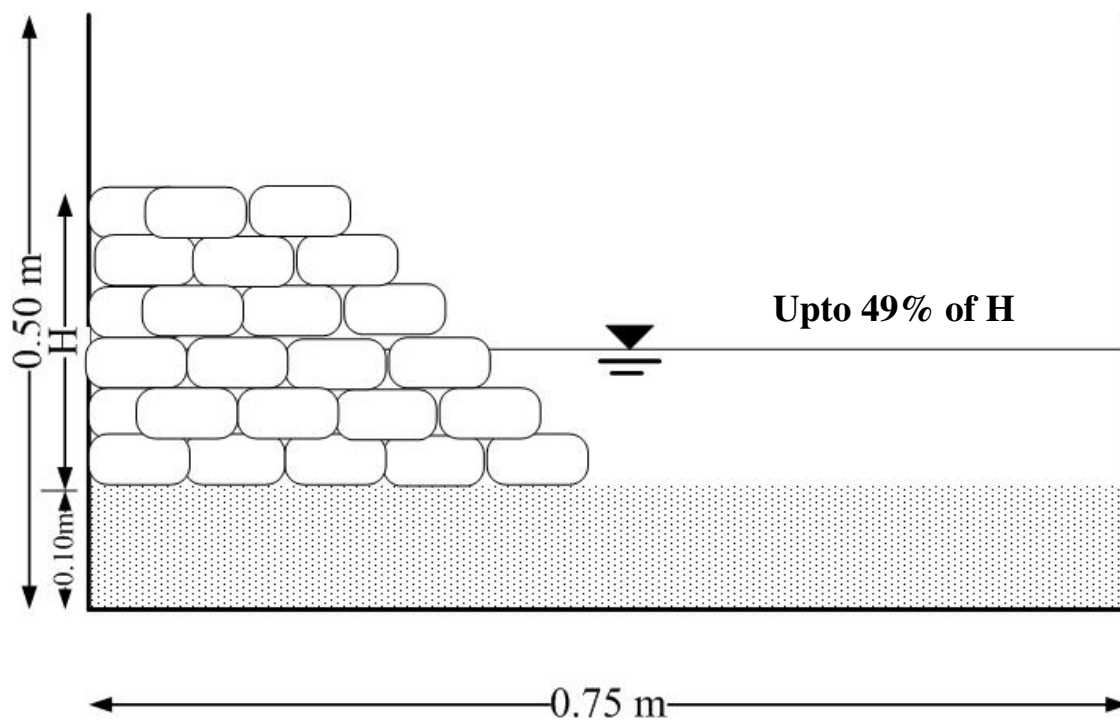


(b) Geobag revetment on sandbed

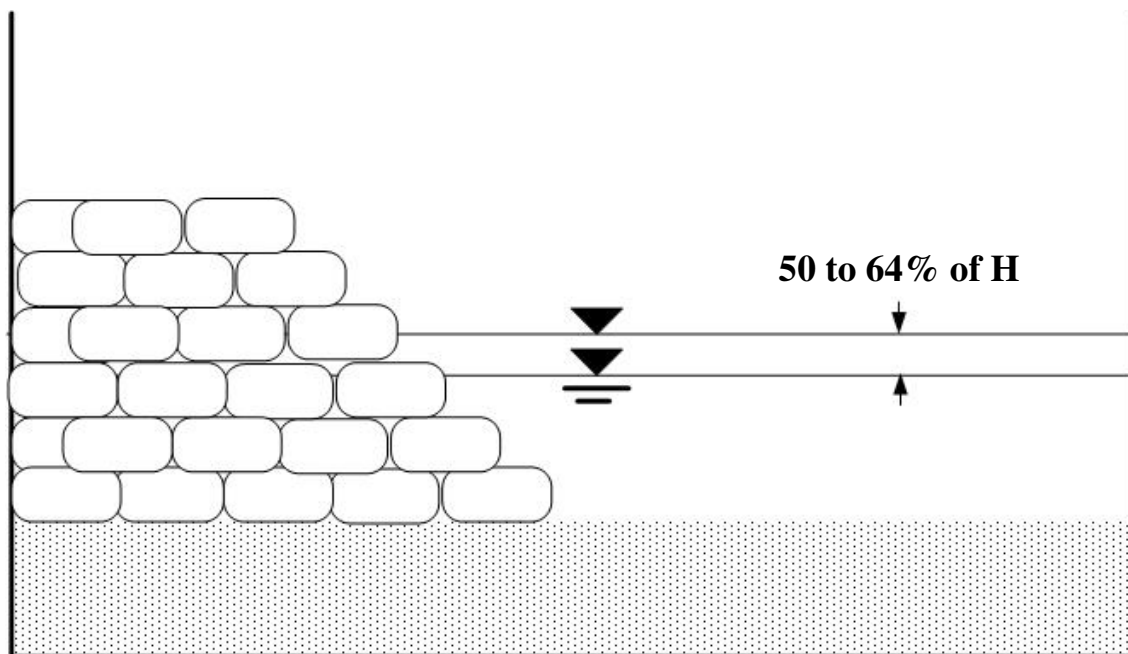
Figure 2.10 (a and b): Experimental setup in flume (mobile bed)

2.4.2 Methodology

Initially, geobag failure modes associated with the earlier stated four different water level conditions (Figure 2.11) and the bed formation were observed. The bed change was recorded in two phases i.e. (i) manually measured depth at an interval of 0.10 m in both streamwise and transverse directions and (ii) photo taken at an interval of 0.50 m for capturing the changes in surface area and then using the *Image J* (Ferreira and Rasband, 2010) version 1.43 software the eroded or deposited area had obtained. The final bed change was derived from the difference between the measurements before and after the experimental tests.

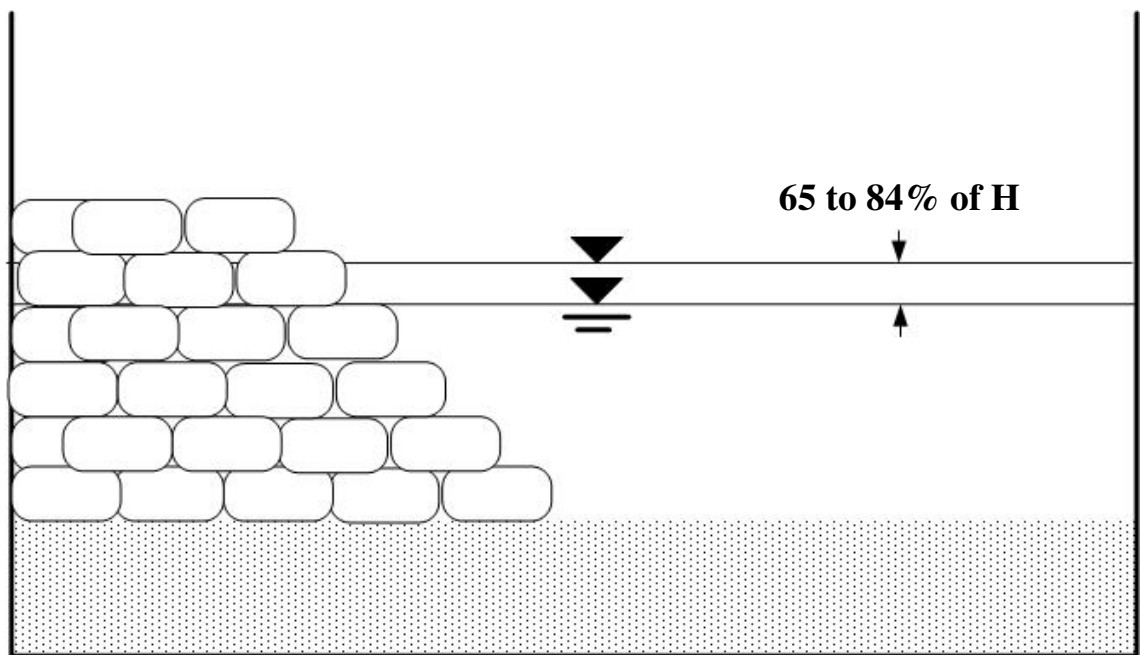


(a) Condition A

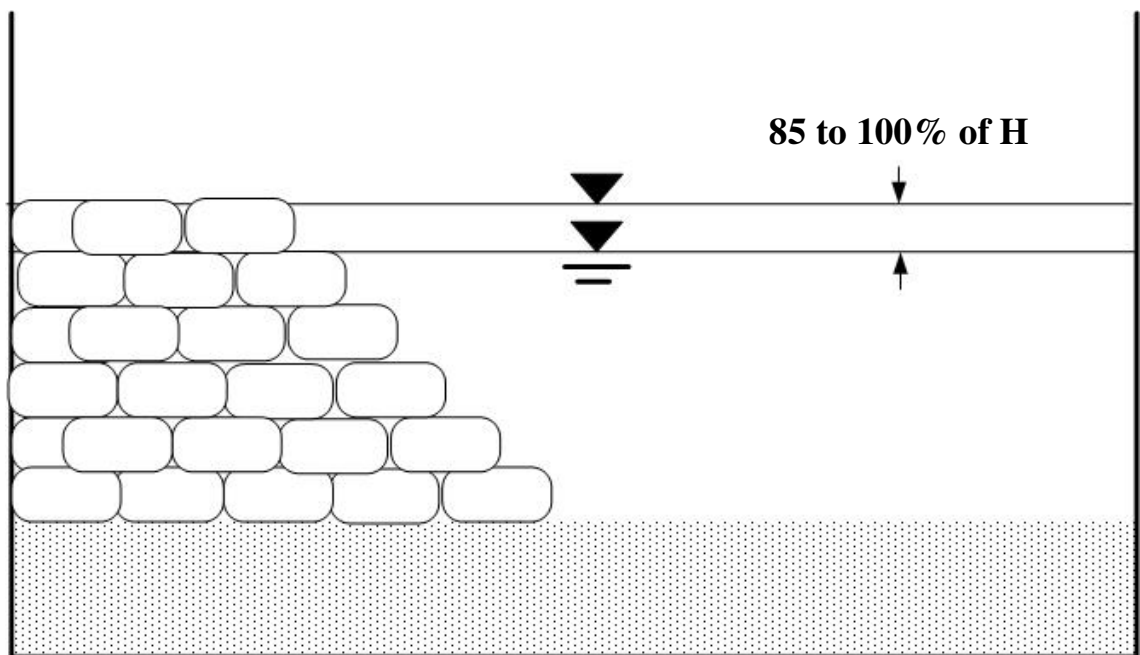


(b) Condition B

Figure 2.11 (a to d): Water depth conditions (mobile sediment bed) (Cont'd)



(c) Condition C



(d) Condition D

Figure 2.11 (a to d): Water depth conditions (mobile sediment bed)

2.4.3 Results

Mobile sediment bed produces two broad sectors of results i.e., failure modes in geobag revetment while mounted on mobile bed and change in mobile sediment under different water depths. The first part of this subsection has considered the incipient failure of geobags under different flow depth and bed formation. Then critically the bed formation was analysed to understand the observed geobag failure modes.

In the flume a number of model runs with the mobile bed show similar failure modes to those found in fixed bed. With the exception in the mobile bed tests failure can occur as a result of toe scour. Additionally the existence of a mobile bed performs sliding of support bags closest to the bed and an increased frequency of failures by this mode (Figure 2.12 a, b, c, d). Geobag displacement in the streamwise direction due to pressure differences between the main flow and void flow was affected by the bed changes underneath the revetment, as a result the bag displacement was more likely to occur in the vertical direction. Uplift, pullout and internal sliding followed similar mechanisms to fixed bed condition, however sliding often ends with scour holes (Figure 2.12 d). The video clip of failure modes in model geobag revetment has enclosed in the thesis CD.

The initial failure modes in each water level condition were:

- Condition A (up to 49% of the geobag revetment height): Ripple bed offered mild toe scour along with pressure differences between the main flow and void flow and internal sliding, geobag displacement observed within test section;
- Condition B (50 to 64% of the geobag revetment height): Dune bed experienced uplifting and sliding of geobags within the test section;
- Condition C (65 to 84% of the geobag revetment height respectively): Failure due to pressure differences between the main flow and void flow, uplifting, sliding or/and pullout. Transition flat bed resulted in displacement of bags from different locations of lower parts of the revetment (i.e. up to 45% of the revetment height) and the washed away bags passed the test section; and

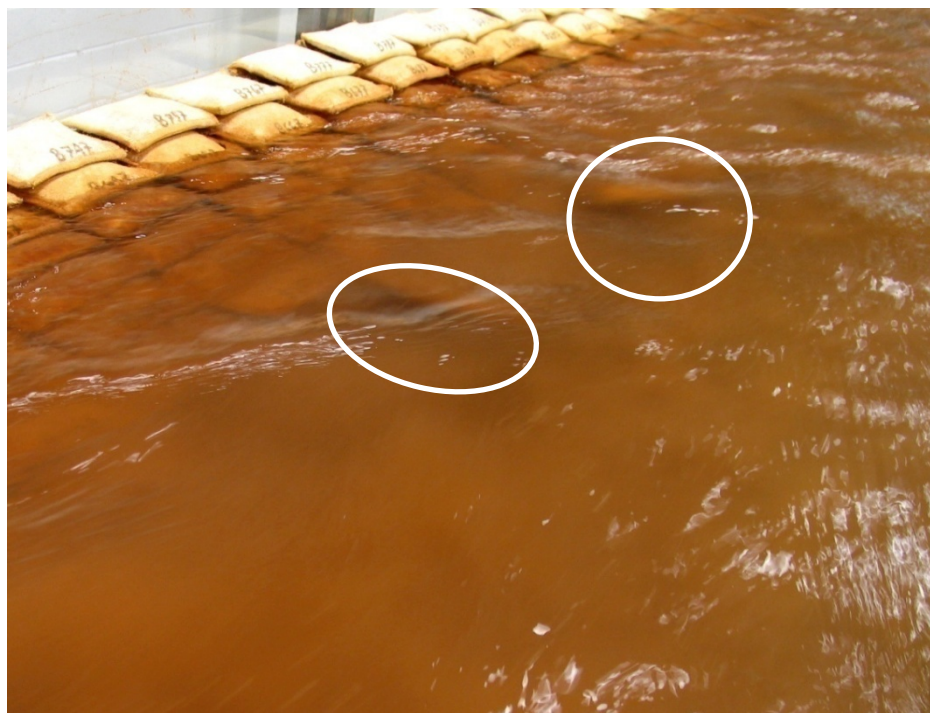
Chapter 2: Physical Model Study

- Condition D (85% to 100% of the geobag revetment height): Transition flat bed associated with overtopping washed away or pull/dislodge geobags from the revetment.

For different water levels and flows the mobile bed setup offered different bed formation along with different failure modes in the geobag revetment. Several researchers have classified the bed form based on visual inspection (Mantz, 1992; Bennett and Best, 1996; Baas, 1999; Friedrich *et al.*, 2006). In the present study sediment is supplied only at the start of each experimental run, to simulate the riverbed (Figure 2.10 b); no further sediment is introduced into the system once an experimental test is commenced. In this stage, the bag failure modes were observed under known water level and flow alongwith bed formation. The observed bed formation was then classified based on the available literatures listed above, to correlate with the geobag failure modes (Figure 2.12, 2.13 and Table 2.3).



(a) Displacement due to (i) pressure differences between the main and void flow and (ii) toe scouring



(b) Uplifting

Figure 2.12 (a to d): Different failure modes in geobag revetment (Cont'd)



(c) Uplifting and sliding



(d) Internal sliding

Figure 2.12 (a to d): Different failure modes in geobag revetment

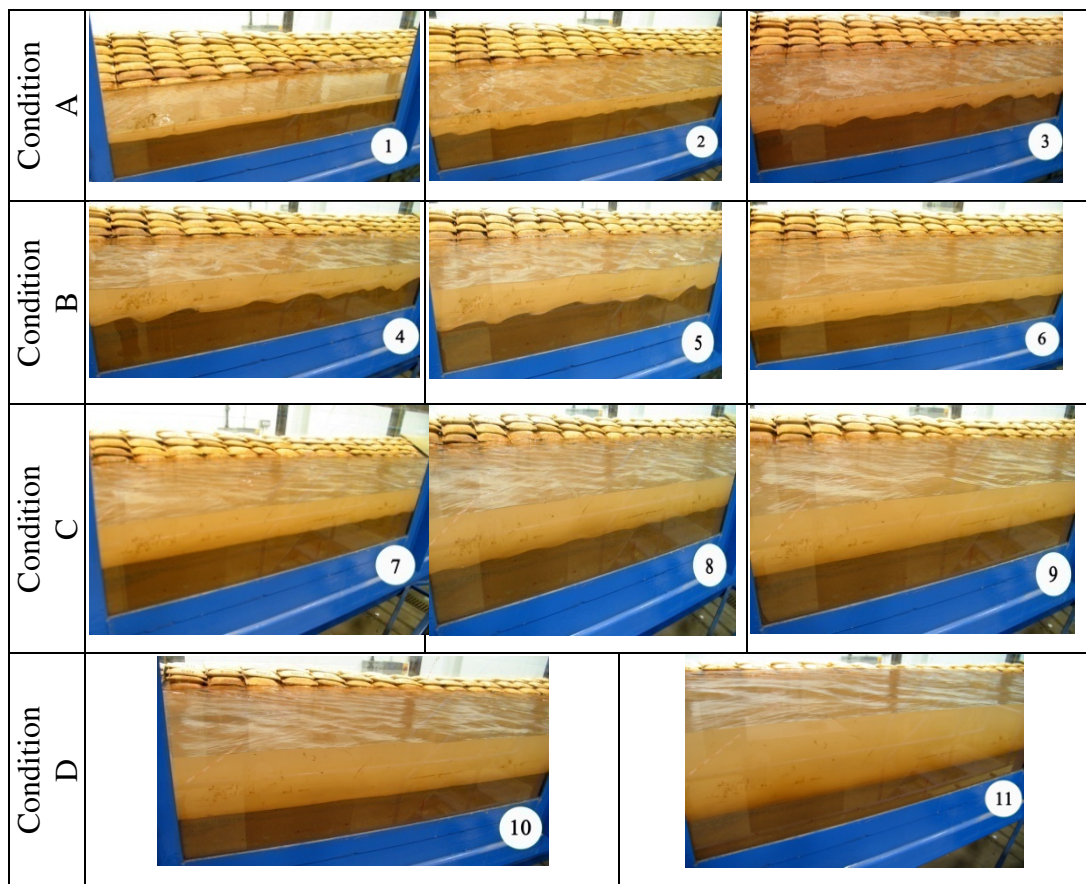


Figure 2.13: Bed formation under different water level and model run time

Table 2.3: Summary of bed formation and associate failure modes in geobag revetment

Water level condition	Run time (min)	Measured			Calculated ⁵			⁶ Change in Bed (visually classified)	Failure mode in geobag revetment
		Above flume bed		Flow (m ³ /s)	Velocity (m/s)	Froude No.	Reynolds No.		
		Mean bed level (m)	Mean Water level (m)						
A [Fig 2.10(1-3)]	10	0.10	0.12	0.0035	0.47	1.05	9296	^{a,c} Primary ripple	Pressure difference and sliding
	30	0.10	0.14	0.0076	0.51	0.81	20186	^a Ripples form	
	40	0.10	0.16	0.0095	0.42	0.55	25232	^a Ripple- ^b dune transition	
B [Fig 2.10(4-6)]	50	0.10	0.170	0.0115	0.44	0.53	30544	^a Dune	Uplifting, sliding and pressure difference
	60	0.10	0.178	0.0147	0.50	0.57	39044	^a Dune	
	70	0.10	0.180	0.0186	0.62	0.70	49402	^a Dune	
C [Fig 2.10(7-9)]	80	0.10	0.185	0.0217	0.68	0.75	57636	^c Transition flat bed	Pressure difference, uplifting, sliding and /or pullout
	90	0.10	0.20	0.0257	0.69	0.69	68260	^a Dune	
	100	0.10	0.21	0.0315	0.76	0.74	83665	^c Transition flat bed	
D [Fig 2.10 (10 -11)]	110	0.09	0.22	0.0382	0.78	0.69	101461	^c Transition flat bed	Pressure difference, uplifting, sliding and /or pullout
	120	0.08	0.26	0.0712	1.05	0.79	189110	^c Transition flat bed	

⁵ Velocity = Measured flow/(Measured water level × Measured average water surface width)
Froude number and Reynolds number calculations were carried out following the similar practice as done in Table 2.2.

⁶ Classified by visual comparison with the available literatures, those are (a) 25 different bed form topography shapes by Friedrich *et al.* (2006) , (b) Bennett and Best (1996), (c) Mantz (1992).

Chapter 2: Physical Model Study

Based on experimental data by Vanoni and Brooks (1957), Raudkivi (1998) has classified the bed formations in terms of shear stress, friction factor and the flow velocity (Figure 2.14). To verify the bed classification presented in Table 2.3, using measure flow and water level the Conveyance Estimation System (CES) is employed to predict the velocity, shear stress and friction factor (described in Chapter 3).

Using *Image J* on the bed changes photos of an interval of 0.50 m, the eroded and deposited area was analysed (Figure 2.15, Table 2.4). The difference in depth measurements at an interval of 0.10 m showed a similar outcome (Figure 2.16). The deposition rate eventually decreases with higher water level condition (Figure 2.16).

The key observations from bed formation observation can be summarized:

- Ending of the condition A and the starting of condition B showed the sand wavelets were on an average of 0.11 m long and in the range of 0.03 m to 0.27 m. The appearance of ripples are described by Mantz (1978) and Baas (1999) with respect to bed material size, their findings showed the ripple length can be in a range of 0.015 m to 0.15 m for the bed material size ($= d_{50}$) of 0.015 mm to 0.238 mm (Mantz, 1978; Baas, 1999);
- In a ripple bed the average deposited area is about twice the area of that under a dune bed. A similar conclusion can be drawn from dune to transition bed;
- The maximum deposited and eroded area observed are over 25% and 30% of the total area respectively;
- The bed depth changes range within the observation section in different conditions, were:
 - Condition A: Mean erosion depth 0.023 m and deposition depth 0.025 m;
 - Condition B: Mean erosion depth became around twice of the ripple condition i.e. 0.05 m and deposition 0.02 m;

Chapter 2: Physical Model Study

- Condition C: Mean deposition depth lowered to about half of the condition B, i.e., 0.013 m and the maximum erosion became 0.09 m; and
- Condition D: Mean deposition depth found as 0.008 m and the maximum eroded depth was 0.093 m.

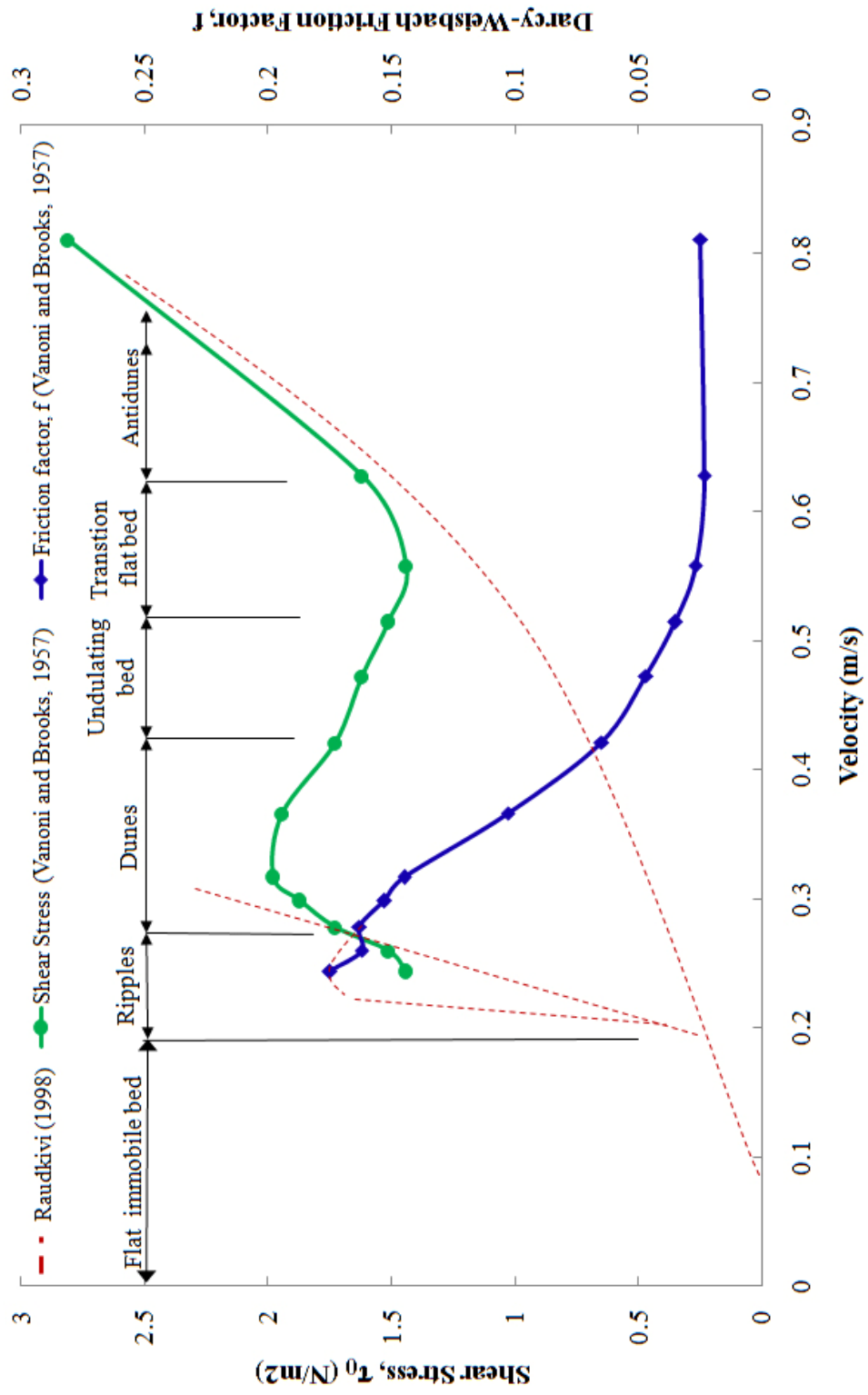


Figure 2.14: Classification of bed forms (based on Figure 6.3 of Raudkivi, 1998)



Figure 2.15: (a) Outline of bed changes after experiment, (b) and (c) Changing bed analysis

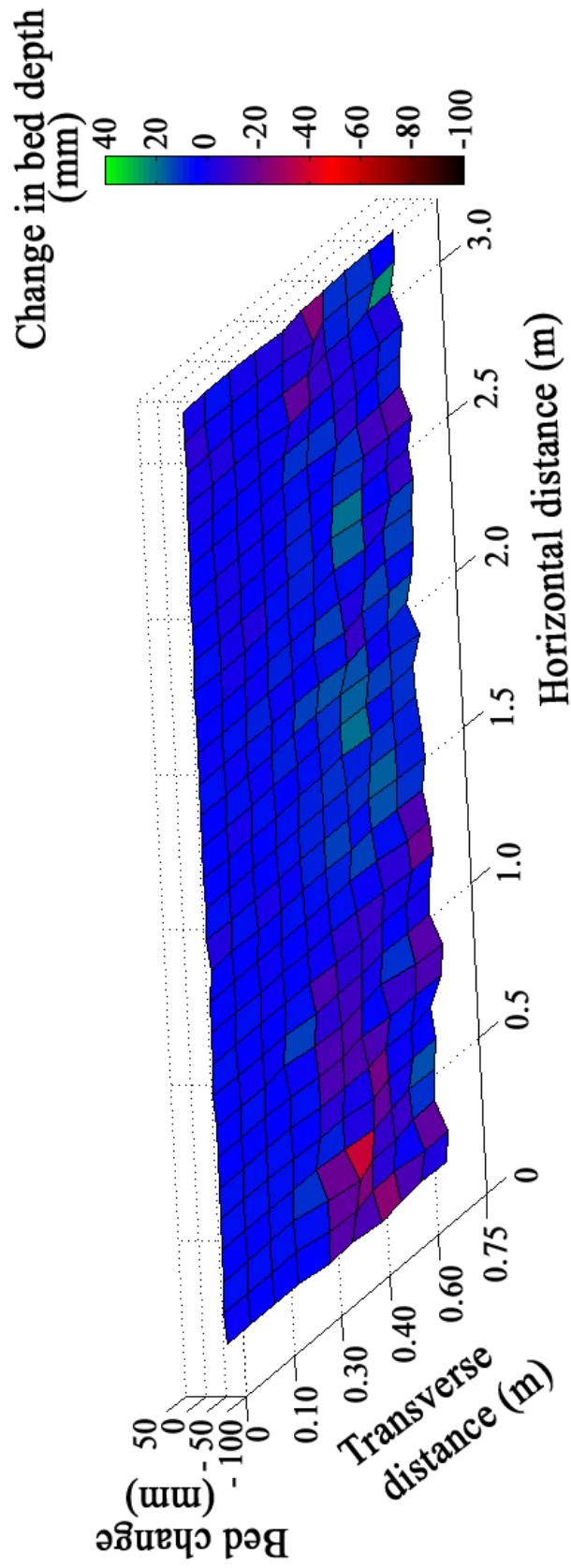
Table 2.4: Summary of the bed changes in terms of total area (streamwise direction)

Condition	Deposited and eroded area (in % of the total area)											
	0–0.5(m)		0.5–1(m)		1–1.5(m)		1.5–2(m)		2–2.5(m)		2.5–3(m)	
	⁷ Dep	⁸ Ero	Dep	Ero	Dep	Ero	Dep	Ero	Dep	Ero	Dep	Ero
A	23	26	21	27	22	11	22	23	25	18	25	30
B	11	18	12	14	18	19	21	17	10	13	11	12
C	4	22	7	14	4	8	11	24	5	28	4	12
⁹ D	1	–	5	–	2	–	1	–	2	–	1	–

⁷ Dep = Deposition

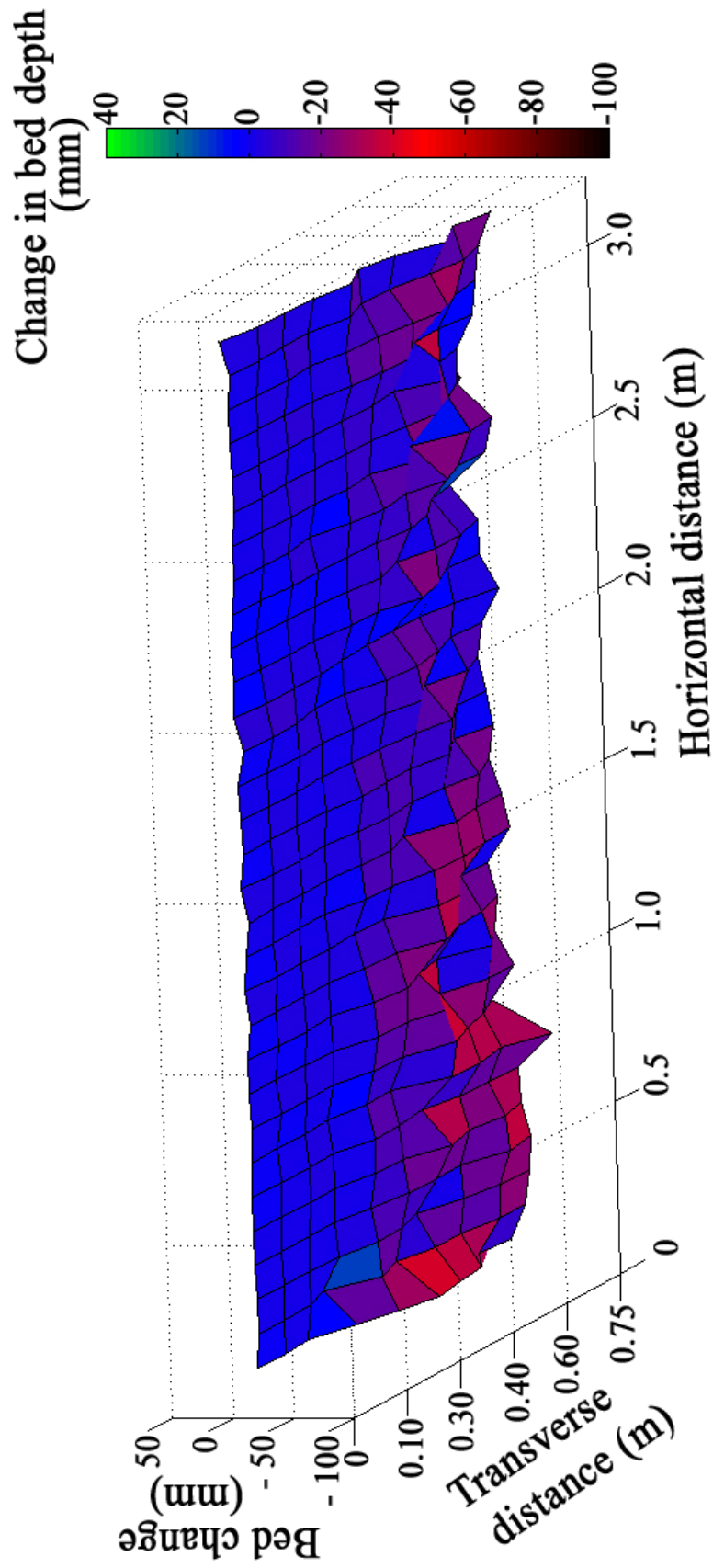
⁸ Ero = Erosion

⁹ In condition D, the final bed formation appeared almost flat due to heavy erosion in observation section except few waves, so the noticeable deposition was not observed.



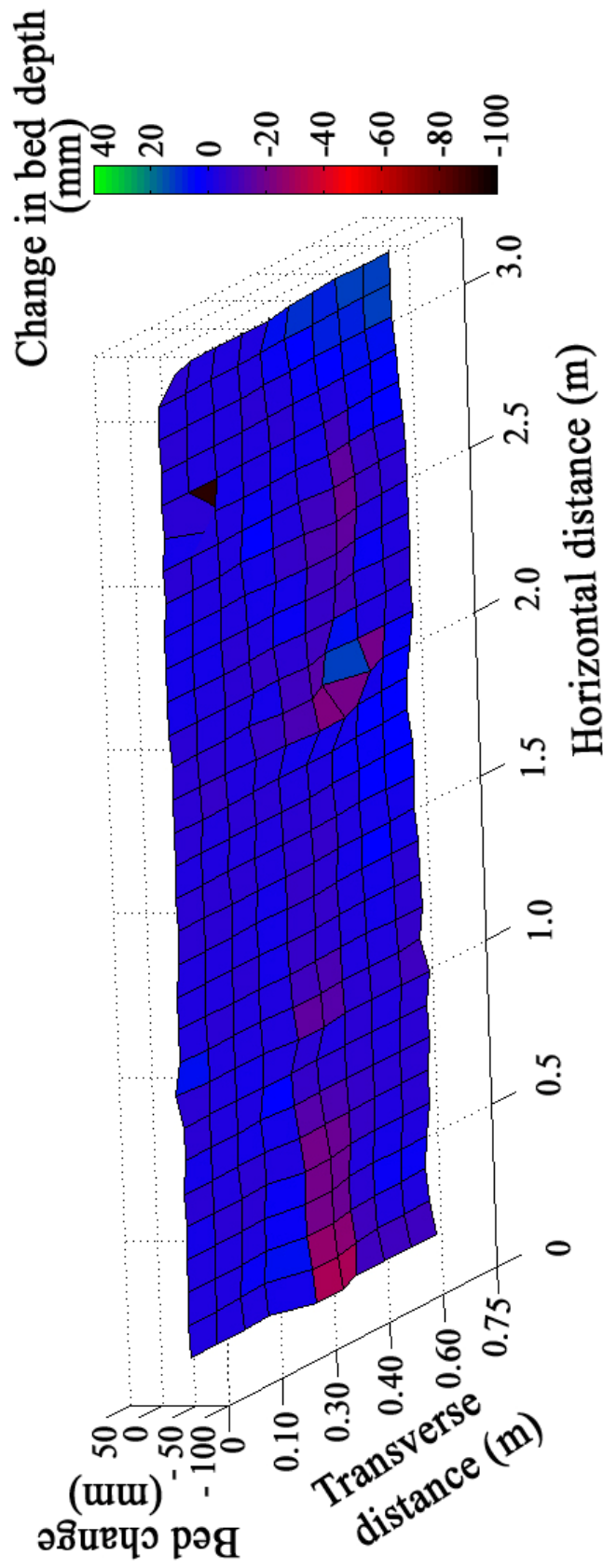
(a) Condition A i.e., water level equal to up to 49% of the geobag revetment height

Figure 2.16 (a to d): Changing bed under four different conditions (cont'd)



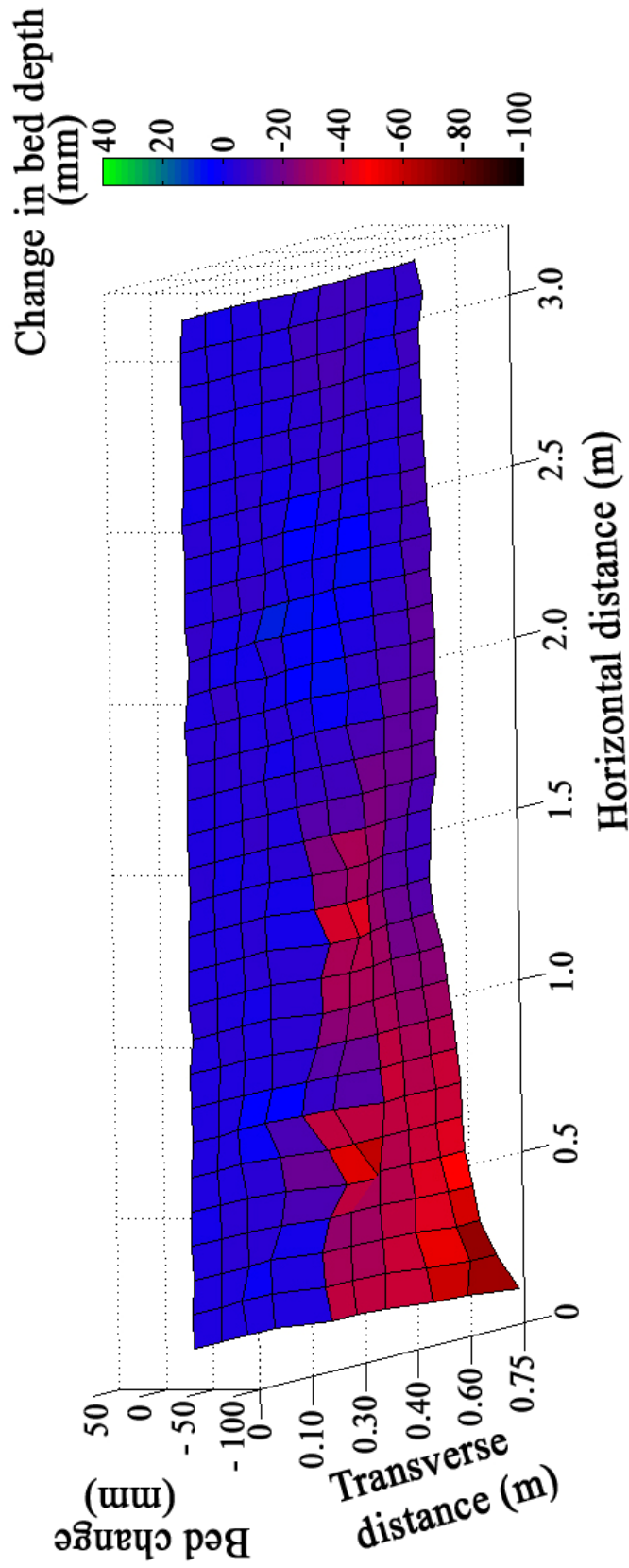
(b) Condition B i.e., water level equal to 50 to 64% of the geobag revetment height

Figure 2.16 (a to d): Changing bed under four different conditions (cont'd)



(c) Condition C i.e., water level equal to 65% to 84% of the geobag revetment height

Figure 2.16 (a to d): Changing bed under four different conditions (cont'd)



(d) Condition D i.e., water level equal to 85% to 100% of the geobag revetment height

Figure 2.16 (a to d): Changing bed under four different conditions

2.5 Analysis of quasi-physical model result

This Chapter deals with three major interactions i.e. friction and hydrodynamic forces and changes in the mobile sediment bed underneath the geobag revetment; those are affecting the geobag revetment performance.

Section 2.2 introduced a simple dry test to illustrate the bag wetness state effect on geobag-geobag sliding initiation. The bag displacement in Figure 2.2 gives an initial idea on failure pattern due to revetment toe scour.

Then in Section 2.3 the failure initiation in the geobag revetment is elaborated on with respect to the hydrodynamic forces. In supercritical turbulent flow the initiation of bag displacement is observed, in all 3 different studied geobag bonds it was within 1.1 to 1.3 m/s, relevant to the prototype velocity of 3.5 to 4 m/s is very close to the *nhc* (2006) findings. The physical state of geobag i.e., bag aging influences on the bag displacement initiation and the settling distance.

Section 2.4 considered the mobile bed along with the hydrodynamic forces. Nominal displacements were recorded under ripple and dune bed formation. Displacement resulted geobag travel away from the test section in transition flat bed. As the bed formation classification is done in this section based on visual comparison with the available literatures, it is expected the classification following Raudkivi (1998) would provide more reliable classification, so CES is employed to predict the required values stated in Chapter 3.

To replicate the failure modes in geobag revetment, details on the observed failures in all these three sections are recorded to validate the application of the commercial Discrete Element Model (DEM) code to be described in Chapter 4.

Chapter 3

Analytical Approach

As quasi-physical model results are influenced by experimental limitations (e.g. scale effects and coverage of frequent velocity measurements), additional analytical approaches are required to determine the hydraulic loading on each individual geobag in a revetment. The specific aim of this chapter is to estimate the shear stress causing incipient failures among the bags in the revetment using analytical approaches.

The first part of the chapter uses the Conveyance Estimation System (CES) to replicate the ADV measured depth average velocity and the validated CES is then applied to estimate the shear stress causing bag incipient motion. The Chow (1959) method was also used for shear stress calculation in this chapter to compare its performance with the CES.

The second part briefly presents the validated CES application in both of the fixed and mobile bed context. This part estimates the hydrodynamic forces on the revetment while the revetment is mounted on a mobile sandbed. In the quasi-physical model, the different bed formations were visually classified. To verify this classification the validated CES was employed, to estimate bed shear stress, water velocity and Darcy Weishbach friction factor 'f' (plotted on Figure 3.5).

The third part deals with the application of the validated CES to predict higher resolution data to prepare a mapped water velocity field for coupling with the DEM described in Chapter 4.

3.1 Active shear stresses on geobag

An attempt has made to extend the quasi-physical model measurements by means of analytical prediction as it is not practical to measure fluid (flowing water) shear stress on the geobag. The purpose of this approach is to use the ADV measured depth-average velocity to estimate the applied fluid shear stress on the geobags in the revetment.

For this study, the shear stresses on the geobag revetments were evaluated using two different methods:

- Conveyance Estimation System (CES) through calibration of the depth average velocities using the measured data, and
- Chow (1959) method based on the membrane analogy for determining the distribution of shear stresses.

3.1.1 Conveyance Estimation System (CES)

As the assumptions underpinning traditional conveyance methods, such as those employing Manning's equation, are not strictly valid (McGahey and Samuels, 2004), and do not yield depth averaged data, the Conveyance Estimation System (CES) was used to calculate the variation in velocity and shear stress with water depth. Based on the depth-integrated Reynolds Averaged Navier Stokes (RANS) equations and the original Shiono-Knight Method (SKM), the CES can estimate the flow in the streamwise direction and laterally across the channel section (Shiono and Knight, 1989; DEFRA/EA, 2003).

Chapter 3: Analytical Approach

$$ghS_o - \frac{f\beta^*q^2}{8h^2} + \frac{\partial}{\partial y} \left[\lambda h \left(\frac{f}{8} \right)^{1/2} q \frac{\partial}{\partial y} \left(\frac{q}{h} \right) \right] = \frac{(1.015 - \sigma^*)}{0.015} \Gamma + \frac{(\sigma^* - 1.0)}{0.015} C_{uv} \frac{\partial}{\partial y} \left[\frac{q^2}{h} \right] \quad 3.1$$

I

II

III

IV

$$ghS_o - \frac{f\beta^*q^2}{8h^2} + \frac{\partial}{\partial y} \left[\lambda h \left(\frac{f}{8} \right)^{1/2} q \frac{\partial}{\partial y} \left(\frac{q}{h} \right) \right] = C_{uv} \frac{\partial}{\partial y} \left[\frac{q^2}{h} \right] \quad 3.2$$

Where:

g	gravitational acceleration (9.807 m/s ²)
q	streamwise unit flow rate (m ² /s)
h	local depth normal to the channel bed (m)
S_o	reach-averaged longitudinal bed slope
y	lateral distance across the channel (m)
β^*	coefficient to account for influence of local bed slope on the bed shear stress
σ^*	reach-averaged sinuosity
f	local friction factor
λ	dimensionless eddy viscosity
Γ	secondary flow parameter – straight channels
C_{uv}	meandering coefficient

Equation 3.1 is applicable for a sinuosity σ of 1.0 for inbank flow and $1.0 \leq \sigma \leq 1.015$ for overbank flow. Equation 3.2 is applicable for a sinuosity greater than 1.0 and greater than 1.015 for inbank and overbank flow respectively. The terms in Equation 3.1 and 3.2 represent:

- I) An approximation to the variation in hydrostatic pressure along the reach ($S_f - S_o$);
- II) energy losses due to boundary friction effects;
- III) turbulence losses due to shearing between the lateral layers; and
- IV) turbulence losses due to secondary currents.

Chapter 3: Analytical Approach

For a known water level, output from the CES includes: (i) in the streamwise direction (for each cross-section): total flow, area, conveyance, average velocity, Reynolds number, Froude number, kinetic energy correction coefficient (α) and momentum correction coefficient (β); and (ii) laterally across the channel section : the distribution of unit flow, unit conveyance, depth average velocity, bed shear stress, shear velocity, Froude number, Darcy–Weisbach friction factor and unit roughness across the cross-section (DEFRA/EA, 2003; McGahey and Samuels, 2004).

In the experimental work reported herein, the closest actual ADV velocity measurements to the geobag revetment were at the centreline of the flume; consequently, the velocity at each geobag was unknown. The CES was therefore calibrated to reproduce the measured centreline depth averaged velocities and then used to predict the streamwise velocity over the geobags in the revetment (Table 3.1); the section was treated as a half-trapezoidal section which is an accurate reflection of the experimental setup (Figure 3.1, section BB).

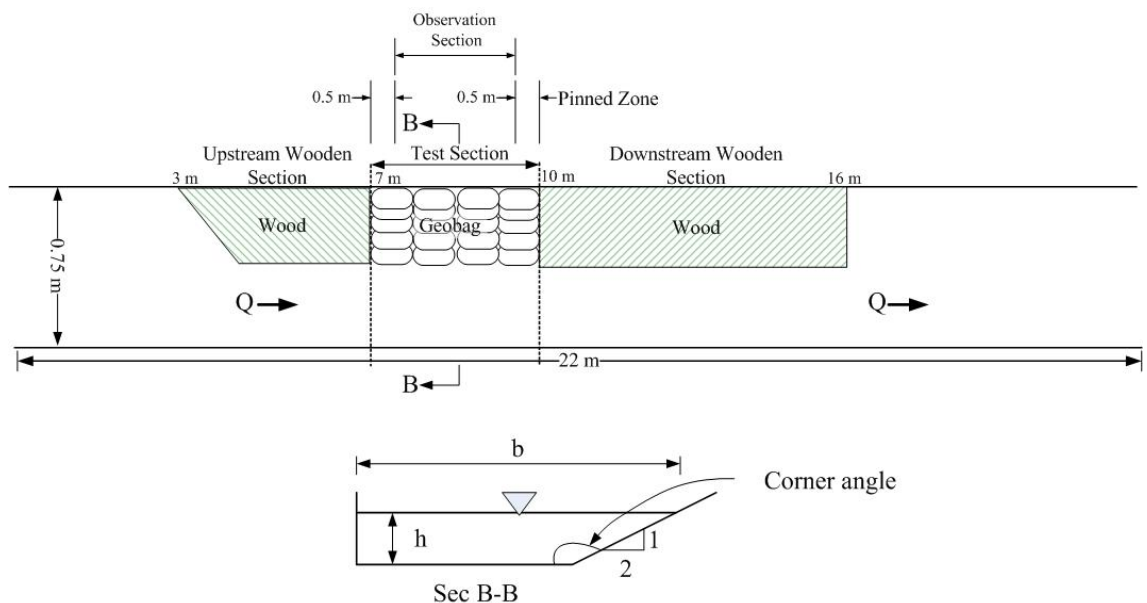


Figure 3.1: Geobag revetment section in experimental setup

3.1.2 Chow (1959) method

It was assumed that the shear force on the geobag slope is similar to the drag force distribution on the slope of a trapezoidal channel. Several researchers have attempted to determine this distribution using a membrane analogy with analytical approaches and finite difference methods for different channel shapes (Leighly, 1932; Olsen and Florey, 1952; Chow, 1959). Based on a membrane analogy study, Chow (1959) provides typical distributions of the drag forces against the width to depth ratio in a trapezoidal channel (Figure 3.2). For this study, stress calculations following the membrane analogy method were conducted using values (i.e., the water depth and channel width ratio as input value to get the relevant distribution fraction of the shear stress) obtained from the chart provided in Chow (1959) and the ADV measured water depth (Table 3.2).

When water flows over the test section in the flume, the active forces can be explained following the force analysis carried out by Chow (1959) on a sediment particle resting on the sloping side of the channel (Figure 3.3 b). Here, two forces are active; the shear or drag force ($a\tau$), and the gravity force component ($W_s \sin\phi$), where: a = effective area of the geobag, τ = shear stress on the side of the channel (i.e. on the slope bags), τ_L = shear stress on the bed, W_s = submerged weight of the geobag (measured) and ϕ = angle of the side slope (26°). The resultant force, R , is the combination of drag and the gravity forces. As the gravity force will be same for both of the CES and the Chow (1959) method, in this study to evaluate the CES prediction over to the Chow (1959) method, only the shear stress was taken into consideration.

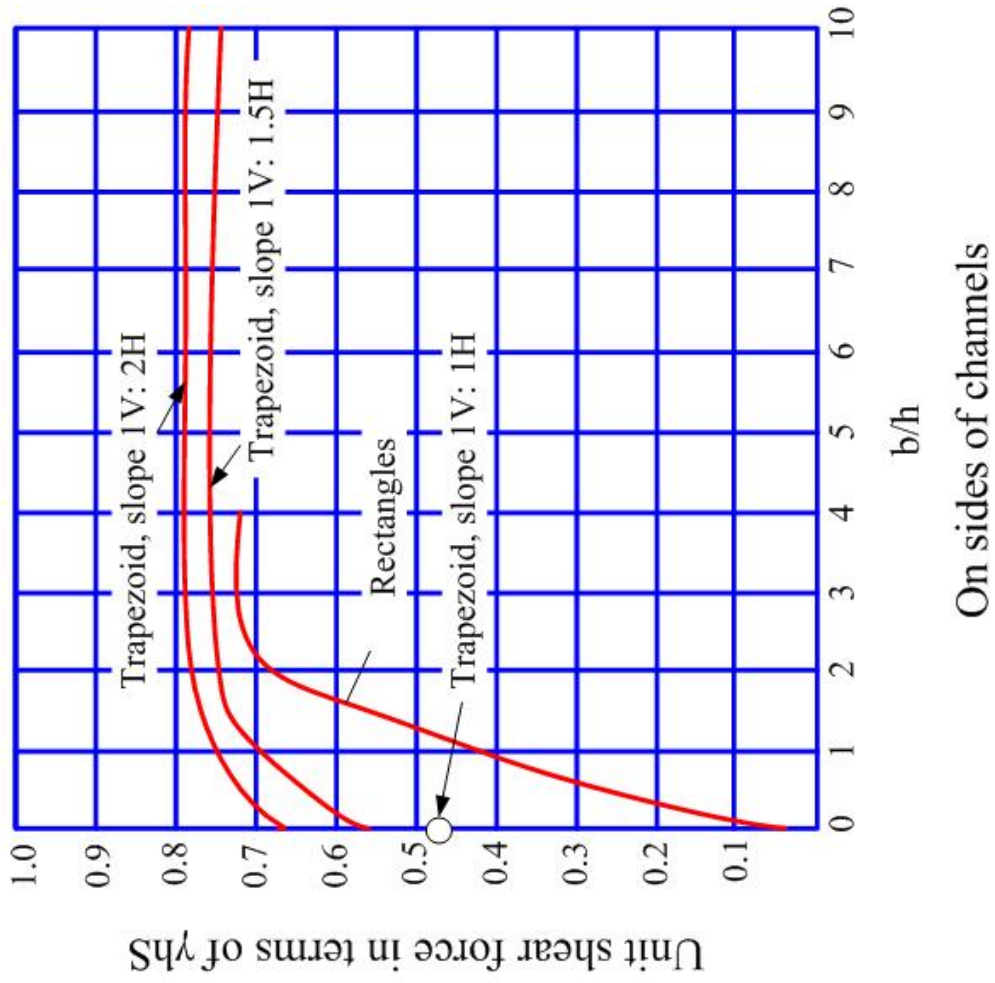
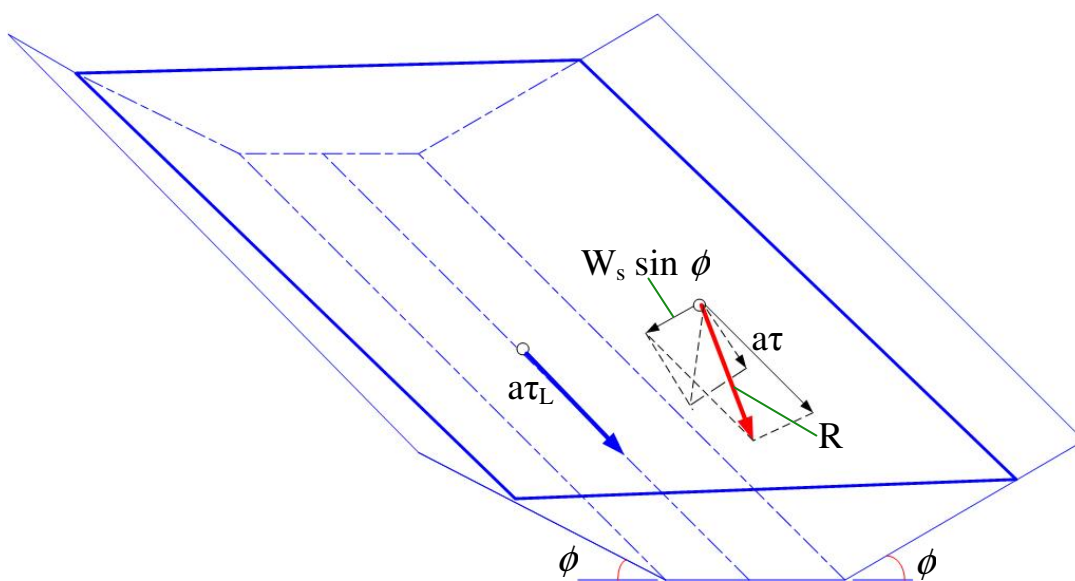


Figure 3.2: Shear force in terms of $\gamma h S$ (based on Chow, 1959)



(a) Force causing geobag movement



$$R = \sqrt{W_s^2 \sin^2 \phi + a^2 \tau^2}$$

(b) Sediment particle resting on the surface of a trapezoidal channel (Chow, 1959)

Figure 3.3: Active forces on (a) washed away geobag, and (b) sediment particle on trapezoidal channel surface

Zarrati *et al.* (2008) derived semianalytical equations for compound open channels based on Chow's chart (1959), and compared this with the analytical data by Shiono and Knight (1991) and the experimental data by Tominaga *et al.* (1989). With three different corner angles (i.e., 120°, 136° and 148°) Zarrati *et al.* (2008) observed their prediction of wall shear stress distribution within a trapezoidal channel underestimates these two dataset as the increment of the corner angle the intensity of the secondary flow increases near the free surface and decreases near the corners (Tominaga *et al.* 1989).

3.2 Results

3.2.1 Conveyance Estimation System

To obtain a reasonable correlation between the experimentally measured and CES predicted velocities, measured flow and water depth data were used to calibrate roughness values for the test section, incorporating the geobag revetment. The unit roughness values were calibrated using data from condition D and validated using the other three condition datasets (coated iron flume bed 0.01, geobags 0.02, and glass flume walls 0.009) (Figure 3.4 a, b, c, d). These acquired values for iron and glass are acceptable as they are within the range of suggested Manning's roughness values of 0.010 to 0.014 (for coated iron) and 0.009 to 0.013 (for glass) (Chow, 1959). The overall mean percentage difference (Λ) and standard deviation (σ) between the experimental data and the CES predicted data indicate that the CES performed better at higher water depths (Table 3.1).

Table 3.1: Summary of the CES prediction against experimental measured value

Number	Water level condition	Water Level		Flow		¹⁰ Velocity	
		Mean Λ (%)	Std Dev σ	Mean Λ (%)	Std Dev σ	Mean Λ (%)	Std Dev σ
1	A	23.79	0.24	0.41	1.48 e-5	20.46	0.09
2		19.61	0.33	0.41	3.05e-5	20.58	0.10
3		14.80	0.38	0.36	4.53e-5	14.14	0.08
4	B	8.32	0.30	3.46	6.50e-3	10.63	0.07
5	C	4.84	0.26	3.52	8.26e-4	6.88	0.05
6		3.68	0.29	0.20	1.71 e-4	2.38	0.04
7	D	0.65	0.33	0.10	4.07 e-5	0.17	0.03

¹⁰ Nearbank depth average velocity

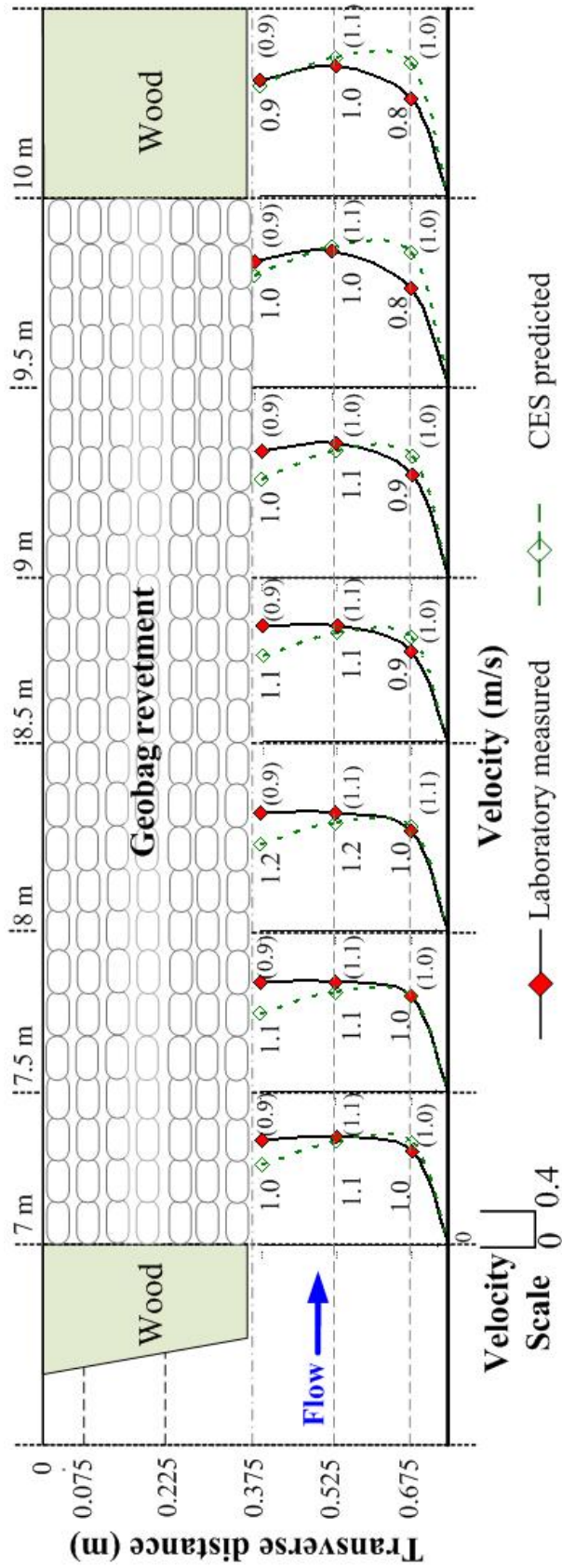


Figure 3.4 (a to d): Comparison of the laboratory measured with CES simulated velocity (Cont'd)

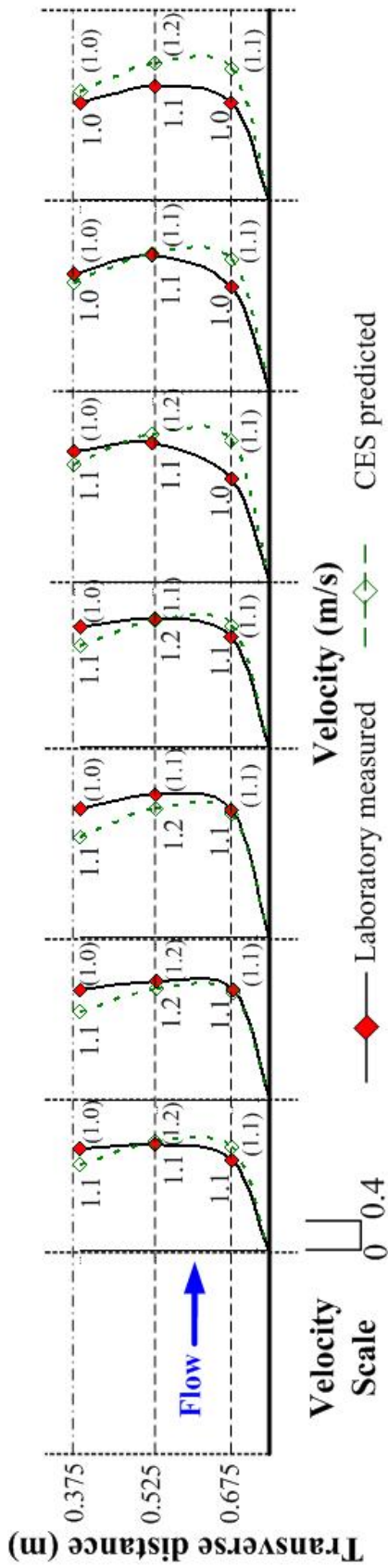


Figure 3.4 (a to d): Comparison of the laboratory measured with CES simulated velocity (Cont'd)

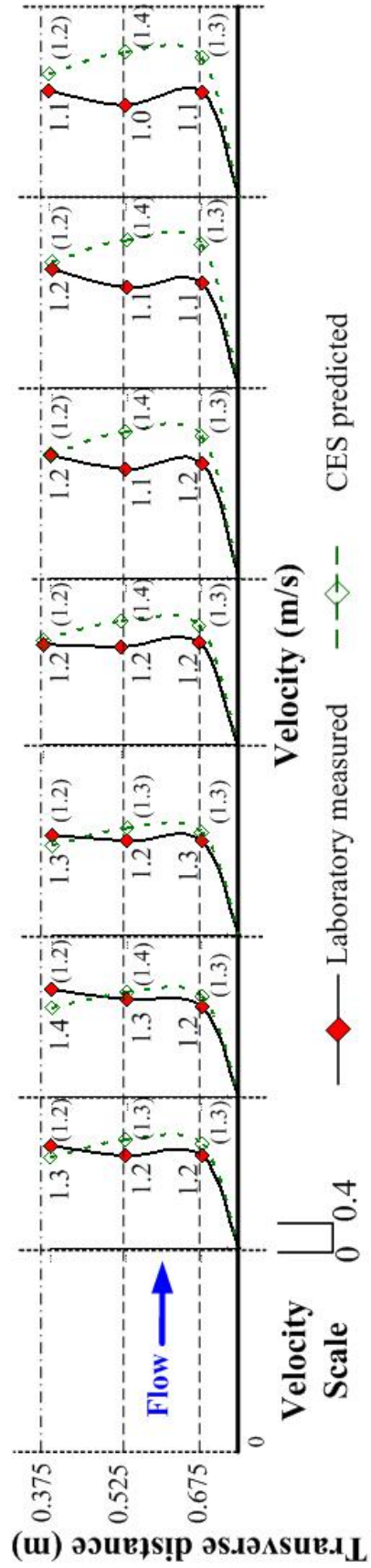


Figure 3.4 (a to d): Comparison of the laboratory measured with CES simulated velocity (Cont'd)

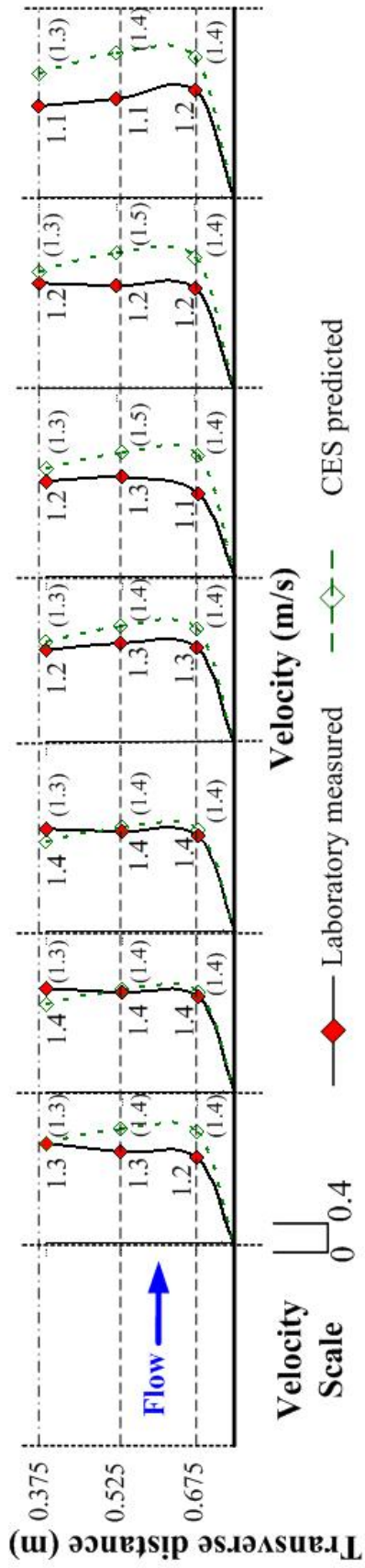


Figure 3.4 (a to d): Comparison of the laboratory measured with CES simulated velocity (Cont'd)

3.2.2 Chow (1959) method

Previous studies showed an interrelation between the corner angle (Figure 3.1) of a channel and the shear stress distribution on the channel's wall, for example, Tominaga *et al.* (1989) and Zarrati *et al.* (2008). In the present study, the corner angle was $154^\circ (= 180^\circ - 26^\circ)$ and the trapezoidal channel wall (i.e. geobag slope) was not uniform (Figure 3.1, Sec B–B). The measured vertical and transverse velocity shows a decreasing trend with respect to increased water depth (Chapter 2). These findings are similar to Tominaga *et al.* (1989), their experimental findings showed:

- (i) secondary flows are strong close to the corner region within a water depth equal to 0.65 h, and
- (ii) there is no effect on the flow mechanism by secondary flow which results in a constant value for the characteristic turbulent flow across the outer region equal to 0.65 h.

The corner angle (the angle between flume bed and geobag revetment slope) in the present study is higher than Zarrati *et al.* (2008) study. Compared to the CES estimation, the Chow (1959) method over predicted the shear stress on the geobag from condition C onwards (more than 65% of the water depth). This can be correlated with the Zarrati *et al.* (2008) study i.e., secondary flows are only significant at depths up to 65% of the revetment depth. This indicates that the CES prediction should be more reliable than the Chow (1959) predictions.

Table 3.2: Comparative shear stress estimation on geobags by Chow (1959) method and CES

¹¹ Condition /Number	Zone	Chow (1959) method (using measured water level)		¹² Shear Stress (N/m ²)	¹² CES Predicted Shear Stress	¹³ Performance statistics for the observed section			
		Based on Figure 3.2				Λ	σ	r	
		b/h	Formula used						
A	1	US	34.98 i.e. > 10	0.785γhS	0.86	0.84	0.00	0.02	0.94
		OS			0.86	0.86			
		DS			1.09	0.93			
	2	US	21.58 i.e. > 10	0.785γhS	1.46	1.63	-12.51	0.09	0.75
		OS			1.42	1.59			
		DS			1.64	1.62			
	3	US	14.25 i.e. > 10	0.785γhS	2.09	2.32	-8.16	0.10	0.66
		OS			2.17	2.34			
		DS			2.54	2.44			
B	4	US	10.61 i.e. > 10	0.785γhS	2.88	2.99	-1.87	0.08	0.84
		OS			2.94	2.98			
		DS			3.29	3.03			
C	5	US	8.51	0.78γhS	3.49	3.49	4.00	0.11	0.92
		OS			3.65	3.49			
		DS			4.08	3.56			
	6	US	7.30	0.78γhS	3.91	3.77	8.74	0.19	0.84
		OS			4.28	3.89			
		DS			4.84	3.99			
D	7	US	6.04	0.77γhS	4.84	4.26	15.35	0.40	0.81
		OS			5.08	4.28			
		DS			5.71	4.38			

¹¹ US= Upstream 0.5 m streamwise geobag section, contains 5 bags/layer;
 OS= Observation (2 m) section, contains 15 bags/layer;
 DS= Downstream 0.5 m pinned streamwise geobag section, contains 5 bags/layer.

¹² The shear stress value represents the mean shear stresses on respective bags in a layer.

¹³ Performance Statistics, Λ = Mean percentage difference; σ = Standard deviation;

r = Coefficient of correlation.

3.3 Summary outcomes of the CES and Chow (1959) method

The calibrated CES predicts the shear stress using a better representation of the underlying physics than Chow (1959) method and is therefore likely to produce more realistic predictions. The findings can be summarized as:

- Although the unit roughness used by the CES is different from the Manning's n value, the unit roughness values for the flume wall and bed seem reasonable, with respect to typical n values. While there are no typical roughness values for geobags for comparison, the obtained 'n' value (0.02) seems lower than would be expected. This is thought to be due to the representation of the geobag revetment slope in the CES setup. In the CES the discrete geobags on the revetment slope were represented by considering a continuous revetment slope, thus the effect of water particles in conjunction with the gaps among bags was absent. However, the CES calibrated values result in good velocity predictions in comparison with ADV measurements (Figure 3.4 a, b, c, d);
- The higher the water depth, the better the velocity representation by the CES for the near bank region, with the best results for a water depth above 85% of the structure height; and
- The comparative study between CES prediction and the use of Chow (1959) chart showed that the first bag to be displaced was subjected to the shear stress of between 2 to 5 N/m^2 , i.e., the prototype shear stress of 63.2 N/m^2 to 158 N/m^2 (calculated using Table 2.1). The range is about 2.5 times more from the minimum to maximum value. This large spread in shear stress is a function of the saturation of the bag and its position in the revetment.

It can be concluded that both methods produce acceptable predictions, although the CES is recommended for further use because of its lower computational time.

3.4 Application of CES

The validated CES has been applied to the fixed bed data to prepare a failure diagram to represent only the water flow – geobag interaction. Then the validated CES is employed to predict depth average velocity of water flow over the mobile sand bed. The bed formations are classified to mimic the Raudkivi (1998) findings. Finally, for which the CES application is meant to be in this study, high resolution data prediction to prepare a mapped water velocity field. Thus CES predicted mapped velocity field works with DEM

3.4.1 Geobag–water flow interaction

A geobag failure diagram is prepared using the CES predicted Froude number of flow and the active shear stress causing incipient bag movement (Figure 3.5). The failure diagram shows, the individual bag movements initiated with flow in a range of Froude number of 1.38 to 1.45, the failures are due to pressure differences between the main flow and void flow (Shear stress, $\tau = 1.32 - 5.17 \text{ N/m}^2$), uplifting ($\tau = 2.81 - 8 \text{ N/m}^2$), pullout ($\tau = 3.8 - 8.068 \text{ N/m}^2$) and overtopping ($\tau = 4.685 - 10.09 \text{ N/m}^2$) (Figure 3.5). The uplifting and pullout often share the same hydraulic properties based on the geobags internal sliding intensity and a similar explanation also can be made for the overtopping.

For practical use of the failure diagram (Figure 3.5), the existing shear stress in y axis should be replaced by “appropriate” non–dimensional parameters (e.g. Shields parameter). Thus the diagram could be presented in order to be of more practical use to engineers and practitioners in conjunction with other factors considerations stated in Chapter 5 (sub–section 5.3.2).

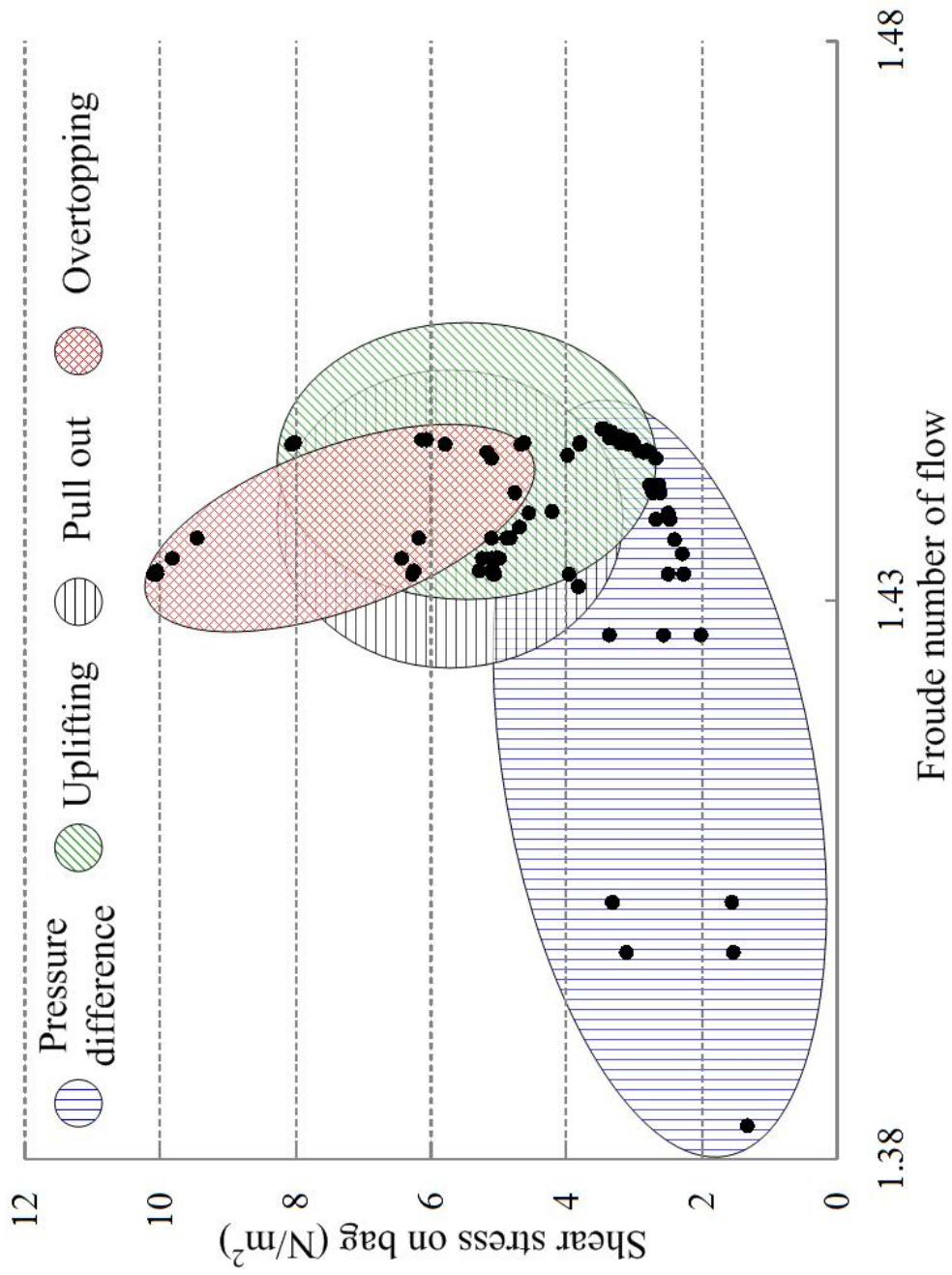


Figure 3.5: Geobag failure diagram due to geobag–flow interaction using CES

3.4.2 Geobag–water flow–mobile sandbed interaction

For a mobile sandbed frequent velocity measurement using ADV is not practical. Using the measured water level and flow data, the validated Conveyance Estimation System (CES) was applied in this study. From the calibration undertaken previously it is shown that the CES can reasonably predict the water level and flow data shown in the rating curve (Figure 3.6).

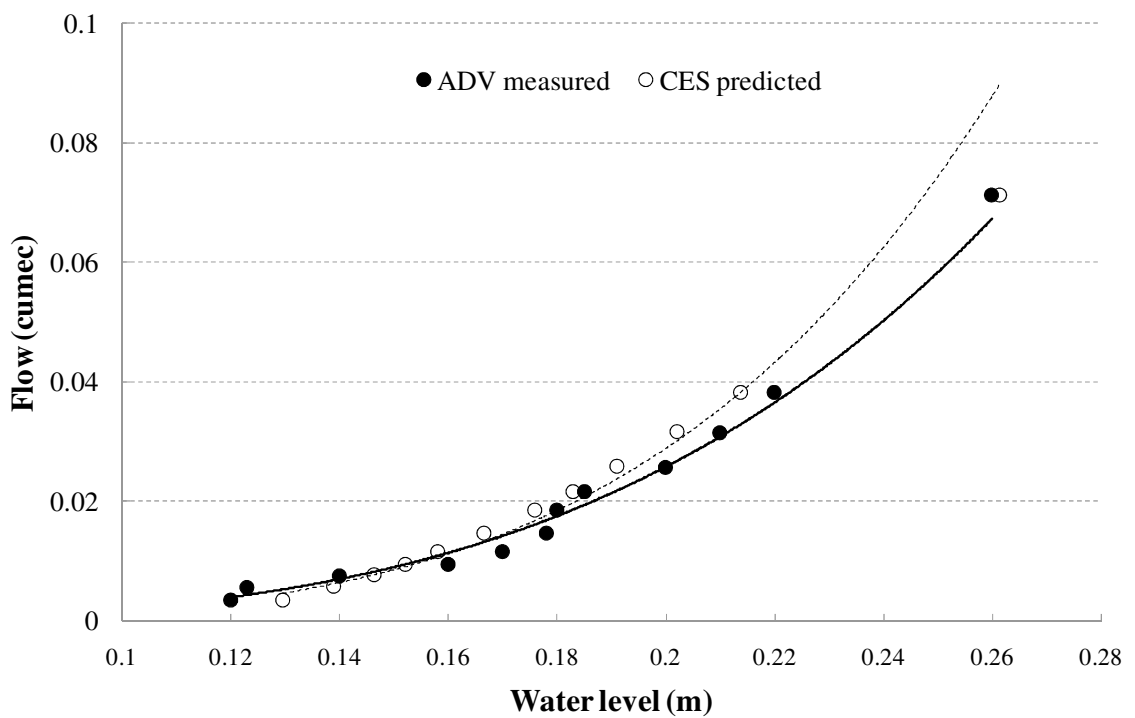


Figure 3.6: Rating curves based on laboratory measure and CES predicted data

Chapter 3: Analytical Approach

The validated CES was employed to predict the depth – average velocity, bed shear stress and friction factor estimation (Table 3.3). The findings are:

- The CES predicted Froude number and Reynolds number confirms the flow in flume was of subcritical – turbulent nature (Table 3.3);
- According to Raudkivi's (1998) classification of sand wavelet, using CES predicted values, dunes started in this study at flow velocity of 0.57 m/s (Figure 3.7). Exactly the same value was also noted for dune initiation by Southard and Boguchwal (1990) i.e., 0.57 m/s. On the other hand, using fine sand bed ($d_{50} = 0.238$ mm) Baas (1999) derived the threshold velocity for dune development as 0.60 m/s. The visual inspection reported in Chapter 2 Section 2.4 (Condition B, Figure 2.16 and Table 2.3) presumed the velocity range for dune were 0.49 m/s to 0.64 m/s (CES predicted velocity values, Table 3.3), showed good agreement with the Raudkivi (1998) classification (Figure 3.7).

Table 3.3:¹⁴ CES predicted hydraulic parameters of flow over mobile bed

Run time (min)	Water level condition	Water Level (m)	Flow (m ³ /s)	Depth-Average Velocity (m/s)	Shear velocity (m/s)	Shear stress (N/m ²)	Froude No.	Reynolds No.
10	A	0.1295	0.0035	0.32	0.020	0.40	0.55	6806
20		0.1390	0.0057	0.39	0.024	0.55	0.61	10647
30		0.1463	0.0077	0.46	0.026	0.69	0.64	13930
40		0.1522	0.0095	0.49	0.028	0.79	0.66	16839
50	B	0.1580	0.0115	0.53	0.030	0.88	0.68	19800
60		0.1665	0.0147	0.59	0.032	1.04	0.70	24348
70		0.1759	0.0186	0.64	0.034	1.17	0.72	29563
80	C	0.1829	0.0217	0.69	0.030	0.92	0.74	33566
90		0.1911	0.0258	0.73	0.032	1.01	0.76	38424
100		0.2021	0.0316	0.79	0.034	1.13	0.77	45079
110	D	0.2137	0.0382	0.84	0.036	1.27	0.79	52279
120		0.2613	0.0712	1.04	0.042	1.80	0.85	82904

¹⁴ Calibrated unit roughness: Flume bed (sand) 0.019, geobag 0.02, flume wall (glass): 0.009

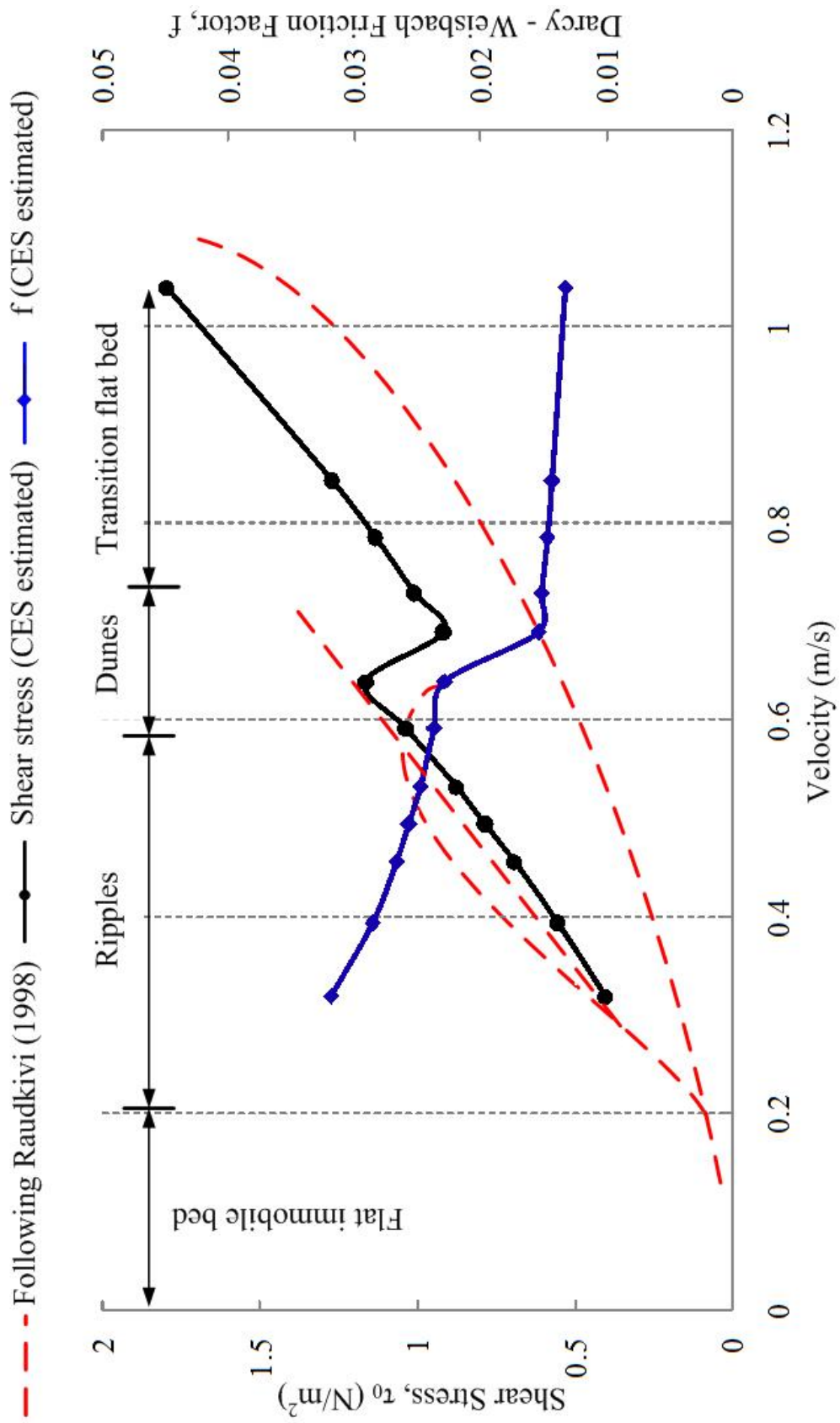


Figure 3.7: Classification of bed formation using CES prediction

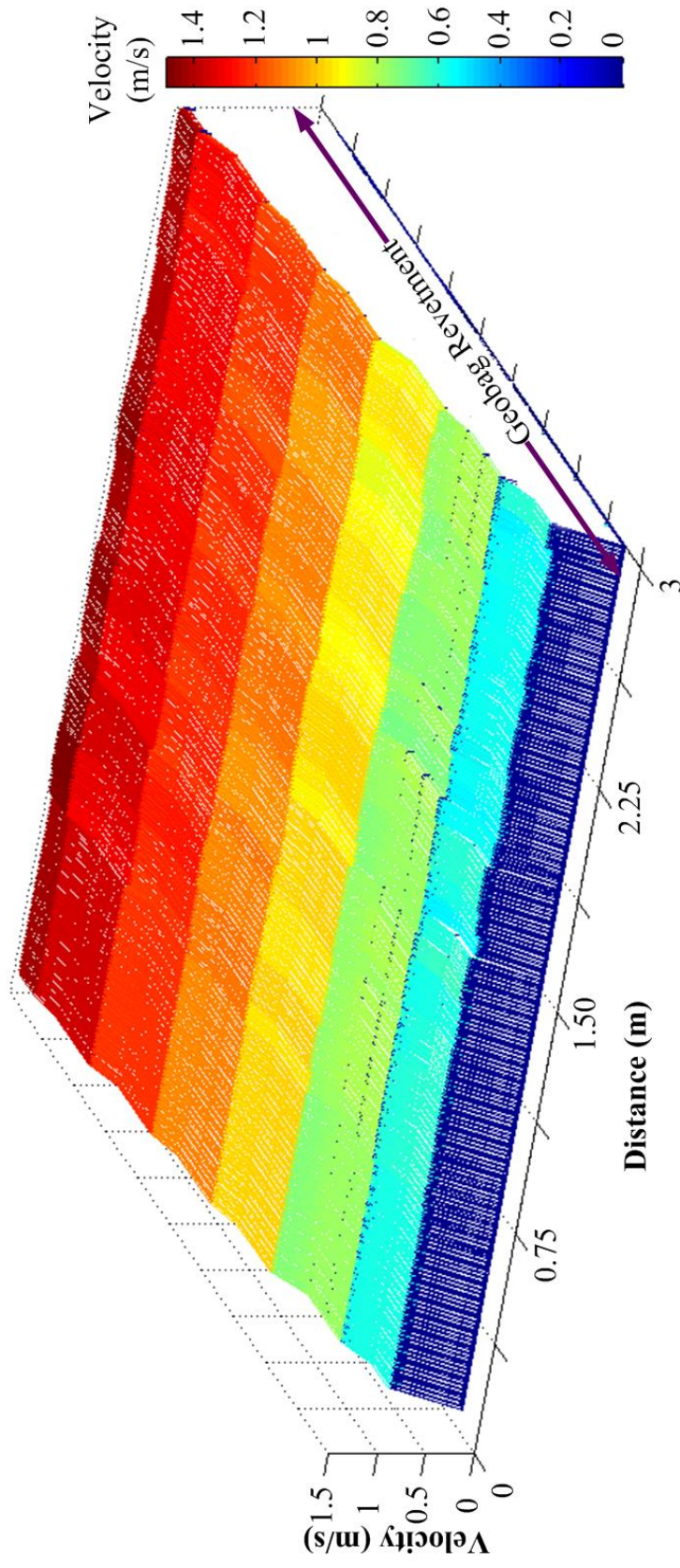


Figure 3.8 : CES predicted high resolution water velocity data on geobag surface

3.4.3 Mapped water velocity field preparation

The measurements made in Chapter 2 for depth average velocity was at an interval of 0.10 m in streamwise direction. In this stage the measured data was extended ten times more frequent, i.e. at an interval on 0.01 m, using the validated CES (Figure 3.8). The details on the application of mapped velocity field are presented in Chapter 4.

3.5 Conclusions

The CES and Chow (1959) method showed good agreement in terms of consistency in predicting shear stresses on the geobags in the revetment. However, both of these two methods are based on a 1D approach; as observations suggest that the failure mechanism in geobag revetments are heavily influenced by pressure differences between the main flow and void flow, a 3D numerical model approach is necessary to adequately simulate local failure mechanisms. In this chapter, the CES results are used to prepare a mapped velocity field for a Discrete Element Model (DEM).

Chapter 4

Numerical Model Study

The quasi-physical model or an 1D analytical approach often fail to fully indentify the complete failure process involved in the geobag revetment. Therefore, an attempt has made in this Chapter to extend the quasi-physical model study by means of numerical simulations. The specific aim of this Chapter is to predict the coefficient of friction, drag and lift forces causing incipient failures among the bags in the revetment.

In first part, the commercial Discrete Element Model (DEM) code EDEM[®] is used to replicate the observed failure modes in Chapter 2 for the geobag – geobag interactions on wooden test rig (Section 2.2) and thereby obtain the coefficient of friction.

The second part of the Chapter uses the DEM model coupled with a water mapped velocity field to reproduce the failures observed in Chapter 2 (Section 2.3) for the geobag – water flow interactions and obtains the coefficient of drag and lift force. Meanwhile, details on the model setup and the mapping of the water velocity field are discussed.

The third part deals with the hydrodynamic forces on the revetment while the revetment is mounted on a mobile sandbed. The coupled model is also used to mimic the observed failures for the geobag – water flow – mobile sandbed interactions in Chapter 2 (Section 2.4).

4.1 General

Mustoe and Miyata (2001) noticed most DEM methods are based on cylindrical or spherical shaped particles, due to the inherent ease in detecting contact between particles in the numerical calculation. In this study it was, necessary to simulate the distinctive shape of the geobag and to implement a three dimensional DEM set up. This was done using the commercial DEM code EDEM[®] (DEMSolutions 2010). This code allows for the creation of non-spherical particles from overlapping spheres of differing sizes. The commercial EDEM[®] model can couple with a three dimensional mapped fluid velocity field (described later in this Chapter).

4.2 Hypothesis

Given variations in precise bag size in the experiment, tolerance limits in their initial placement and ignorance of the bag permeability and state of wetness (as described in Chapter 2), the hypothesis is that the initial response of any layer of geobags in the DEM model would indicate the critical location for bag instability in the revetment.

4.3 EDEM[®] model

Here, a single geobag was represented by using a total of 110 spheres, 66 spheres of 11 mm diameter, 28 spheres of 20 mm and 16 spheres of 28 mm diameter. The spheres were rigidly connected at their point of contact (Figure 4.1 a). Within EDEM[®], the 110 spheres were treated as an individual body, with spatial properties such as its location being indexed to the overall centre of mass. For most post processing, a bag template (based on measured coordinates of the model geobags of 0.103 m × 0.07 m used in laboratory described in Chapter 2) was placed over the individual sphere grouping (Figure 4.1 b). This distinguishes between the bags, but it is important to recognize that the template is not the interaction surface of the particles; it is merely

applied during post-processing to aid in visualizing the individual bags. In fact, the bags can overlap at their edges when the maximum diameter of a sphere protrudes into the ‘valley’ between adjacent spheres. In DEM, the total contact forces of the geobags were summed over each sphere within a geobag. All bags were identical.

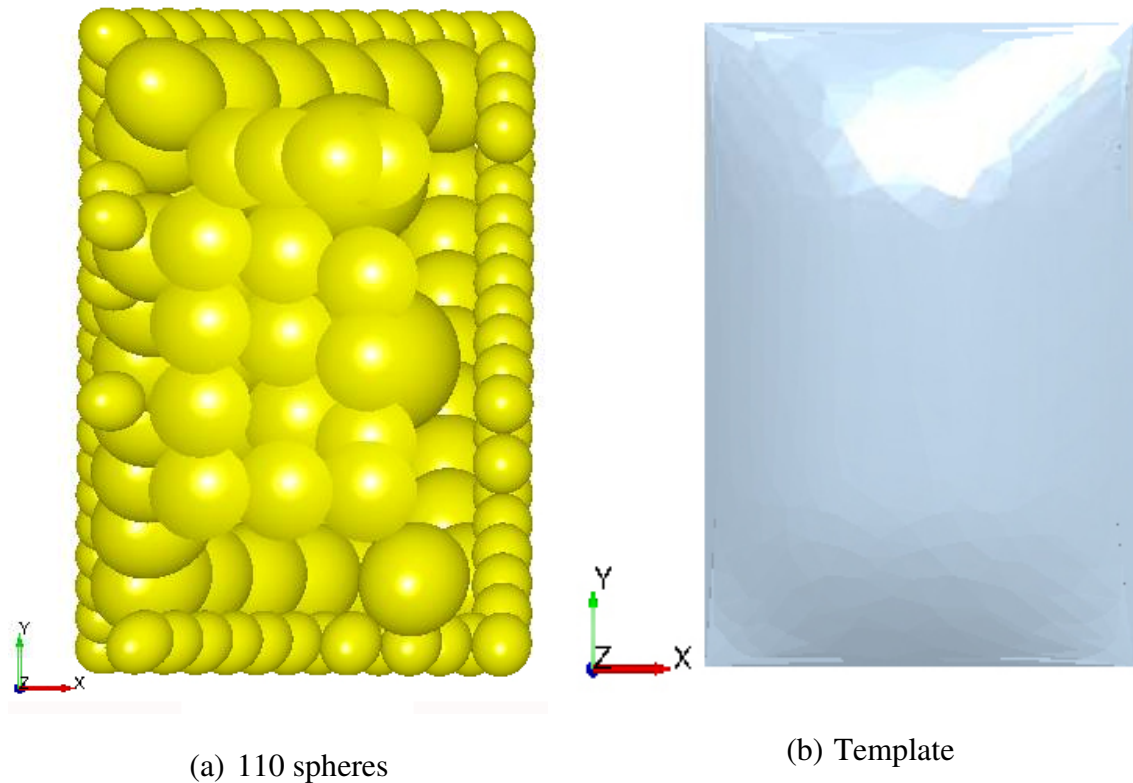


Figure 4.1 (a and b): Laboratory model geobag representation in EDEM

Chapter 4: Numerical Model Study

The default contact model in the EDEM[®] software is the Hertz Mindlin model (Mindlin, 1949), which is regarded as accurate and efficient in force calculation for elastic solids (DEMSolutions, 2010).

The normal force, F_n , is a function of normal overlap δ_n and is given by

$$F_n = \frac{4}{3} E^* \sqrt{R^*} \delta_n^{\frac{3}{2}} \quad 4.1$$

Where the equivalent Young's Modulus E^* , the equivalent radius R^* are defined as:

$$\frac{1}{E^*} = \frac{(1 - \nu_i^2)}{E_i} + \frac{(1 - \nu_j^2)}{E_j} \quad 4.2$$

$$\frac{1}{R^*} = \frac{1}{R_i} + \frac{1}{R_j} \quad 4.3$$

With E_i , ν_i , R_i and E_j , ν_j , R_j being the Young's Modulus, Poisson ratio and radius of each sphere in contact. Additionally there is a damping force, F_n^d , given by

$$F_n^d = -2 \sqrt{\frac{5}{6}} \beta \sqrt{S_n m^* v_n^{rel}} \quad 4.4$$

Where $m^* = \left(1/m_i + 1/m_j\right)^{-1}$ is the equivalent mass, v_n^{rel} is the normal component of the relative velocity and β and S_n (the normal stiffness) are given by

$$\beta = \frac{\ln e}{\sqrt{\ln^2 e + \pi^2}} \quad 4.5$$

$$S_n = 2E^* \sqrt{R^* \delta_n} \quad 4.6$$

With e the coefficient of restitution. The tangential force, F_t , depends on the tangential overlap δ_t and the tangential stiffness S_t .

$$F_t = -S_t \delta_t \quad 4.7$$

With

$$S_t = 8G^* \sqrt{R^* \delta_n} \quad 4.8$$

Here G^* is the equivalent shear modulus. Additionally, tangential damping is given by:

$$F_t^d = -2 \sqrt{\frac{5}{6}} \beta \sqrt{S_t m^*} v_t^{rel} \quad 4.9$$

Where v_t^{rel} is the relative tangential velocity. The tangential force is limited by Coulomb friction $\mu_s F_n$ where μ_s is the coefficient of static friction.

For simulations in which rolling friction is important, this is accounted for by applying a torque to the contacting surfaces.

$$\tau_i = -\mu_r F_n R_i \omega_i \quad 4.10$$

With μ_r the coefficient of rolling friction, R_i the distance of the contact point from the centre of mass and ω_i the unit angular velocity vector of the object at the contact point.

So, this contact model deals with three mechanical properties for each material used in a simulation – the modulus of rigidity, Poisson’s ratio and density, and three particle interaction properties, the coefficient of restitution, Coulomb or static friction coefficient and the coefficient of rolling friction. Recio and Oumeraci (2009b) noted the modulus of rigidity for their geobags as 1.1 GPa. As there are no available standard methods for determining the required mechanical properties of the geobag, some tests were done to get suitable estimates (Table 4.1 and 4.2). The maximum value for the coefficient of rolling friction, unity, was taken to avoid any unrealistic rolling of the simulated geobags. A minimum value of coefficient of restitution (0.0001) was selected to reflect the low ‘bounce’ of the bags.

4.4 Geobag-geobag interaction

4.4.1 Model setup

The EDEM[®] model setup was done by using a similar number of geobags i.e., 120 geobags on a test rig comprise of a mobile and a fixed base (Figure 4.2). The frictional force test model require the input of three mechanical properties for each material used in a simulation and three interaction properties for each pair of materials that may come into contact during a simulation (Table 4.1).

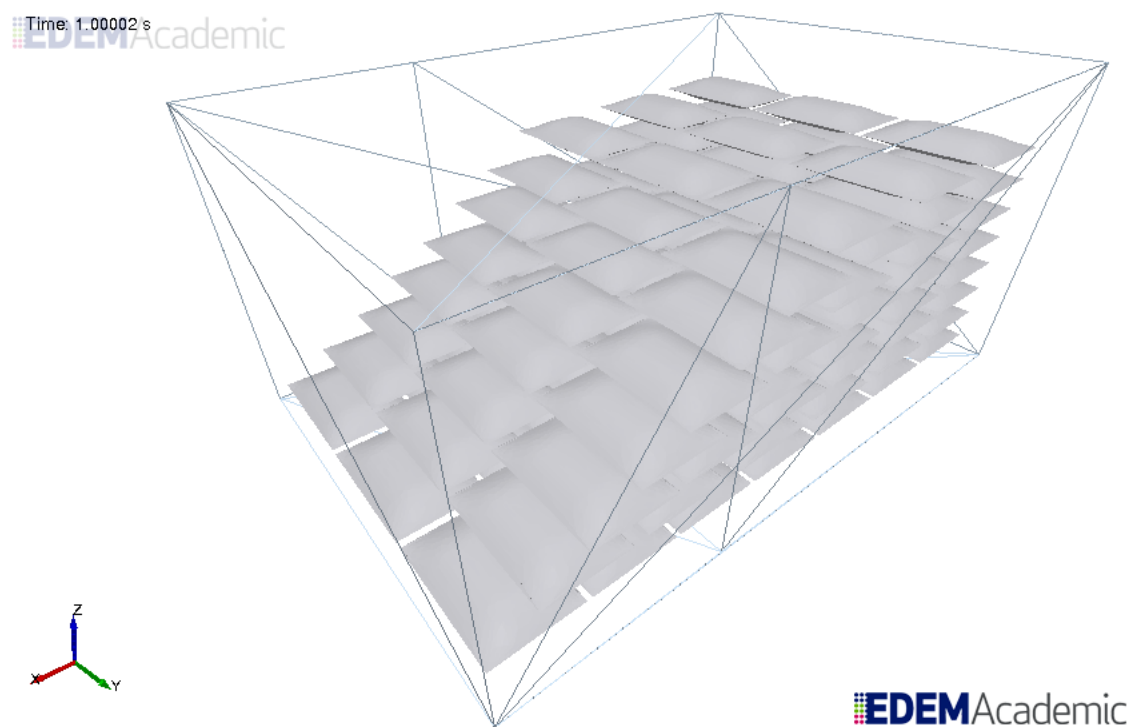


Figure 4.2: Model setup for the dry test on wooden test rig

Table 4.1: Required material and interaction properties for the Geobag Model

Material Properties			Interaction Properties	
Details	Geobag	Wood	Details	Value
Modulus of rigidity (G) (pa)	¹⁵ 1.1×10^6 1.9×10^6	¹⁶ 1×10^{10}	Coefficient of static friction	0.5 – 0.6
Poisson's ratio (ν)	0.42	¹⁷ 0.33	Coefficient of rolling friction	1
Density (ρ) (kg/m^3)	1596	¹⁶ 700	Coefficient of restitution	0.0001

The total simulation time had selected 800 s and the first 200 s allow the bags to fully settle after their introduction to the model domain. The mobile bed was allowed to move in a downward direction at the rate of 0.167 mm/s for rest of the 600 s. the movement of a subgroup of 24 bags (i.e. the surface bags) of 120 bags were visually observed on test rig experiment to determine their displacement through time (Figure 4.3). While bags are on the joint of the two beds namely – the fixed bed and mobile bed, bags have the best opportunity to make contact with each other in response to the local scour. Ideally, all of the bags on test rig would have been tracked, however according to the laboratory observation this was not practical and selection had to be made of the 24 surface bags. Figure 4.3 is based on the modulus of rigidity and the calibrated coefficient of static friction being taken as 1.9×10^6 pa and 0.55 respectively. The coefficient of static friction was obtained as 0.55 from several model runs using EDEM®, and verified with the dry experimental results as described in Chapter 2 (Section 2.2).

¹⁵ Recio and Oumeraci, 2009 b

¹⁶ Abdalla and Sekino, 2006

¹⁷ Ganev *et al.*, 2005

4.4.2 Validation process

Validation by means of a visual comparison has been the most common approach taken for discrete element modelling due to its simplicity (Yang *et al.*, 2006). For this study, visual comparison has made with the laboratory results (Figure 4.3). Details of the simulation can be found in Appendix C.

In this study, a coefficient of friction of 0.55 was found to give the best results; this is close to that published for dry geotextile – sand interaction which gives a coefficient of friction of 0.57 to 0.70 (Garcin *et al.*, 1995; NAUE, 2006; Chapter 1) and to the finding by Yang *et al.* (2008) for geobag – geobag interaction, which was 0.554.

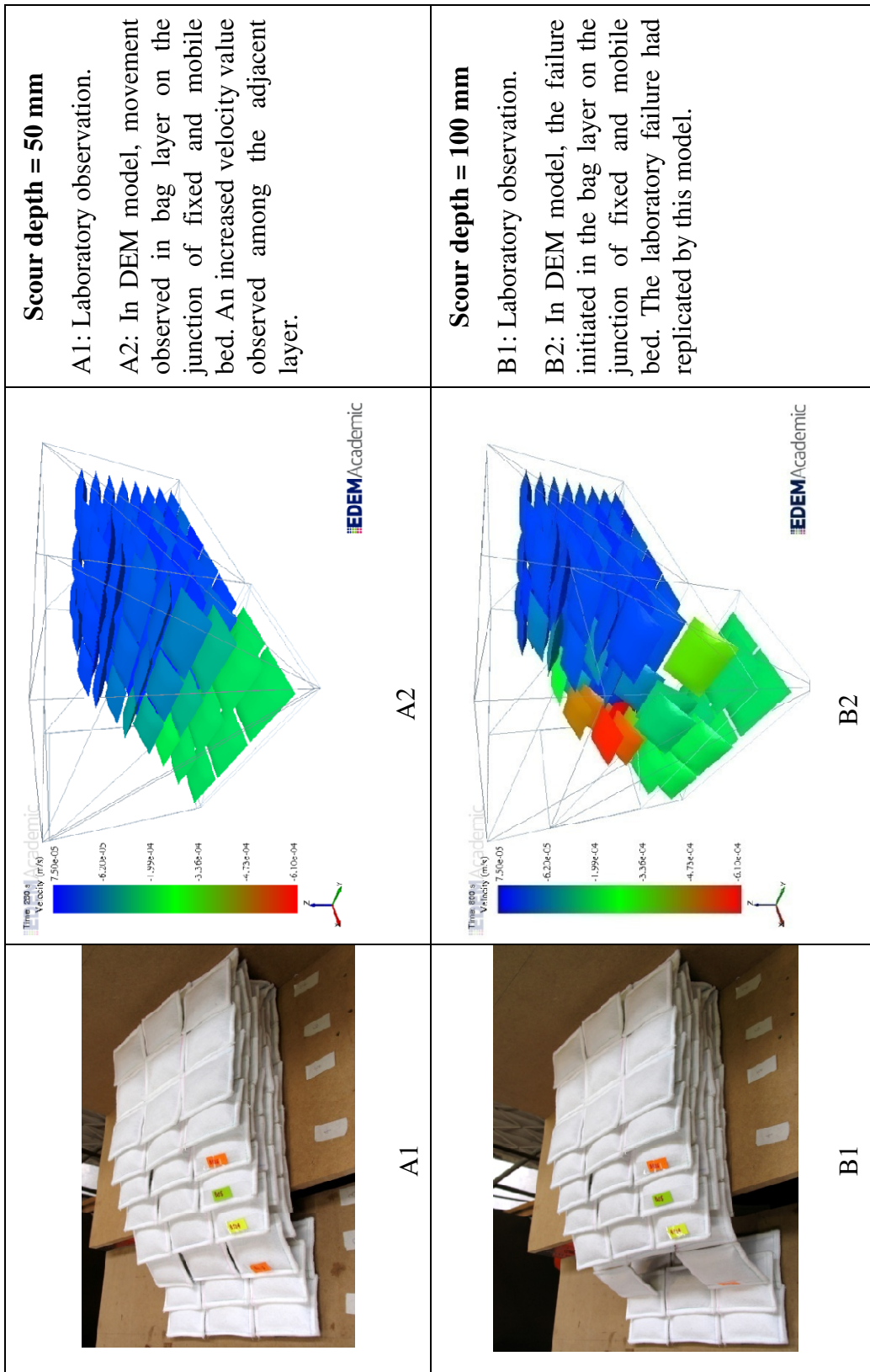


Figure 4.3 (A1 to B2): Comparison between laboratory and EDEM® prediction on test rig

4.5 Geobag – water flow interaction

The geobag – water flow interaction is evaluated using the DEM couple to the Mapped velocity field estimated using the CES.

4.5.1 DEM couple model

In the dynamics of spherical particles in fluid, drag is the dominant force. Lift forces such as Saffman and Magnus forces only become influential when the spheres are in the high-shear region (Yin *et al.* 2003). For non-spherical particles, the lift force is also important at lower shear due to the aspect ratio of the particle shapes. Torque will be exerted on the particles as the centre of pressure on the non-spherical particles shifts, and if there is a non-uniform fluid velocity gradient along the surface of the particles. This will cause the particles to try to rotate, to which geobags may be approximated.

In a uniform flow, for flat plate type particles, there are semi-empirical formulas to calculate the coefficient of moment for the particles with a fixed rotation axis. However, in a non-uniform flow field with high velocity gradients, without using high fidelity models such as immersed boundary methods, it is difficult to determine exactly the position of the centre of pressure and to calculate the total torque acting on the particles. Yin *et al.* (2003) developed a model that tracks the motion of cylinders in fluid. They included various hydrodynamic forces including torque on the cylinders. However, their model is more suitable for a flow-field without high velocity gradients and it is developed specifically for cylindrical type particles.

Models such as immersed boundary methods are computationally intensive. In this study, a new simple model is used that approximates the hydrodynamic forces and torques acting on a non-spherical particle in a non-uniform flow field. The model discretises the particle into sections with equivalent size by simple geometrical calculations. In this case, the geobags are approximated as a number of inter-connected, simple rectangular flat plates. Drag and lift are calculated for each plate based on

Chapter 4: Numerical Model Study

semi-empirical drag models, such as the drag model for non-spherical particles from Hölzer and Sommerfeld (2008) and the lift model from Yin *et al.* (2003). Then, the drag and lift coefficients were set manually by the user in the model to replicate the experimental observation. The buoyancy force is included in the calculations. The drag equation utilised here is written as:

$$F_D = \frac{1}{2} \rho_f C_D A_{\text{sect}} V_{\text{rel}} |V_{\text{rel}}| \quad 4.11$$

Where,

ρ_f = Fluid density

C_D = Drag coefficient

V_{rel} = Relative velocity

A_{sect} = Cross-sectional area, calculated by the diameter of an equivalent sphere of the volume of the discretised section

The lift equation is adopted from Yin *et al.* (2003)

$$F_L = \frac{1}{2} \rho_f C_L A_{\text{sect}} \frac{\vec{z} \cdot V_{\text{rel}}}{|V_{\text{rel}}|} [\vec{z} \times V_{\text{rel}}] \times V_{\text{rel}} \quad 4.12$$

Where,

\vec{z} = the particle major axis direction

The total force is then summed up for all sections. The total torque acting on the particle is calculated by summing up the torque generated by the total of the hydrodynamic forces of each discretised sections with respect to the centre of gravity of the particle as a whole.

The model is implemented in the Application Programmable Interface (API) in EDEM®. The API allows the user to implement custom contact and non-contact type models, such as drag models for DEM modelling.

4.6 DEM model for the geobag – water flow interaction

To replicate the laboratory observations, the EDEM[®] model setup was done for the geobag revetment setup in the flume using the same configuration for revetment build up (as described in Section 2.3) (Figure 4.4). The interaction properties are tabulated in Table 4.2.

With this setup, the simulation was run for first 100 s to allow the bags to fully settle after their introduction to the model domain. Thereafter, the mapped water velocity was applied and used as a basis for calculating the drag and lift forces on the geobags, according to the coupling model described in Section 4.4.1.

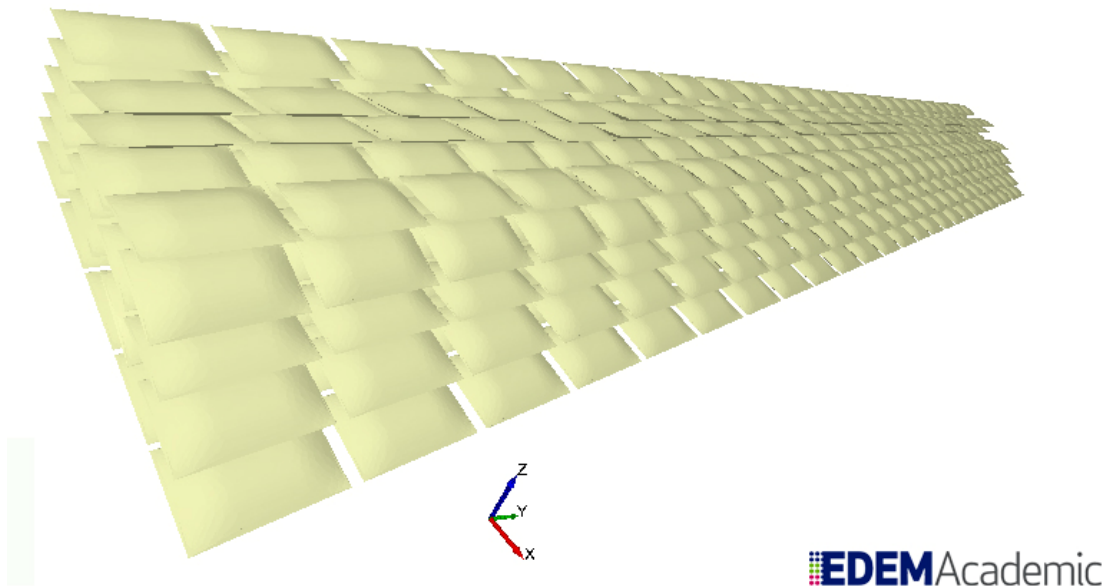


Figure 4.4: Model setup for the geobag revetment in flume

Table 4.2: Required material and interaction properties for the EDEM® geobag revetment model

Material Properties			Interaction Properties	
Details	Geobag	¹⁸ Flume bed	Details	Value
Modulus of rigidity (G) (pa)	¹⁹ 1.9×10 ⁶	8.16×10 ¹⁰	Coefficient of static friction	0.55
Poisson's ratio (ν)	²⁰ 0.42	0.293	Coefficient of rolling friction	1
Density (ρ) (kg/m ³)	²¹ 1596	7852	Coefficient of restitution	0.0001

4.6.1 Mapped velocity field

The required input data for fluid force calculations were water density (998.2 kg/m³) and viscosity (1.003 × 10⁻⁶ m²/s) (at 20°C, Chow, 1959), the coefficient of drag and lift force for the bags, and the local velocity. The streamwise velocity predicted by the CES (described in Chapter 3) was used to prepare a mapped velocity field with 0.01m intervals as input for the DEM modelling. To determine the lateral and vertical component of the mapped velocity field, the same proportion of the streamwise velocity for a particular water depth as that derived from the experimental measurements was used (Chapter 2, Table 2.2). It was assumed that only the 150 surface bags were exposed to flow, and the negligible drag on the rear, buried geobags was ignored.

The velocity for the drag calculations on each bag was derived by interpolating the CES velocity field based on a weighted distance average between the geobag centroid and the four closest grid nodes.

¹⁸ Considered Iron properties from Tilley, 2004.

¹⁹ Geobag in shearbox experiment was carried out following the BS 6906–8:1991.

²⁰ Young's modulus was obtained for only geotextile following the BS EN 29073–3:1992.

²¹ Considering geobag as coarse aggregate, experiment carried out following the BS 812: 1995.

4.6.2 DEM model results

The purpose of this study was to find out the initiation of bag movement, and the visual validation was carried out by comparing failure modes with the experiments for the associated water level. For the flow simulations, the drag and lift coefficients, C_D and C_L were calibrated using data from condition D and validated using the other three condition data sets (Figure 4.5).

The results can be summarized as follows:

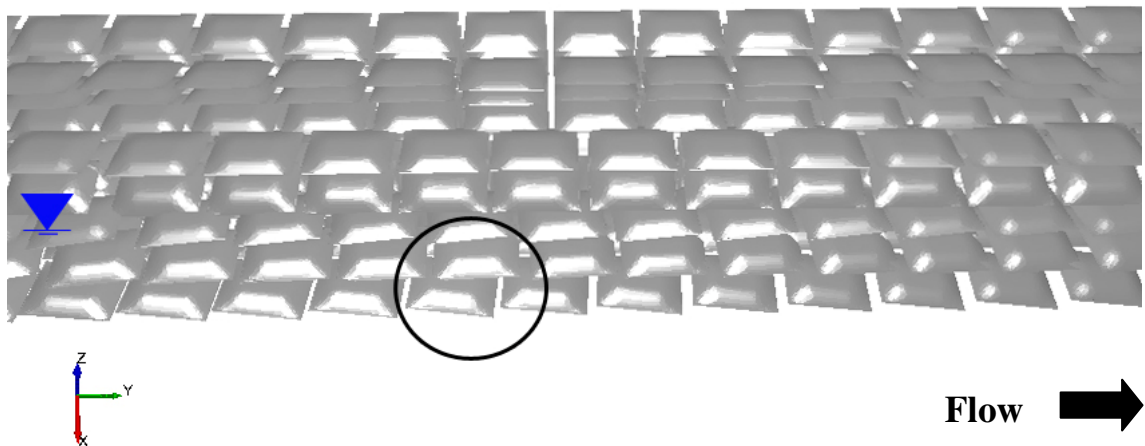
- A coefficient of drag of 0.5 and coefficient of lift of 0.8 showed good agreement with laboratory observations in conditions B to D;
- In condition A with the same coefficient value, the movement of bags started in the bottom most layer due to pressure differences between the main flow and void flow; the DEM model did not predict this, although it did reproduce to some extent the bag movement in the surface level layer and the one adjacent to this.

The DEM results for conditions B to D were reasonably good and the model has allowed the exploration of potential failure modes in the laboratory data collected for a fixed bed.



(A1) Laboratory

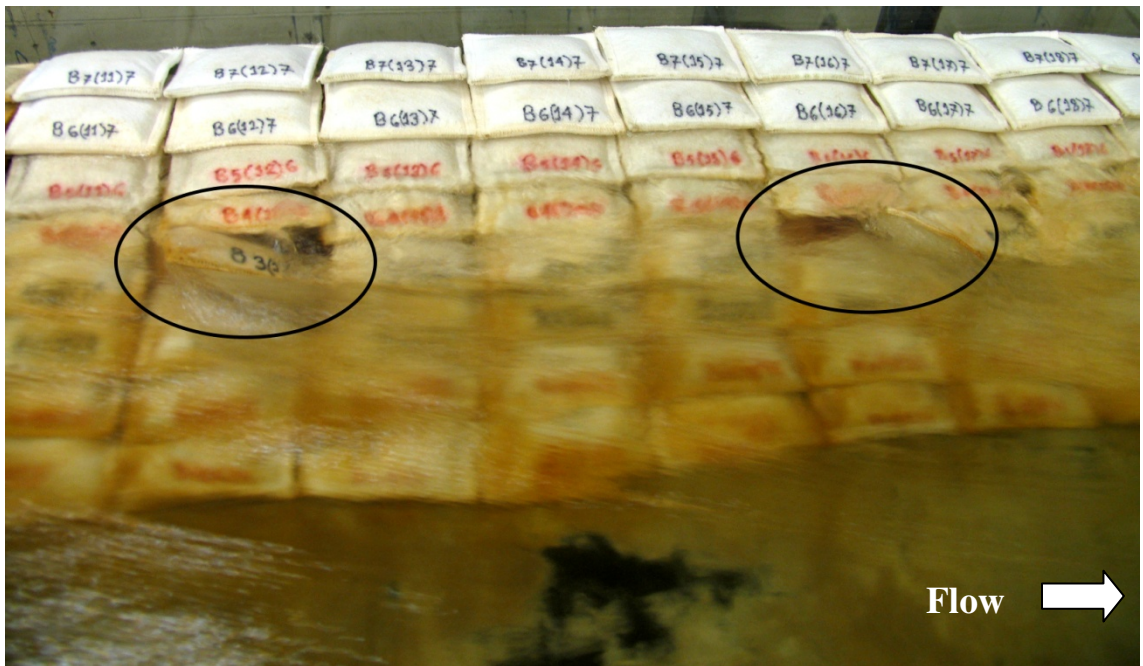
Pressure differences between the main flow and void flow initiated in the bottom most layer of bags and propagated to the next layer as this became less supported.



(A2) DEM model

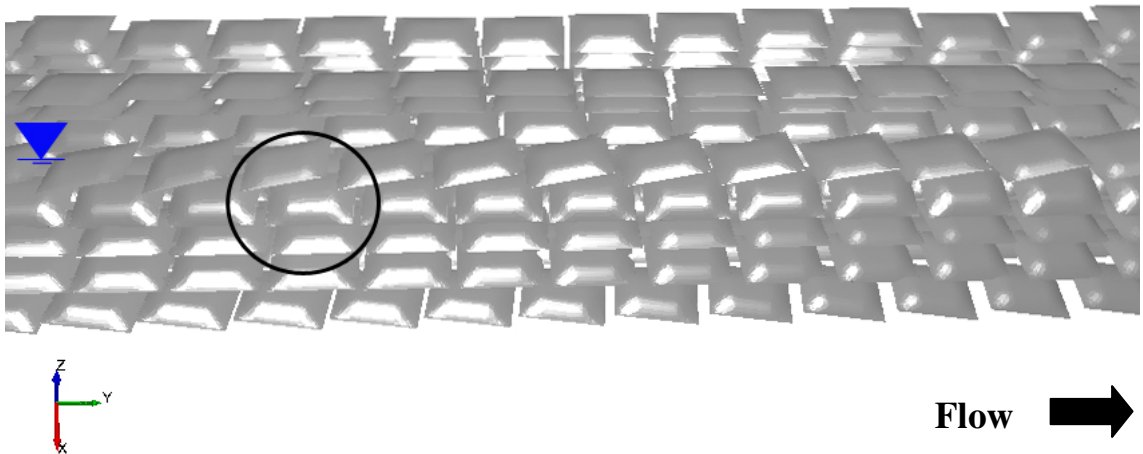
The surface water level layer and the next layer showed outward movement of the upstream outer corner. Thus the bottom most layers became exposed to water.

Figure 4.5(A1 and A2): Visual validation of the DEM simulation against laboratory observations (for condition A)



(B1) Laboratory

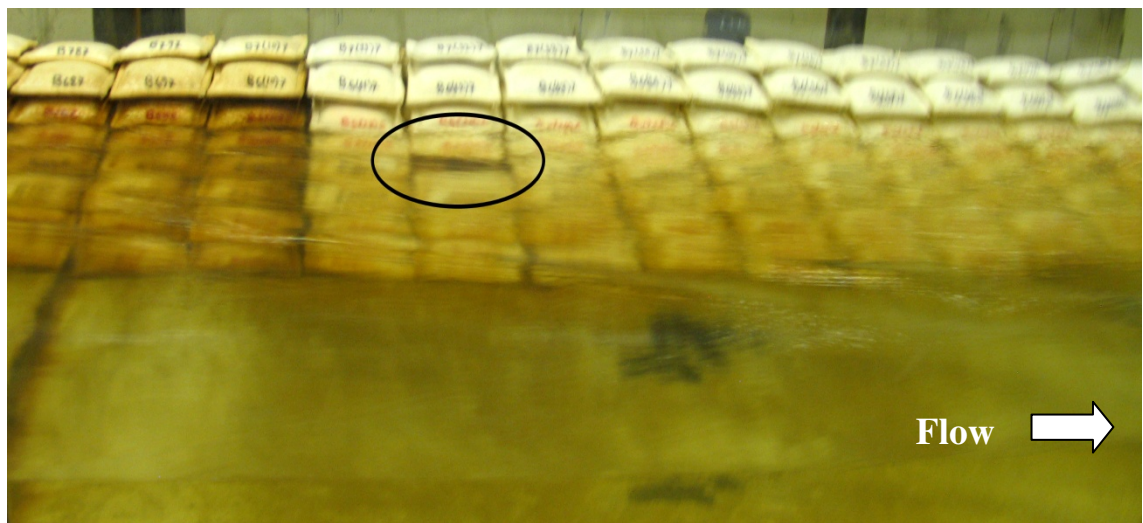
Partial uplifting observed in the layer nearest to the water surface.



(B2) DEM model

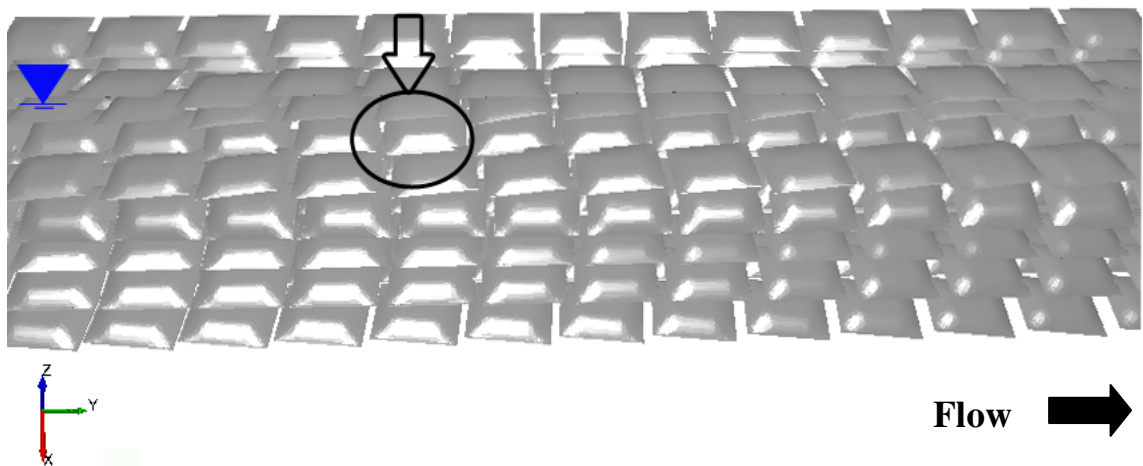
Bag movement observed in the layer nearest to the water surface.

Figure 4.5(B1 and B2): Visual validation of the DEM simulation against laboratory observations (for condition B)



(C1) Laboratory

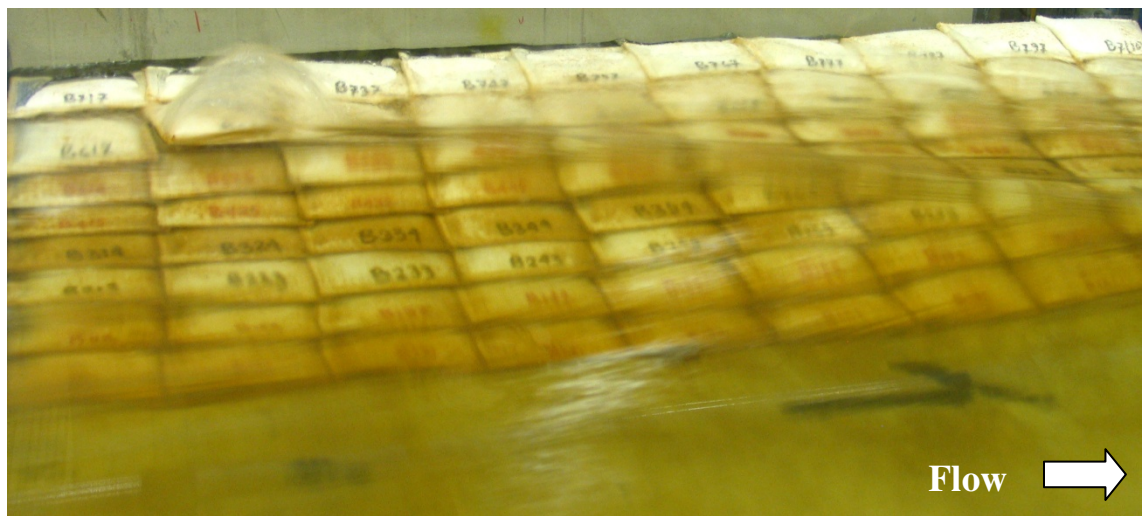
Full uplifting observed adjacent to water surface.



(C2) DEM model

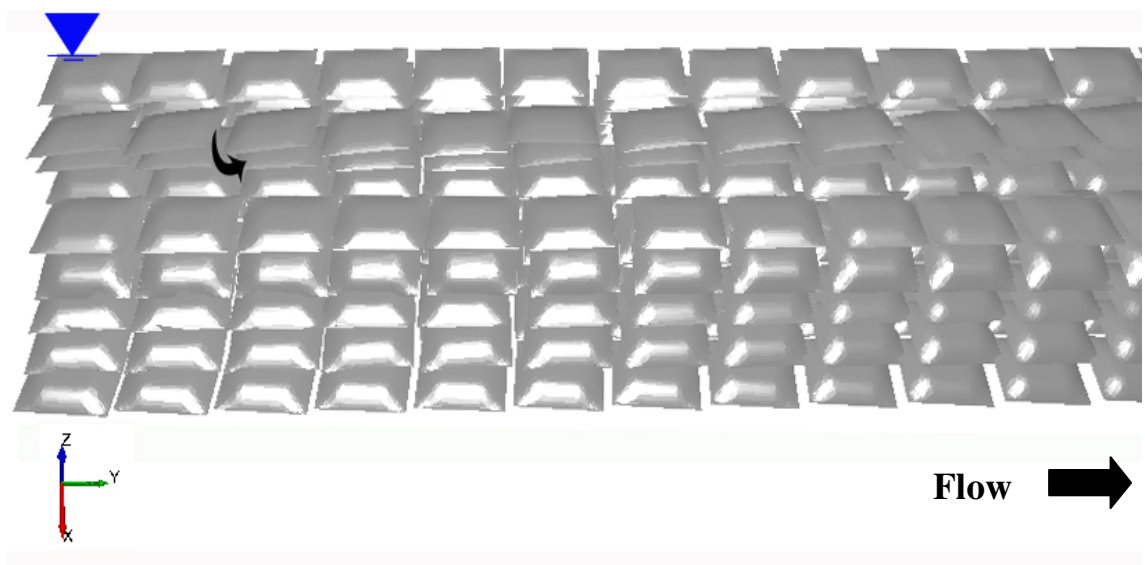
Displacement starts from water surface level.

Figure 4.5(C1 to C2): Visual validation of the DEM simulation against laboratory observations (for condition C)



(D1)Laboratory

Outward movement of upstream outer corner adjacent to water surface.



(D2) DEM model

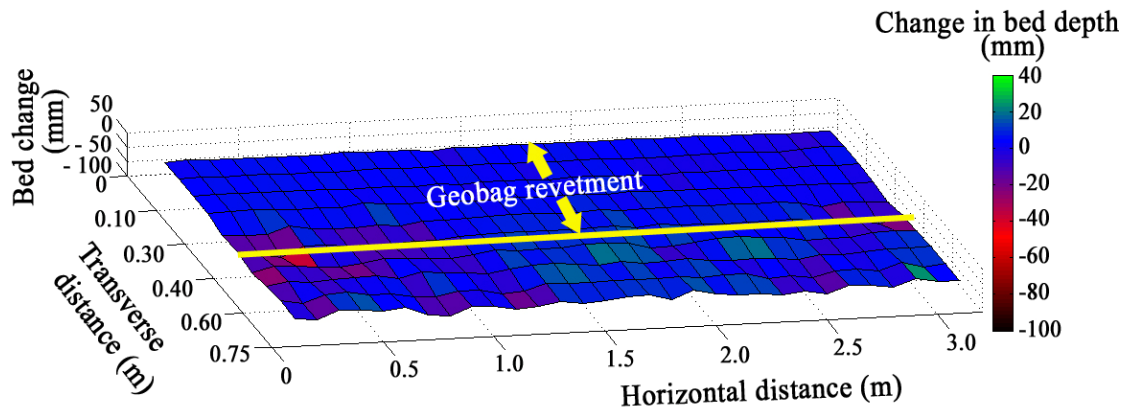
Outward movement of upstream outer corner adjacent to water surface.

Figure 4.5(D1 to D2): Visual validation of the DEM simulation against laboratory observations (for condition D)

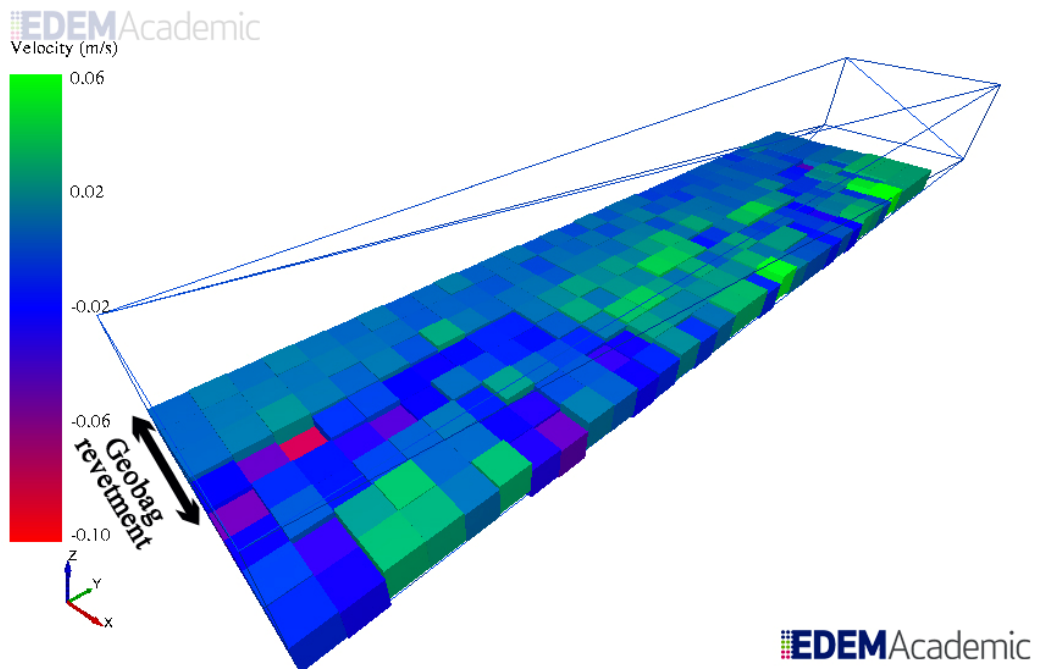
4.7 DEM model for the geobag - water flow- mobile bed interactions

The sandbed underneath the geobag revetment needed to be represented in such a way that DEM can simulate the response to bed erosion and scouring. In the model setup, the 3 m long, 0.75 m wide and 0.10 m deep sandbed was represented by using total 265 square of 0.10 m length as the laboratory measurement were taken at 0.10 m intervals (Figure 4.6 a). Within EDEM[®], all of these squares were treated individually, so the linear translation feature allowed movement of the square either downward or upward based on the laboratory measured data (Figure 4.6 b).

For model setup (Figure 4.7) the required values for the mobile (sand) bed were taken as the Modulus of rigidity (G) and Poisson's ratio (ν) 1.25×10^7 pa and 0.2 respectively as these values represent the Jamuna Riverbed (Tomlinson and Woodward, 2008). Density (ρ) of the sand, used in flume had been tested following the standard (BS 812: 1995) and found to be 1830 kg/m^3 .



(a) Change in bed under condition A (reproduced figure 2.16 a, Chapter 2)



(b) Representation of the sandbed change within EDEM®

Figure 4.6: Bed change (a) laboratory measurement and (b) DEM representation

EDEM Academic

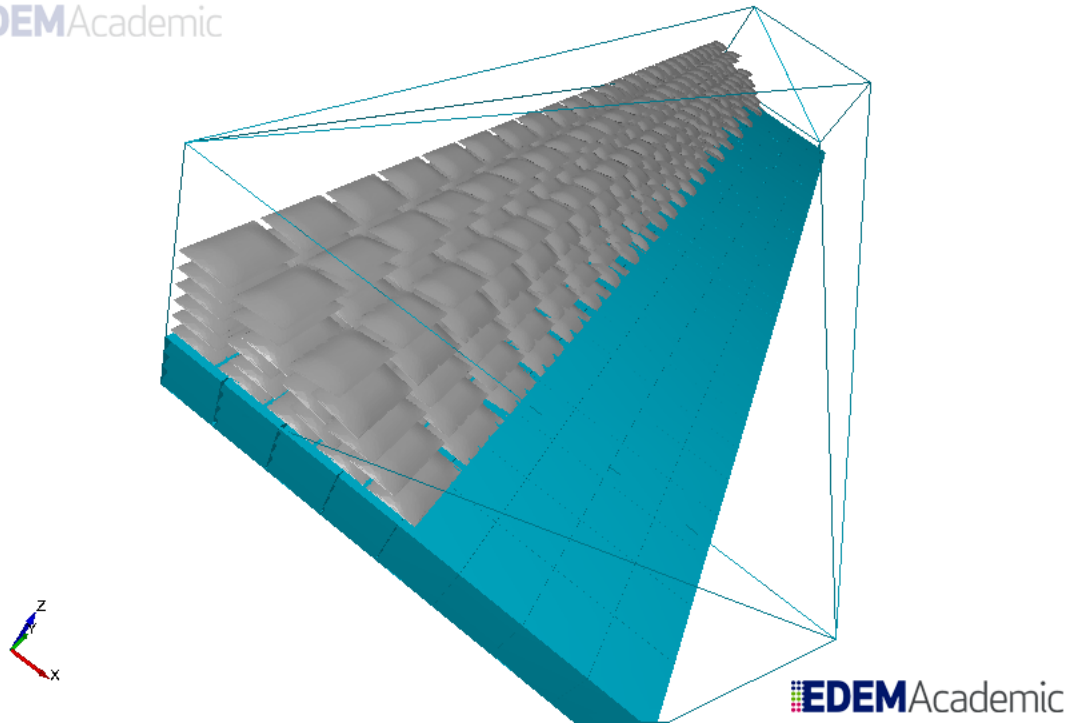


Figure 4.7: Initial setup of geobag revetment using EDEM®

The simulation was carried out following the same practice as done for fixed bed context. Initially the 100 s simulation run allowed for bag settlement to the model domain, and then the mapped water velocity was applied followed by the bed movement described in subsection 4.4.1.

The mapped velocity field of 0.01 m intervals was prepared using the CES predicted streamwise velocity. The lateral and vertical component of the mapped velocity field was derived from the same proportion of the streamwise velocity, as used in the fixed flume bed.

4.7.1 DEM model results

The key results can be summarized:

- A coefficient of drag of 0.5 and coefficient of lift of 0.8 showed good agreement with laboratory observations in all four water level conditions;
- In condition A, bag displacement in the DEM model represented an outward movement of the upstream outer corner of bags;
- Bag incipient movement in condition B was reproduced in the DEM model by the outward movement of the downstream corner of bag, i.e. the reverse direction from that in condition A;
- The location of failure initiation in condition C was predicted by the DEM model and the outward movement of the downstream corner of bag had observed i.e., same direction that in condition B; and
- In condition D, two types bag movement were observed simultaneously at the bottom most layer and next to the surface water level. In the bottom most layer, the bag movement modelled was an outward movement of the downstream corner of the bag as in conditions B and C. In the next to the surface water level, the modelled bag movement was in the same direction movement as in the fixed bed observation and also in condition A in mobile bed study.

Consideration of these model results suggests that in the DEM model, the bag displacement occurs in different directions, based on the active force. The outward movement of the upstream corner of the bags arises due to drag force on the bags, whilst the outward movement of the downstream corner of the bag represents the effect of displacement due to bed erosion.

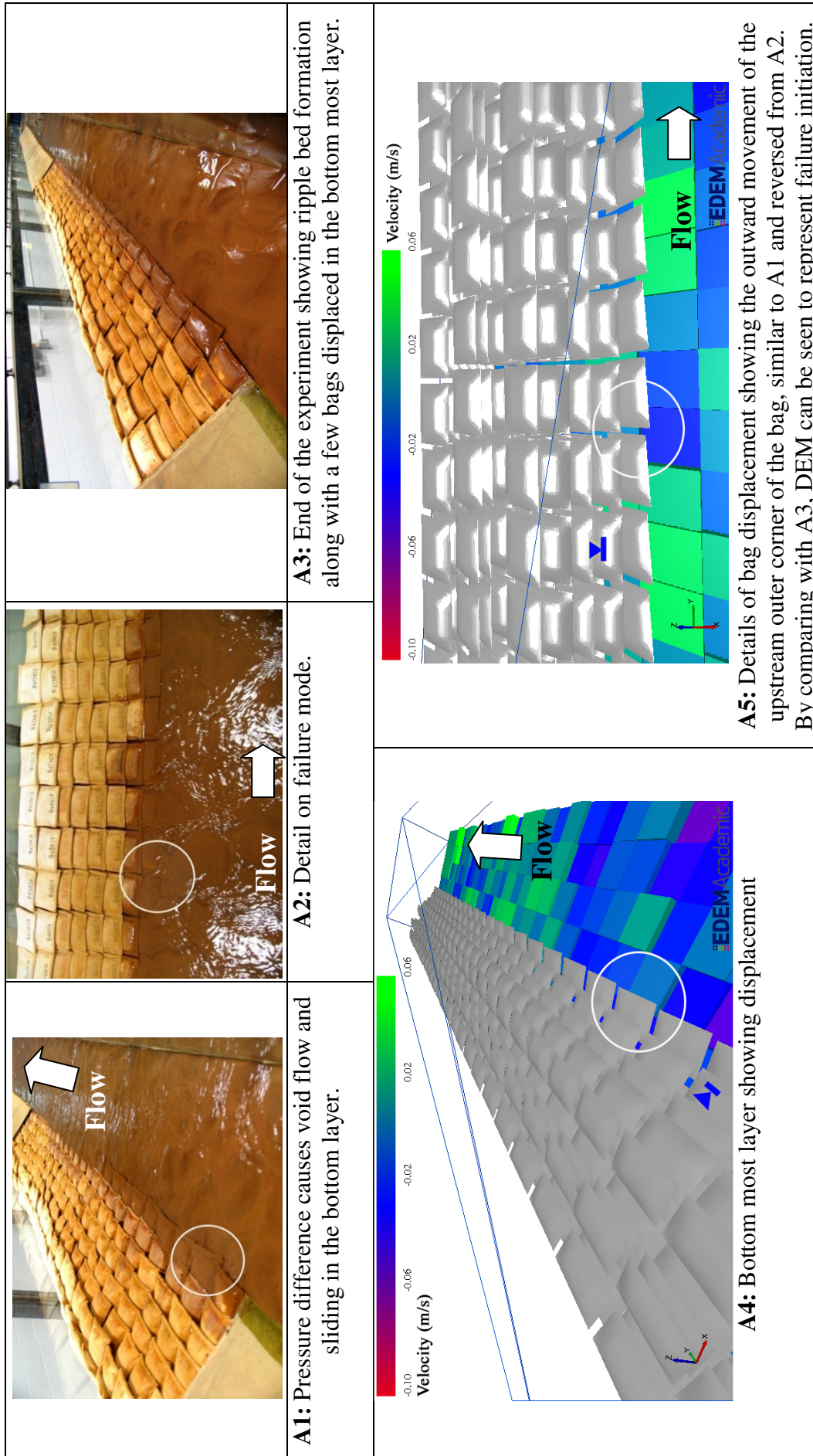


Figure 4.8 (A1 to A5): Comparison of laboratory observation and DEM outcome for condition A

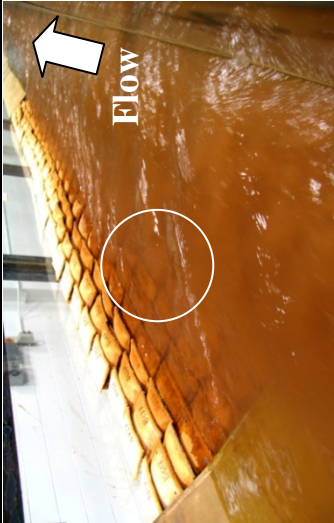
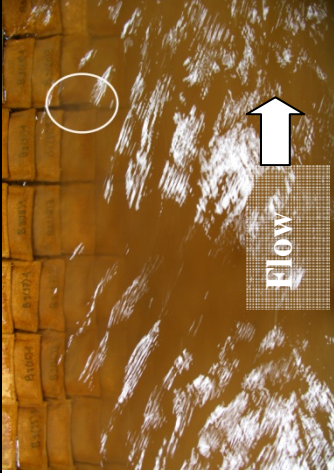

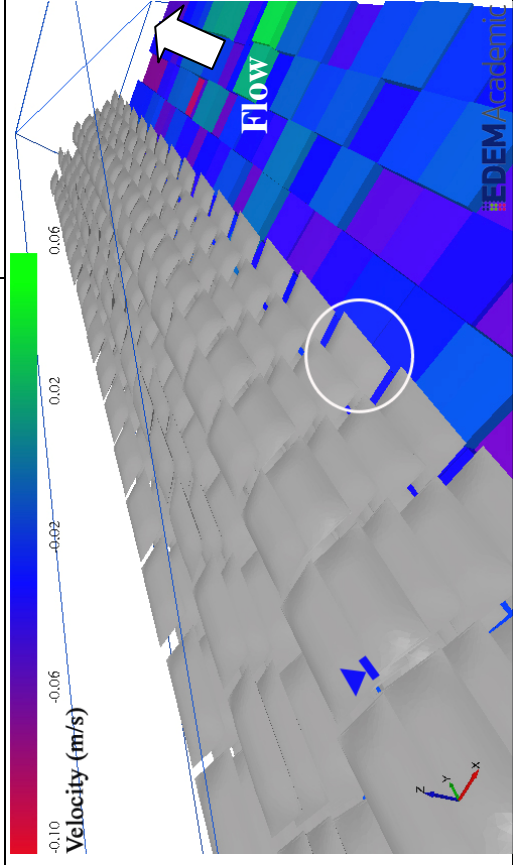
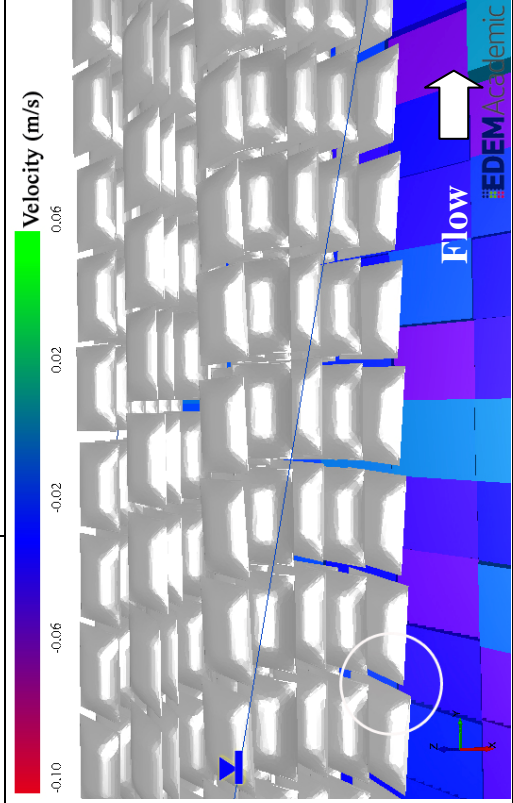
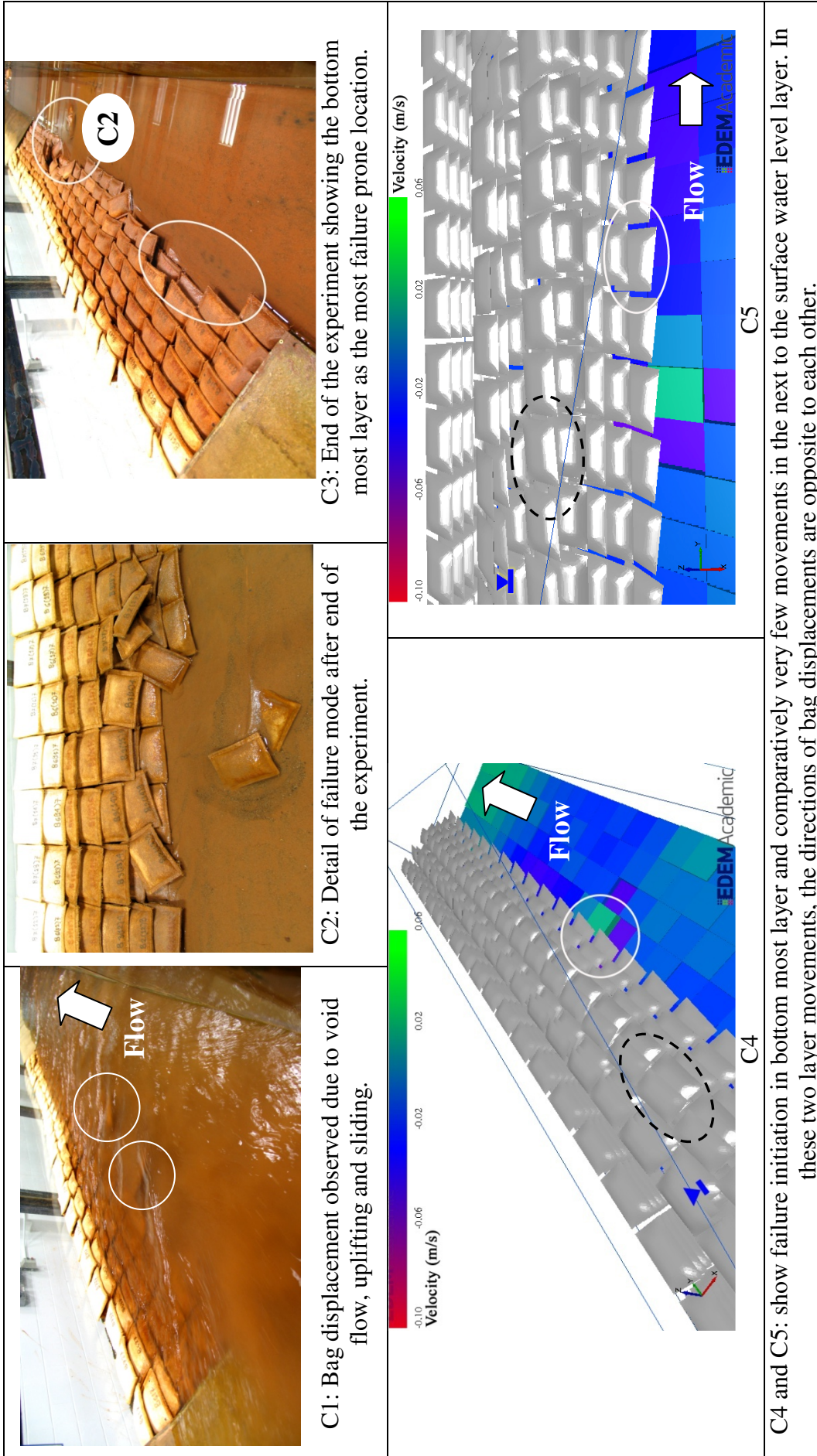
			<p>B1: Pressure difference causes void flow and sliding in the bottom layer.</p>	<p>B2: Negligible uplifting due to void flow but bottom most layer movement observed.</p>	<p>B3: End of the experiment confirms displacement in the bottom most layer.</p>
		<p>B4: DEM represents the incipient failure location, i.e., the bottom most layer.</p>	<p>B5: Both B4 and B5 show outward movement of the downstream outer corner of the bag similar to the laboratory observation for B2, but reversed movement compared to the A2 and fixed bed case (Figure 4.5B2).</p>		

Figure 4.8 (B1 to B5): Comparison of laboratory observation and DEM outcome for condition B



C4 and C5: show failure initiation in bottom most layer and comparatively very few movements in the next to the surface water level layer. In these two layer movements, the directions of bag displacements are opposite to each other.

Figure 4.8 (C1 to C5): Comparison of laboratory observation and DEM outcome for condition C

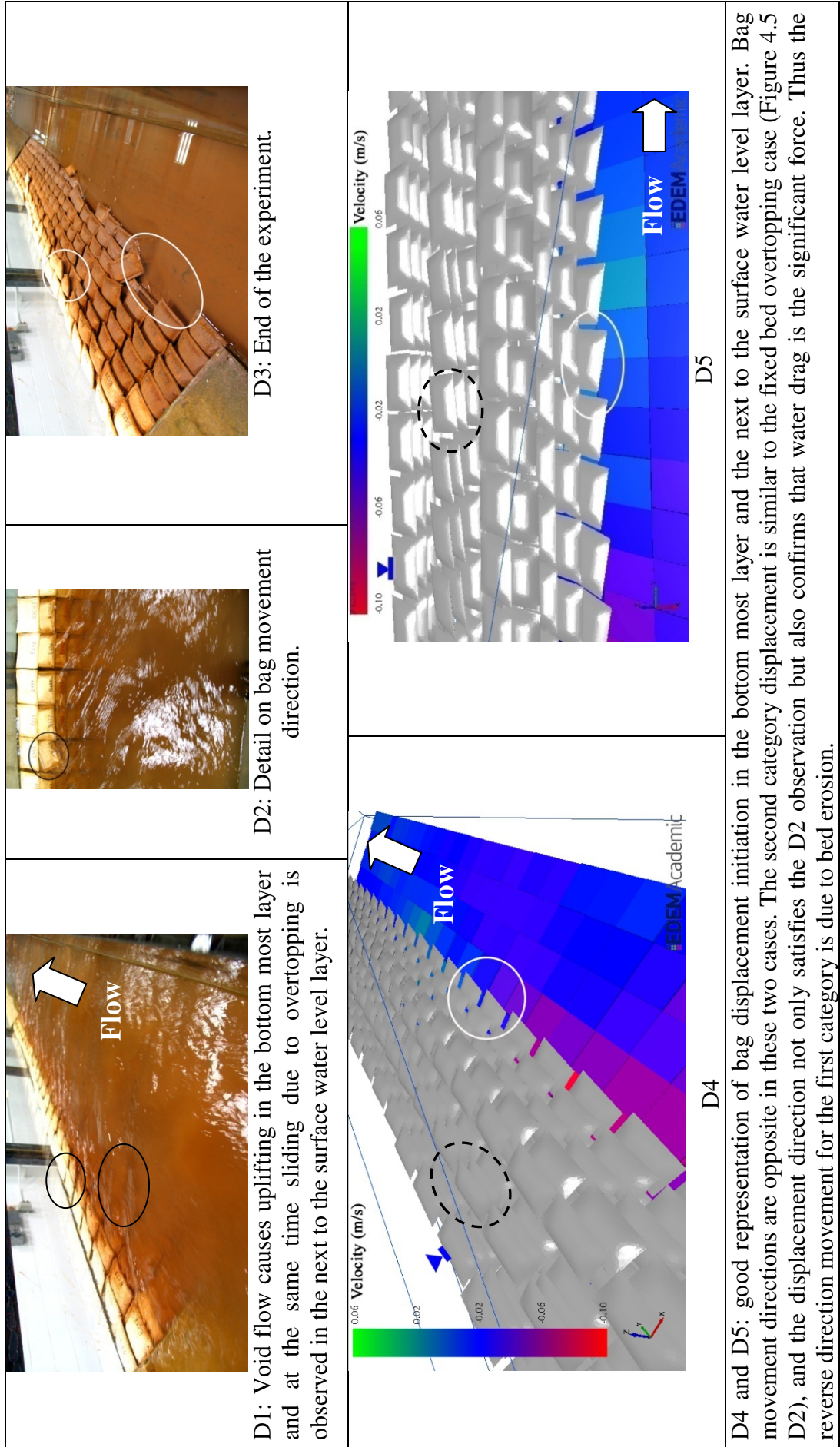


Figure 4.8 (D1 to D5): Comparison of laboratory observation and DEM outcome for condition D

4.8 Analysis of numerical model results

The coefficient of friction of geobag–geobag was found as 0.55 to reproduce the similar bag displacement obtained in laboratory dry experiments. Although there is no standard method for determining this value, this is close to the published values under different circumstances, i.e., dry geotextile and sand interaction, geobag–geobag under wave action. So, for revetment design this value can provide more realistic guideline as this test was solely done on geobag–geobag interaction and the DEM model maintain the precise bag size.

In the DEM couple model on the fixed bed, a coefficient of drag of 0.5 and the coefficient of lift of 0.8 of flow around the geobag caused bag displacement initiation from the revetment. The DEM model could replicate the laboratory observed incipient bag movement direction. Generally, through anti–clockwise bag movement with respect to streamwise direction (i.e., outward movement of upstream outer corner of bag) revetment failure observed both in laboratory and DEM model. In this model setup, the DEM model showed better performance in higher water level.

Using same coefficient of drag and lift in the DEM couple model the failure initiation in the geobag on the mobile sediment bed could be well represented. Including similar bag movement direction close to surface water level in fixed bed, the DEM model produced opposite directional movement in the bottom most bag layer. These two different bag movement directions suggest that for bag movement initiation due to drag force (anti-clockwise bag movement with respect to streamwise direction) or toe scour (clockwise bag movement with respect to streamwise direction).

4.9 Conclusion

The failure processes in a geobag revetment has been studied using a DEM model, validated against quasi-physical model observations. The validated numerical model was employed to estimate the coefficient of friction, drag and lift in different water depths. The DEM model gave good representation of revetment failure modes at water levels above 50% of the revetment height and provides a useful tool for characterizing revetment failure on a fixed bed.

To investigate the DEM model applicability in river management, the second part of this chapter considered a mobile sediment bed. In this case, toe scouring including bed formation in different water depths had a significant influence on geobag performance.

The DEM model gave good representation of revetment failure modes in all of selected water level conditions, and provides a useful tool for characterizing incipient revetment failure.

Chapter 5

Practical Application

This chapter aims to influence the future practical design guidelines for riverbank geobag revetments to enable them to withstand geobag – water flow interaction on mobile sandbed. The first part of this chapter summarizes the available guidelines around the world for both coastal and river bank applications.

Scope of the DEM model for reproducing the real features are discussed in a manner ‘if – then’. Finally the guideline is described in light of DEM applicability in river bank geobag revetment.

5.1 Published geobag guidelines

The first published paper on sand filled bags for bank protection appeared over more than four decades by Venis (1968). For emergency flood protection sand bags are the first choice for temporary protection. So, there are a large number of guidelines available around the world on bag design specifications, construction method and placement. These features are different than this thesis meant to be. For reviewing the existing guidelines, the emergency sand bag guidelines are not considered for protection against the significant amount of hydraulic forces arising in riverbank revetment.

The complete design guideline for long term use in coastal or riverbank protection is still not available. In 1994, probably for large scale protection the first guideline was recommended in Germany. According to Saathoff *et al.* (2007) the German recommendations 'EAG-CON' by German Geotechnical Society (DGGT) is expected to describe the principles of geobag application, material parameters and system requirements, design, quality assurance, construction and installation possibilities; and execution with bag filling method towards the final bag positioned and prefilled bag handling . The EAG-CON is still under preparation (personal communication Prof. Oumeraci Hocine).

More detailed guidance is covered by the Australian guidelines on geobag application in coastal protection (NSW, 2010) (Table 5.1). UK and USA have some guidance on bag design and revetment construction specifications (Scottish Natural Heritage, 2000; US Army Corps of Engineers, 2004; CAMA, 2008; NDSU & U.S. Department of Agriculture, 2010).

In Asia, riverbank experiences from Khando, Bagmati and Lalbakeya Rivers in Nepal (CFM, 2004), and Mekong River in Thailand (Mekong River Commission, 2009) show lack of proper engineering design of river training works and the guidelines for geobag construction appeared following the general rules of revetment. So, special requirements of geobag revetment in terms of hydraulic stability are absent.

Table 5.1: Published geobag guideline obtained for both coastal and riverbank protection works

Structure zone	Bag design Specification			Construction Specification				Life cycle (Year)	Maintenance and Inspection	Labour Safety	Year	Reference
	Sand d ₅₀ (mm)	Fabric (Thickness)	Fill ratio (%)	Bag size Weight Volume	Bond bag-bag	Thickness	Placement (streamwise)					
Coastal	–	Geotextile	–	3m x 1.5m x 0.5m 3 tonnes –	Running bond	2–3bag widths	Parallel	≤1:1.5	Adaptive management	≤ 50 kg	2000	Scottish Natural Heritage
	–	–	–	2–4.5m x 1–1.5 m –	–	–	Parallel	≤1:3.3	Following standards 15A NCAC 7H Section .0308(a)	–	2008	²² CAMA
	0.15–0.50	Geotextile (5 mm)	67–100	– ≥ 18 kg 0.75 m ³	Running bond	2 layer	Perpendicular	1:1.5	Coastal protection Act 1979 Section 55R(1)(c)	–	2010	²³ NSW
Riverbank	–	Burlap and plastic	50 – 67	0.61 m x 0.36m – –	–	–	–	1:1	–	–	2004	US Army Corps of Engineers
	–	Woven polypropylene	50	0.61 m x 0.36m 16–18 kg –	Running bond	–	Parallel	1:2 1:3	–	–	2010	NDSU & U.S. Dept. of Agri.

²² Coastal Area Management Act (CAMA)²³ This draft document has been prepared to support the Coastal Protection Act 1979 once amended by the Coastal Protection and Other Legislation Amendment Bill 2010, which is currently being considered by the NSW Parliament. Department of Environment, Climate Change and Water, NSW.

Chapter 5: Practical Application

In Bangladesh, the first design guidelines on 'Guide to planning and design of river training and bank protection works' was published in 1993. This was followed by the FAP (Flood Action Plan) 21/22 publication on 'Guidelines and design manual for standardized bank protection structures'. Afterwards a guideline for 'Design of river bank protection and manual' was published in 2007 under Jamuna Meghna River Erosion Mitigation (JMREM) project. Since the publication of two earlier guidelines, there have been some advances in understanding of river bank protection materials and of the design and behaviour of the river training works in the river environment. The publication under JMREM project has reviewed both of the earlier guidelines and also introduces on the use of geobags as a new construction materials and also a concept of an adaptive approach in the constructions and strengthening of the river bank protection works.

According to JMREM (2006 a) , the adaptive approach contains five elements, these are (i) revetment construction in an emergency, (ii) first major construction provides the first level protection which takes usually two years to complete, (iii) length of the monitoring and adaption phase might be several years depends on the river erosion nature, (iv) if required, the second level protection is adopted to upgrade the existing protection and (v) normal maintenance would carried out on the protected riverbank.

Thus after the first major construction, the rest of the adaptive approach depends on the knowledge of failure mechanisms of the geobag revetment. To achieve the desire performance of the designed geobag revetment, there is an urgent need to predict the failure modes.

The experience from laboratory geobag revetment and field can provide details hydraulic stability knowledge on the geobag performances in a riverbank. Hence an acquired experience can make best use of a 3D numerical model prediction for failure mechanism of geobags in a revetment.

5.2 Lessons from JMREM project

5.2.1 Bag design specification

According to JMREM (2006 a) the original specifications of sand is of non-plastic, non-saline, free from silt, clay, roots, and other organic materials. The minimum grain size was 0.08 mm and the range of Fineness Modulus is from 1 to 1.3 (JMREM, 2006 a). Bag size of 1.03 m × 0.70 m with 80% fill ratio provides a weight of 126 kg.

5.2.2 Construction specification

In the field, the most commonly achieved pattern after launching is one layer of geobags (JMREM, 2006 a). But using a running bond of placement, a complete coverage could be achieved with two layers of bags (JMREM, 2006 a) whereas the JMREM (2006 c) suggested that the bag layers should be 3 layers. However, presently there is no precise rule for target bonds among bags while revetment constructed.

As dumping of bags resulted in reduction in thickness, the JMREM (2006 c) project concluded with two concepts, are:

- (i) A mechanized system to provide a more reliable coverage through lowering the bag wastage;
- (ii) Manually bag dumping from river surface.

Due to practical and local interest the second concept has been practicing even though this requires more bags.

Geotechnical slope instability is a common immediate reason for failure of riverbank protection. In the consolidated soils commonly found along river banks, slopes of 1V:2H are at the borderline of stability (JMREM, 2006 c).

5.2.3 Maintenance and inspection

The normal maintenance for geobag revetment is expected to start about 5 to 10 years after implementation of protection upto deeper scour levels (JMREM, 2006 a). JMREM (2006 c) recommended monitoring as an integral part against revetment stability. As per recommendation these can be done through:

- (i) large scale river survey (bathymetry and flow measurements);
- (ii) river survey along the protected banks by means of diving investigations both for general checks at locations of specific interest and annual checks with detailed bankline survey.

Presently the Maintenance and Evaluation division of Bangladesh Water Development Board (BWDB) is responsible for monitoring.

5.2.4 Hydraulic parameters

The JMREM (2006 c) suggested:

- design velocity is of 3 m/s; and
- in determining design depth, a consideration of 7 m toe scour should allow for implemented geobag revetment;

For major rivers in Bangladesh, the prediction of riverbank erosion and future planform developments has been carried out by the Center for Environmental and Geographic Information Services (CEGIS). The prediction tool based on low–water satellite images is relevant for riverbanks. Daily water level and flow velocity measurements are carried out by the BWDB in specified stations.

5.3 Application of this thesis in design guideline

In this thesis, as the quasi-physical model was carried out using the scaled down geobags, an intensive measurement program of performance details could be acquired from the laboratory experiences and thus contribute to construction specifications and hydraulic parameters for the design guideline preparations. On the other hand the DEM model was well calibrated against laboratory observations, so for further applications this calibrated DEM model could be use.

Next three subsections are presenting a critical evaluation on achieving a practical guideline for geobag application using the knowledge from this thesis.

5.3.1 Quasi-physical model study

The present practice of JMREM is to place a batch of geobags near the top of the bank literally just below low surface water level and the launching on slope of the river followed by the same manner of the quarry rocks (JMREM, 2006 a). The assumption behind this practice was that the geobags would slide from the dumped batch in an orderly manner in layers while toe scour progresses and thus a protected slope of 1V:2H could be achieved (JMREM, 2006 a). Here an important factor was unknown i.e. the portion of batch revetment height, contributing to slope formation. Possibly an idea can be drawn from the findings noted down in subsection 2.4.3, under condition C while the near bank mobile sand bed changed to transition flat bed then from bottom part of the revetment height (upto 45% of the revetment height from the bottom) experienced bag displacements.

Overtopping observed in laboratory under both fixed and mobile sediment bed conditions as described in subsections 2.3.3 and 2.4.3. The possible negative effect of this observation can be easily predicted in terms of achieving the revetment performances. In JMREM, this feature is considered through a geo-mechanical slope stability conclusion and the remedial approach above the low water level is adopted by

using a sand/cement grout-filled mattress, concrete blocks, or other hard elements in geobag revetment. As this thesis meant to focus only the hydraulic stability concern so within the thesis scopes the present practice seemed a good practice and should continue to withstand against the overtopping.

During geobag-flow interaction evaluation in laboratory, findings showed the water flow velocity of 3.5 m/s to 4 m/s causes geobag movement initiation (subsection 2.3.3). This can confirm the required design velocity (i.e., 3 m/s) for JMREM can be achieved reasonably with geobags (JMREM, 2006 c).

5.3.2 Analytical approach

In this thesis, the comparative study between CES prediction and the use of Chow (1959) chart showed the first washed away bag was possibly subjected to the shear stress of 63.2 N/m^2 to 158 N/m^2 . This estimation can not be verify with the field values as there is no such value is available from JMREM and it also not practical to measure in the field. But the CES application can help to boost the prediction of bag displacement initiation (described in Chapter3, subsection 3.4.1) and thus the failure zone through relevant and frequent data prediction. Mc Gahey et al. (2008) had reported that CES could not properly estimate the roughness values for large river such as Brahmaputra. The lower part of Brahmaputra river, which flows over Bangladesh is the Jamuna River. Probably this is a major challenge for CES applications, however, as the JMREM implemented location is in further down, thus CES can possibly show better estimation than for the Brahmaputra River.

5.3.3 DEM model

The importance of a 3D representation of geobag revetment is well understood in terms of performance evaluation. The unique significance of this thesis is to replicate the laboratory observation using a 3D DEM model. The commercial EDEM[®] model is the

tool to serve this purpose. In subsection 4.5.2, the acquired coefficient of friction among the geobags is of 0.55 which confirmed by replication the experimental observation on geobag revetment performance.

The DEM model showed a good representation of geobag–water interaction in subsection 4.5 as well as more acceptable representation of geobag–water–mobile sediment bed interaction stated in subsection 4.6. During geobag–water–mobile sediment bed interaction, the displacement of geobag could well recognize in laboratory experiments. The sliding was prominently observed in the laboratory and it can easily mislead how this failure is progressing, as the similar kind of displacement is also observed in geobag–water interaction? The DEM model showed a clear difference on the bag displacement and active forces.

5.4 DEM model application in design guideline

To prepare a design guideline aimed to ensure a geobag revetment hydraulic performance, the DEM model prediction can play a vital role. As the calibrated DEM model showed promising performances to replicate the laboratory observations, so it can be envisaged that to some extent the DEM can provide distinguishable information on bag movement due to active forces on them.

So the DEM model will work while the following relevant information is available:

5.4.1 Bag design specification

Following the present geobag size and preparation specifications as used in the JMREM (2006 a). As the change in bag size could restrain from presently manually bag launching.

5.4.2 Construction specification

Using the jack on jack revetment construction method, the revetment should be constructed to achieve a 1V:2H protected slope through 50% layer-to-layer overlapping. The longest axis of the bag should be in the streamwise direction.

5.4.3 Maintenance and inspection

The proper inspection can offer the required maintenance prediction for geobag revetment. The best prediction of the DEM model could also be achieved through model calibration using field inspection.

The JMREM (2006 c) observed that the project work presently consider natural riverbanks for survey in comparison to the common practice of 10 to 25 m line spacing survey density. So they made a recommendation for the BWDB M&E subdivisions were to undertake a comparison survey with 5 m, 10 m and 25 m spacing along one reach within a few days and to compare 3D presentation of the data to assess which type of riverbank failure can be found (JMREM, 2006 c). If the next phase of inspections can consider these features, the DEM model would be trained sufficiently to provide reasonable prediction on geobag revetment performances.

5.5 Summary

The quasi-physical model study could provide information on geobag practical application in some extent. The flow nature in the field, which would be different from the experimental setup in laboratory, and also the riverbed erosion and the scouring nature of riverbank needs careful consideration.

The presently calibrated DEM model needs the following field information to be useable in field geobag revetment performance evaluations:

- water depth and systematic evaluation of relevant 3D water flow velocity;
- their relationship with riverbank erosion and scour rates, so a 3D bed profile should be included; and
- all of the above mentioned parameters should be considered along with the specific failure mode identification in geobag revetment.

Chapter 6

Conclusions

This thesis is concerned with the application of a 3D Discrete Element Model (DEM) in design guideline preparation for geobag revetment. This can be summarised as follows:

In Chapter 2, detailed quasi-physical model studies were carried out considering the possible revetment construction methods, different water depths and bed formations, to enhance the basic knowledge on active friction and hydrodynamic forces on the revetment performance. The observations are made of failure modes and zones in the geobag revetment. The scaled model geobags showed good agreement with the previous physical model study carried by *nhc* (2006) in terms of the incipient velocity for movement. The physical state of the geobags was also considered and recorded in due course. Settling distance of the displaced bags was also recorded to evaluate along with the initial state of geobags while the experiment was started. Thus based on the laboratory experimental data, relationship among geobag failure modes, associated water depth and bed formation have produced a failure map, Figure 2.9.

Chapter 6: Conclusions

A number of limitations are noted for the quasi-physical model study detailed in Chapter 2, including the highly turbulent flow in flume and the absence of a continuous sediment supply. As this study was focussed on the initial stages of geobag revetment failures, these limitations are considered acceptable from an experimental point of view. However, they would certainly need cautious consideration for real field applications

Apart from the scale effect in quasi-physical model, frequent manually data measurement is a big challenge in a quasi-physical model study. In Chapter 3, an analytical approach was adopted to extend the laboratory measurements. In this regards, the Conveyance Estimation System (CES) was used to replicate the measured depth-average velocity data. The calibrated CES model was then applied to estimate the water flow shear stress on geobag failure initiation. To verify the CES predicted shear stress, membrane analogy method as presented by Chow (1959) was also used. Both CES and the Chow (1959) method showed good agreement in terms of shear stress determination. However, for frequent data prediction, CES was selected due to its lower computational effort.

The Chapter 3 attempted to determine a unit roughness value for geobags, which initially seemed lower than expected. This is a limitation, as long as there is any specific study showed the standard or acceptable value for geobag.

The available published literature showed this is the first time a 3D numerical model has been used to predict geobag revetment performance, details are described in Chapter 4. The DEM model could mimic the failure modes due to geobag-flow and geobag-flow-mobile sediment bed interactions. The DEM model performed better with mobile sediment bed than the fixed bed when compared with observations from the laboratory. The most important contribution, of the DEM model to the understanding of geobag performances, was the distinguishable representation of geobag displacement due to drag force and toe scour. It is envisaged that the DEM model could also be applicable in field geobag revetment performance evaluations.

Chapter 5 is dedicated to discussing a design guideline for geobag revetments. A details review is carried out of available guidelines or recommendations for long term geobag revetments. Except for the recent Australian guideline, there is no such complete guideline. The Australian guideline is for coastal geobag structures, so literally riverbank protected geobag application guidance are absent. The calibrated DEM model from this thesis could provide important information in this regards and thus as per river dynamism a more practical design guideline can be achieved.

6.1 Conclusions

The most important conclusions of this thesis can be summarised as follows:

- A number of the experimental runs illustrated some distinct incipient failure mechanisms related to water level and revetment construction method. In general, these failures were initiated through combinations of pressure differences between the main flow and void flow, partial or full uplifting, overtopping, pullout, or internal sliding.
- The quasi-physical model highlighted the influence of the water level on the failure modes of geobag revetments. Despite the difference in model scale, the incipient velocity measurements showed good agreement with previous experimental work by *nhc* (2006).
- In the present study, the CES was found to replicate the measured depth average velocities to a reasonable degree. The CES and Chow (1959) method showed good agreement in terms of consistency in predicting shear stresses on the geobags in the revetment. Both methods produce acceptable predictions, although the CES is recommended for further use because of its sound theoretical basis and ease of application.

Chapter 6: Conclusions

- The CES can reasonably predict the bed formation in mobile sandbeds against the known water flow rate and water level in the flume.
- The failure processes in a geobag revetment has been studied using a DEM model, validated against quasi-physical model observations. The validated numerical model was employed to estimate the coefficient of friction, drag and lift in different water depths. The DEM model gave good representation of geobag – water flow interaction at water levels above 50% of the revetment height and provides a useful tool for characterizing revetment failure on a fixed bed.
- To investigate the DEM model applicability in river management, the second part of DEM model study considered a mobile sediment bed. In this study, toe scouring including bed formation in different water depths had a significant influence on geobag performance. The DEM model gave good representation of revetment failure modes in all of the selected water level conditions, and provides a useful tool for characterizing incipient revetment failure.
- The aim of this thesis is to contribute to prepare a practical design guideline, the present calibrated DEM can be expected to provide reasonable information to withstand the desired performance of geobag revetment through prediction of bag displacement considering the active forces.

6.2 Further research recommendations

An immediate potential research issue concerns the implementation of geotechnical stability models of the geobag revetment. This will allow simulation of features of permeability and durability of geobags in terms of river bank environment. This needs to be more on basic geotechnical knowledge based. So that this can work in coupled with DEM model or might work based on sharing information and thus can provide more realistic prediction. A further development of the numerical simulation would be the representation of fluid forces using a Monte Carlo simulation.

In practical application of this thesis, JMREM has taken as a case study area and finding of this thesis has evaluated in this context. In further research, DEM can be applied in evaluating the performance of other discrete riverbank protective materials, for example concrete blocks or riprap.

References

- Achenbach, E., 1971. Influence of surface roughness on the cross-flow around a circular cylinder. *Journal of Fluid Mechanics*, **46** (2), pp. 321-335.
- Achenbach, E., 1972. Experiments on the flow past spheres at very high Reynolds numbers. *Journal of Fluid Mechanics*, **54** (3), pp. 565-575.
- Abdalla, A. M. A. and Sekino, N., 2006. Veneer strand flanged I-beam with MDF or particleboard as web material IV: Effect of web material types and flange density on the basic properties. *Journal of Wood Science*, **52** (2), pp. 167-172.
- Baas, J.H., 1999. An empirical model for the development and equilibrium morphology of current ripples in fine sand. *Sedimentology*, **46**, pp. 123-138.
- Bennett, S. J., and Best, J. L., 1996. Mean flow and turbulence structure over fixed ripples and the ripple-dune transition. in Ashworth, P. J. Bennett, S. J. Best, J. L. and McLelland, S. J. (ed.) *Coherent flow structures in open channels*, Wiley, New York, pp. 281–304.
- Bertrand, F., Leclaire, L. A., and Levecque, G., 2005. DEM – based Models for the Mixing of Granular Materials. *Chemical Engineering Science*, **60**, pp. 2517 - 2531.
- Bezuijen, A., Adel, H. D., Groot, M. B., and Pilarczyk, K.W., 2000. Research on geocontainers and its application in practice. *Proceedings of the. 27th Conference of Coastal Engineering* (Sydney, Australia, ASCE), pp. 2331-2341.
- Bezuijen, A., Groot, M. B., Breteler, M. K., and Berendsen, E., 2004. Placing Accuracy and Stability of Geocontainers. *Proceedings 3rd Geosynthetics Conference*, Munich, Technische Universität München, Cent, Geotech, **1**, pp. 123-128.
- Brand, E.W. and Pang, P.L.R., 1991. Durability of geotextiles to outdoor exposure in Hong Kong. *Journal of Geotechnical Engineering*, American Society of Civil Engineers, **117**, pp. 979-1000.
- Breteler, M. K., Pilarczyk, K.W and Stoutjesdijk, T., 1998. Design of Alternative Revetments. *Proceedings of the 26th International Conference on Coastal Engineering*, Copenhagen, Denmark.
- British Standard, 1991. *BS 6906-8:1991 Methods of test for Geotextiles - Part 8: Determination of sand-geotextile frictional behaviour by direct shear*. BSI.
- British Standards, 1992. *BSEN 29073 Methods of tests for Nonwovens - Part 3: Determination of tensile strength and elongation*. BSI.
- British Standards, 1995. *BS 812 Testing aggregates Part 2. Methods of determination of density*. BSI.
- British Standard, 2007. *BS EN ISO 748: 2007 Hydrometry –Measurement of liquid flow in open channels using current-meters or floats*. pp. 8-17.
- Coastal Area Management Act (CAMA)
<http://www.nccoastalmanagement.net/handbook/section4.htm>.

References

- CFM, 2004. Manual for Community-Based Flood Management in Nepal. *Asia Pacific Journal on Environment and Development*, **11**(1&2), pp. 227-304.
- Chow, V. T., 1959. *Open-Channel Hydraulics*. London, McGraw-Hill Book Company, Inc.
- Corbet S. 2005. *Geosynthetics in Construction*. Geotechnical Faber Maunsell Limited, United Kingdom.
- Crapper, M., Ooi, J., Favier, J. and Golz, P., 2005. Coupled Continuum-Discrete Modelling of Solid-Fluid Phase Flow. *7th World Congress of Chemical Engineering*.
- Dassanayake, D. and Oumeraci, H., 2010. Sinking Behaviour and Deformation of Geotextile Sand Containers (GSCs) during construction of fully submerged GSC-structures. *International Workshop on Geosynthetics and Modern Materials in Coastal Protection and Related Applications*. IIT Madras, Chennai, India.
- DEFRA/EA, 2003. *Reducing Uncertainty in River Flood Conveyance, Interim Report 2: Review of Methods for Estimating Conveyance*. Project W5A- 057, HR Wallingford Ltd., United Kingdom.
- DEM solutions, 2010. *EDEM 2.3 user guide*. United Kingdom, Available on <http://www.dem-solutions.com/>.
- Ferreira, T. A. and Rasband, W., 2010. *The ImageJ user guide version 1.43*.
- Friedrich, H., Nikora, V., Melville, B. W. and Coleman, S. E., 2006. Statistical interpretation of geometric differences in ripple and dune shapes. *Proceedings of the 7th International Conference on Hydroscience and Engineering (ICHE 2006)*, ISBN: 0977447405 , pp. 1 - 14.
- Gadd, P. E., 1988. Sand Bag Slope Protection: Design, Construction and Performance. *Arctic Coastal Processes and Slope Protection Design*, ASCE, pp. 145-165.
- Ganev, S., Cloutier, A., Gendron, G. and Beauregard, R., 2005. Mechanical properties of MDF as a function of density and moisture content. *Wood and Fiber Science*, **37** (2), pp. 314-326.
- Garcin, P., Faure, Y. H., Gourc, J. P. and Purwanto, E., 1995. Behaviour of geosynthetic clay liner (GCL): Laboratory tests. *Proceedings 5th International Symposium on Landfill*, Calgary, **1**, pp. 347-358.
- Goring, D. and Nikora, V. 2002. De-spiking ADV data. *Journal of Hydraulic Engineering*, ASCE, **128** (1), pp. 117-126.
- Gutman, A. L., 1979. Low-cost Shoreline Protection in Massachusetts. *Coastal Structures '79*, **1**, ASCE, New York, pp. 373-387.
- Grüne, J., Sparboom, U., Schmidt-Koppenhagen, R., Wang, Z. and Oumeraci, H., 2006. Stability tests of geotextile sand containers for monopile scour protection. *Proceedings 30th International Conference Coastal Engineering (ICCE)*, **5**, San Diego, California, USA, pp. 5093-5105.

References

- Heerten, G., Jackson, L.A., Restall S. and Stelljes K., 2000 a. Environmental benefits of sand filled geotextile structures for coastal applications. *GeoEng 2000*, Melbourne, Australia.
- Heerten, G., Jackson, L. A., Restall, S. and Saathoff, F., 2000 b. New developments with mega sand containers of non-woven needle-punched geotextiles for the construction of coastal structures. *International Conference on Coastal Engineering 2000*, Sydney, Australia.
- Heerten, G., Klompmaker, J., and Partridge, A., 2008. Design and construction of waterfront structures with special designed nonwoven geotextiles. *PIANC-COPEDEC VII, 7th International Conference on Coastal and Port Engineering in Developing Countries*, Paper No: H-06, pp. 1-10.
- Heibaum, M. H. 1999. Coastal scour stabilization using granular filter in geosynthetic nonwoven containers, *Geotextiles and Geomembranes*, **17**(5-6), pp. 341–352.
- Hornsey, W. P., Jackson, L. A., Restall, S.J. and Corbett, B., 2003. Large sand filled geotextile containers as a construction aid over poor quality marine clay. *Coasts & Ports Australasian Conference*, pp. 1-8.
- Hölzer, A. and Sommerfeld, M., 2008. New simple correlation formula for the drag coefficient of non-spherical particles. Short Communication, *Powder Technology*. **184** (3), pp. 361-365.
- Individual Consultants, 2003. *Geobags Protection, project concept, experience, future, Jamuna-Meghna Erosion Mitigation Project, Part A*. Report prepared for Bangladesh Water Development Board and Asian Development Bank.
- Jackson, L. A., Tomlinson, R., McGrath, J. and Turner, I., 2002. Monitoring of a multi functional submerged geotextile reef breakwater. Paper 359. *In: 28th International Conference on Coastal Engineering 2002*, 7-12 July, Cardiff, United Kingdom.
- Jackson, L. A., Corbett, B. B., and Restall, S., 2006. Failure modes and stability modelling for design of sand filled geosynthetic units in coastal structures. *30th International Conference on Coastal Engineering*, San Diego.
- Jackson, L. A. and Hornsey, W., 2002. An artificial reef to protect surfers paradise beach - developing & implementing the science. Soil Filters Australia Pty Ltd.
- JMREM, 2006 a. Jamuna-Meghna River Erosion Mitigation Project Part B. *Special Report 17, Geobag Revetments*. Government of the People's Republic of Bangladesh, Asian Development Bank and Bangladesh Water Development Board.
- JMREM, 2006 b. Jamuna-Meghna River Erosion Mitigation Project Part B. *Special Report 22, Geotechnical Report*, Government of the People's Republic of Bangladesh, Asian Development Bank and Bangladesh Water Development Board.

References

- JMREM, 2006 c. Jamuna-Meghna River Erosion Mitigation Project Part B. *Special Report 21, Site Data and Details of Work*, I, Government of the People's Republic of Bangladesh, Asian Development Bank and Bangladesh Water Development Board.
- Kim, H. T., Yoo, D., Park, S. S., Lee, J. H. and Lee, C. J., 2004. A fundamental approach for an investigation of behaviour characteristics of the vegetation structures using sandbags. *Proceedings of GeoAsia 2004*, pp. 225-232.
- Kobayashi, N. and Jacobs, B. K., 1985. Experimental study on sandbag stability. *Coastal Zone 85: 4th Symposium on Coastal and Ocean Management*, ASCE, pp. 1612-1626.
- Korkut, R., Martinez, E. J., Morales, R., Ettema, R. and Barkdoll B., 2007. Geobag performance as scour countermeasure for bridge abutments. *Journal of Hydraulic Engineering*, ASCE, **133** (4), pp. 431-439.
- Krahn, T., Blatz, J., Bathurst, R. and Alfaro, M., 2004. Assessment of sandbag dike interface shear using two direct shear devices, *57th Canadian Geotechnical Conference*, Canada.
- Krahn, T., Blatz, J., Alfaro, M., and Bathurst, R. J., 2007. Large-scale interface shear testing of sandbag dyke materials. *Geosynthetics International*, **14**(2), pp. 119 - 126 , ISSN: 1072-6349.
- Leighly, J. B., 1932. Toward a theory of morphological significance of turbulence in the flow of water in streams. University of California, Publication in *Geography*, Berkeley, **6**(1), pp. 1-22.
- Mc Gahey, C. and Samuels, P.G., 2004. River roughness – the integration of diverse knowledge. In Greco, M., Carravetta, A. and Della Morte, R. (ed.) *Proceedings of the 2nd International Conference on Fluvial Hydraulics*, River Flow 2004, Naples, London: Taylor and Francis Group, ISBN 90 5809 658 0, **1**, pp. 405-414.
- Mc Gahey, C., Samuels, P.G., Knight, D.W. and O'Hare, M.T., 2008. Estimating river flow capacity in practice. *Journal of Flood Risk Management*, **1**(1), pp. 23-33.
- Mantz, P. A. 1978. Bed forms produced by fine, cohesionless, granular and flakey sediments under subcritical water flows. *Sedimentology*, **25**, pp. 1-21.
- Mantz , P. A., 1992. Cohesionless, fine-sediment bed forms in shallow flows. *Journal of Hydraulic Engineering*, **118** (5), Paper No. 1003, pp. 743 – 764.
- Mekong River Commission, 2009. Best practise guidelines for structural measures and flood proofing, *The Flood Management and Mitigation Programme, Component 2: Structural Measures & Flood Proofing in the Lower Mekong Basin*, Draft Final Report.
- <http://www.mrcmekong.org/>
- Mindlin, R. D., 1949. Compliance of elastic bodies in contact. *Journal of Applied Mechanics* **16**, pp. 259–268.

References

- Mori, E., Aminti, P. L. and D'eliso, C., 2008 a. Field experiment on a groin system built with sand bags. *International Conference on Coastal Engineering*, pp. 219.
- Mori, E., D'eliso, C. and Aminti, P. L., 2008 b. Physical modeling on geotextile sand containers used for submerged breakwater. *Proceedings on the second international conference on the application of physical modelling to port and coastal protection*, CoastLab 2008, Italy.
- Mustoe, G. G. W. and Miyata, M., 2001. Material flow analyses of non-circular shaped granular media using Discrete Element Methods. *Journal of Engineering Mechanics*, ASCE 2001, **127**(10), pp. 1017-1026.
- NAUE GmbH & Co. KG, 2006. Advantages of Needle-punched Secutex® and Terrafix® Nonwoven Geotextiles. NAUE GmbH & Co. KG, Germany.
- NDSU and U.S. Department of Agriculture, 2010 Sandbagging for flood protection. Prepared by Kenneth Hellevang, Extension Engineer. AE-626 (Revised), www.ag.ndsu.edu
- northwest hydraulics consultants (nhc), 2004. *Mega-container concept -hydraulic model tests in Edmonton, Canada*. prepared for the Bangladesh Water Development Board, Government of the People's Republic of Bangladesh, as a part of Jamuna-Meghna River Erosion Mitigation Project.
- northwest hydraulics consultants (nhc), 2006. Jamuna-Meghna River Erosion Mitigation Project Part B. *Special Report 11, Physical Model Study* (Vancouver, Canada), Final Report, Government of the People's Republic of Bangladesh, Asian Development Bank and Bangladesh Water Development Board.
- NSW, 2010. *Minister's Requirements under the Coastal Protection Act 1979*. Department of Environment, Climate Change and Water, NSW. www.environment.nsw.gov.au
- Oberhagemann K. and Kamal M. S., 2004. Geobag protection in Bangladesh. *4th international Conference on filters and Drainage in Geotechnical and Environmental Engineering*, Geofilters 2004, pp. 205-216.
- Olsen, O. J. and Florey, Q. L., 1952. Sedimentation studies in open channels boundary shear and velocity distribution by Membrane Analogy, Analytical and Finite-Difference Methods, U.S. Bureau of Reclamation, SP-34.
- Oumeraci, H., 2003. Review and Analysis of Vertical Breakwater Failures - Lessons learned. *Coastal Engineering, Special Issue on "Vertical Breakwaters"*, Amsterdam, The Netherlands: Elsevier Science Publishers B.V., **22** (1/2), pp. 3-29.
- Pilarczyk, K.W., (ed.), 1998. *Dikes and revetments*. A.A Balkema, Rotterdam.
- Pilarczyk, K.W., 2000. *Geosynthetics and geosystems in hydraulic and coastal engineering*. A.A. Balkema, Rotterdam, Netherlands.
- Porraz, M., Maza, J. A. and Medina, R., 1979. Mortar-filled Containers, Lab and Ocean Experience. *Coastal Structures '79*, **1**, ASCE, pp. 270-289.

References

- Raudkivi, A. J., 1998. *Loose boundary hydraulics*. A. A. Balkema/ Rotterdam/Brookfield, pp. 122-123.
- Recio, J. and Oumeracia, H., 2007. Effect of deformations on the hydraulic stability of coastal structures made of geotextile sand containers. *Geotextiles and Geomembranes*, **25** (4-5), pp. 278-292.
- Recio, J. and Oumeraci, H. 2009 a. Process based stability formulae for coastal structures made of geotextile sand containers. *Coastal Engineering*, **56**, pp. 632-658.
- Recio, J. and Oumeraci, H., 2009 b. Processes affecting the hydraulic stability of coastal revetments made of geotextile sand containers. *Coastal Engineering*, **56**, pp. 260-284.
- Restall, S. J., Jackson, L. A., Heerten, G., and Hornsey, W. P., 2002. Case studies showing the growth and development of geotextile sand containers an Australian perspective, *Geotextiles and Geomembranes*, **20** (5), pp. 321-342.
- Saathoff, F., Oumeraci, H and Restall, S., 2007. Australian and German experiences on the use of geotextile containers. *Geotextiles and Geomembranes*, **25**(4-5), pp. 251-263.
- Scottish Natural Heritage, 2000. <http://www.snh.org.uk/>
- Shiono, K. and Knight, D.W., 1989. Two-dimensional analytical solution for compound channel. *Proceeding 3rd International Symposium on Refined Flow Modeling and Turbulence Measurements*, Universal Academy Press, pp. 591 -599.
- Shiono, K., and Knight, D.W., 1991. Turbulent open – channel flows with variable depth across the section. *Journal of fluid mechanics*, **222**, pp. 617-646.
- Southard, J. B. and Boguchwal, L. A., 1990. Bed configurations in steady unidirectional water flows. Part 2. Synthesis of flume data. *Journal of Sedimentary Research*, **60** (5), pp. 658-679.
- Tilley R. J. D. *Understanding solids: the science of materials*, Wiley 2004.
- Tominaga, A., Nezu, I., Ezaki, K., and Nakagawa, H., 1989. Three dimensional turbulent structure in straight open channel flows, *Journal of Hydraulic Research*, **27** (1), pp. 149–173.
- Tomlinson, M. J. and Woodward, J., 2008. *Pile design and construction practice*. Routledge, pp.234.
- US Army Corps of Engineers, 2004. *Sandbagging Techniques*. Northwestern Division, USA.
- Vanoni, V. A. and Brooks, N. H., 1957. *Laboratory studies of the roughness and suspended load of alluvial streams*. Technical Report E-68. California Institute of Technology, Pasadena, CA.
- Venis, W. A., 1968. Behaviour of dumping material when exposed to current and wave action, *Closure of Estuarine Channels in Tidal Regions*, *De Ingenieur*, **50**, pp. 159 -167.

References

- Wahl, T., 2002. Analyzing ADV data using WinADV. In Wahl, T. L., Pugh, C. A., Oberg, K. A., and Vermeyen, T. B. (ed.), *Hydraulic Measurements and Experimental Methods 2002*, Proceedings of the Specialty Conference, Reston, VA. ASCE.
- Weerakoon, S., Mocke, G., P., Smit, F. and Zahed, K. A., 2003. Cost effective coastal protection works using sand filled geotextile containers. COPEDEC VI, Colombo, Sri Lanka.
- Yang, R. Y., Jayasundara, C. T., Yu, A. B. and Curry, D., 2006. DEM simulations of the flow of grinding media in IsaMill. *Minerals Engineering* **19** (10), pp. 984-994.
- Yang, S. Q., Shu, Y. M. and Yang, X. C., 2008. Flume experiment and numerical analysis for bank reinforcement with geocontainer. *Proceedings of the 4th Asian Regional Conference on Geosynthetics*, Shanghai, China, pp. 630-636.
- Yasuhara, K. and Recio-Molina, J., 2007. Geosynthetic-wrap around revetments for shore protection. *Geotextile and Geomembranes*, **25**, pp. 221-232
- Yin, C., Rosendahl, L., Kær, S. K., Sørensen, H., 2003. Modeling the motion of cylindrical particles in a nonuniform flow. *Chemical Engineering Science*, **58**, pp.3489-3498.
- Zarrati, A. R. , Jin, Y. C. and Karimpour, S., 2008. Semianalytical model for shear stress distribution in simple and compound open channels, *Journal of Hydraulic Engineering*, **134** (2), pp. 205-215.
- Zhu, L., Wang, J., Cheng, N.S., Ying, Q. and Zhang, D., 2004. Settling distance and incipient motion of sandbags in open channel flows. *Journal of Waterway, Port, Coastal and Ocean Engineering*, ASCE, pp. 98-103.
- Zhu, C. R. , Shu, Y. M. and Jiang, J. H., 2008. Study on the experiment of stability of unarmored flat geotube dike under wave action, *Proceedings of the 4th Asian Regional Conference on Geosynthetics*, June 17 - 20, 2008 Shanghai, China, Published in: *Geosynthetics in Civil and Environmental Engineering 2009, Part 8*, pp. 625-629.

Appendix A

Wooden test rig











<p>Scour depth = 0.01 m</p> 	<p>Scour depth = 0.02 m</p> 	<p>- No signification bag movement observed.</p>
<p>Scour depth = 0.03 m</p> 	<p>Scour depth = 0.04 m</p> 	<p>- No signification bag movement observed.</p>
<p>Scour depth = 0.05 m</p> 	<p>Scour depth = 0.06 m</p> 	<p>- Sliding observes from scour depth 0.05 m; and - Steepness of the slope observes in scour depth 0.06 m.</p>
<p>Scour depth = 0.07 m</p> 	<p>Scour depth = 0.08 m</p> 	<p>- Sliding continues.</p>
<p>Scour depth = 0.09 m</p> 	<p>Scour depth = 0.10 m</p> 	<p>- Steepness of the structure increased and a bag was missed at the scour depth of 0.097 m.</p>

Figure A1: Failure observation due to friction forces using dry geobag











<p>Scour depth = 0.01 m</p> 	<p>Scour depth = 0.02 m</p> 	<p>- No signification bag movement observed.</p>
<p>Scour depth = 0.03 m</p> 	<p>Scour depth = 0.04 m</p> 	<p>- No signification bag movement observed.</p>
<p>Scour depth = 0.05 m</p> 	<p>Scour depth = 0.06 m</p> 	<p>- No signification bag movement observed.</p>
<p>Scour depth = 0.07 m</p> 	<p>Scour depth = 0.08 m</p> 	<p>- Failure line observed in 0.08 m scour depth.</p>
<p>Scour depth = 0.09 m</p> 	<p>Scour depth = 0.10 m</p> 	<p>- Bag sliding continues, however none of the bag leave the test rig.</p>

Figure A2: Failure observation due to friction forces using 24h saturated geobag

Appendix B

ADV measured velocity

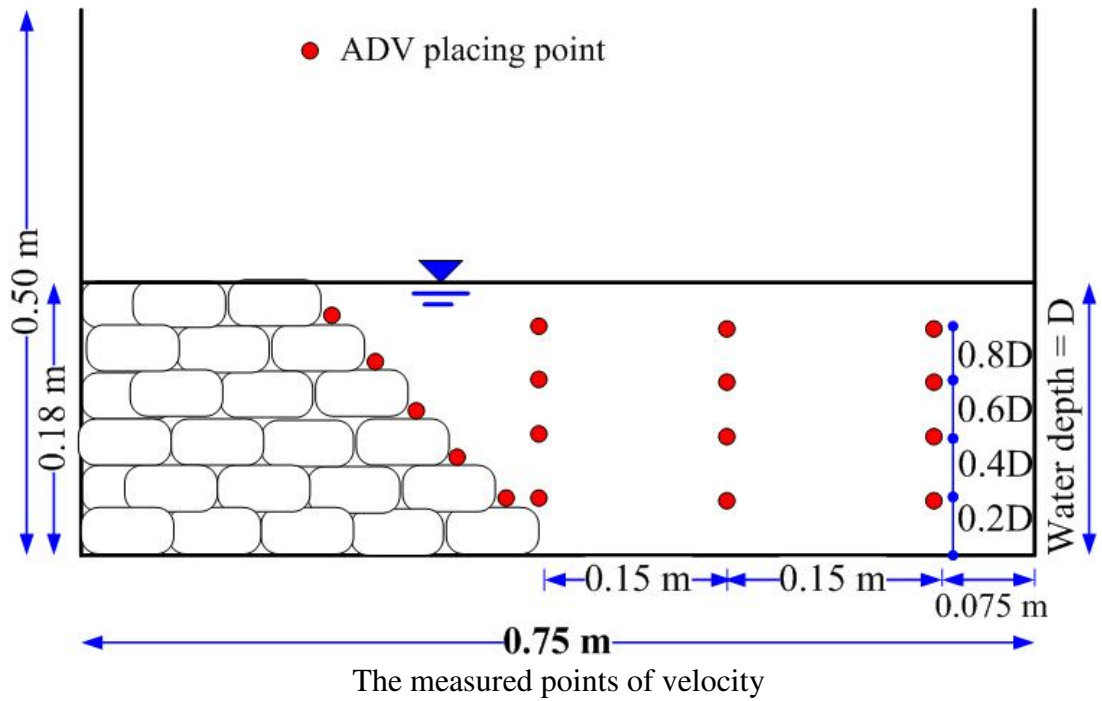
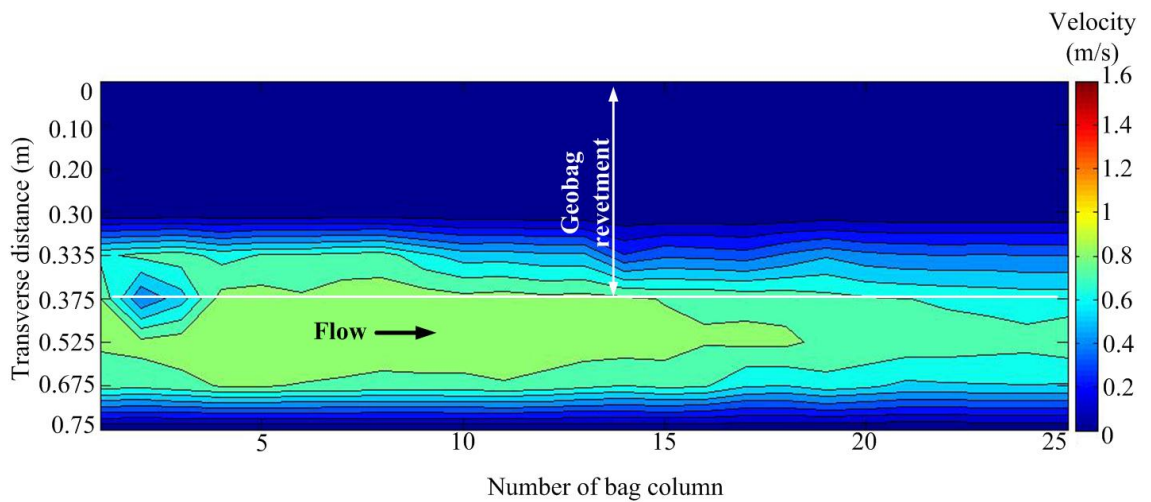


Figure B.1: The details on AVD measuring points



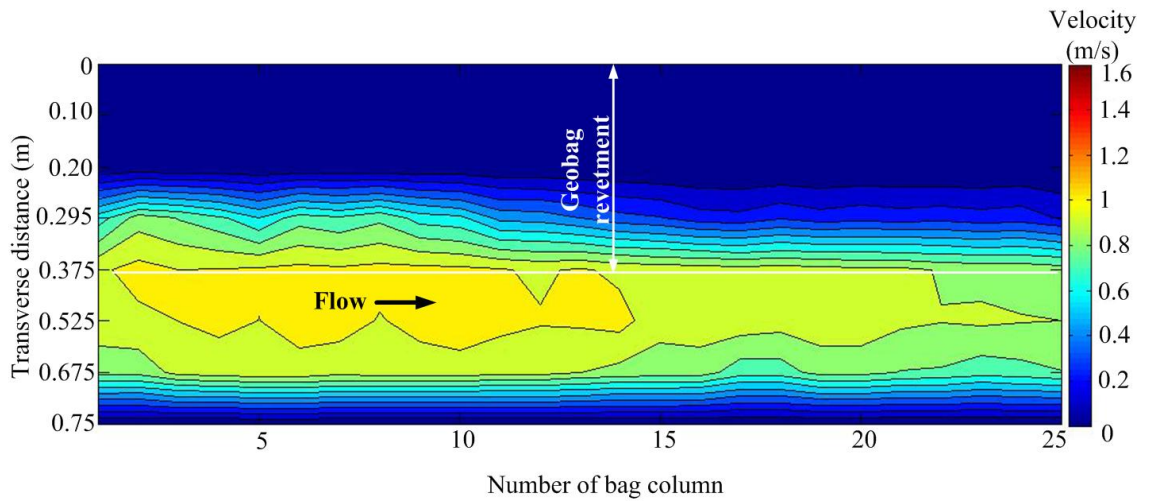
Mean water level = 0.0214 m (equal to 16.5% of the total revetment height)

Mean flow = 0.0072 m³/s

Note: Transverse distance axis is not in scale

Figure B2: ADV measured flume velocity profile (Condition A)

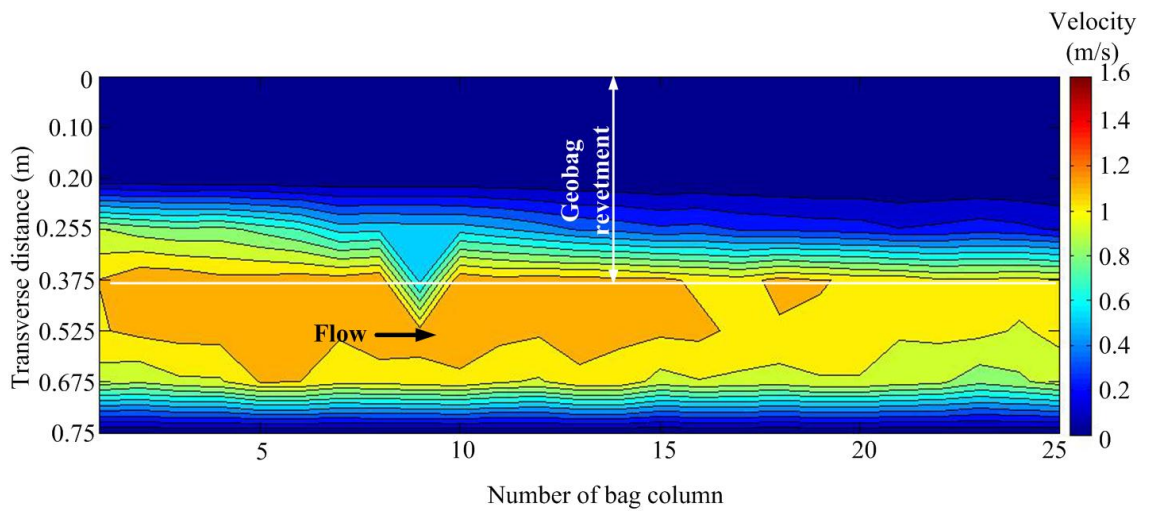
Appendix B: ADV measured velocity



Mean water level = 0.034 m (equal to 26.7% of the total revetment height)
Mean flow = 0.015 m³/s

Note: Transverse distance axis is not in scale

Figure B3: ADV measured flume velocity profile (Condition A)

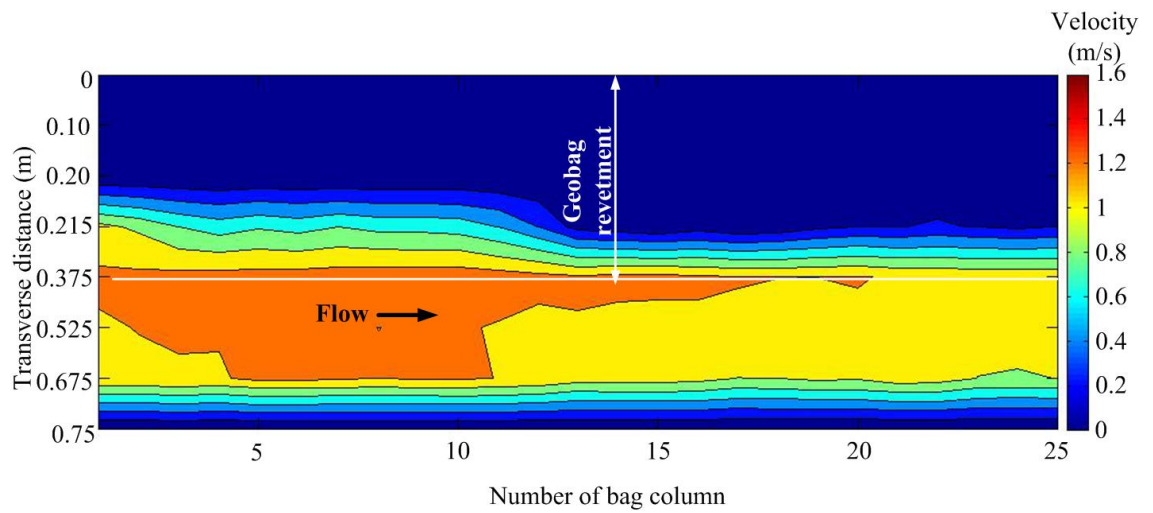


Mean water level = 0.052 m (equal to 40.5% of the total revetment height)
Mean flow = 0.025 m³/s

Note: Transverse distance axis is not in scale

Figure B4: ADV measured flume velocity profile (Condition A)

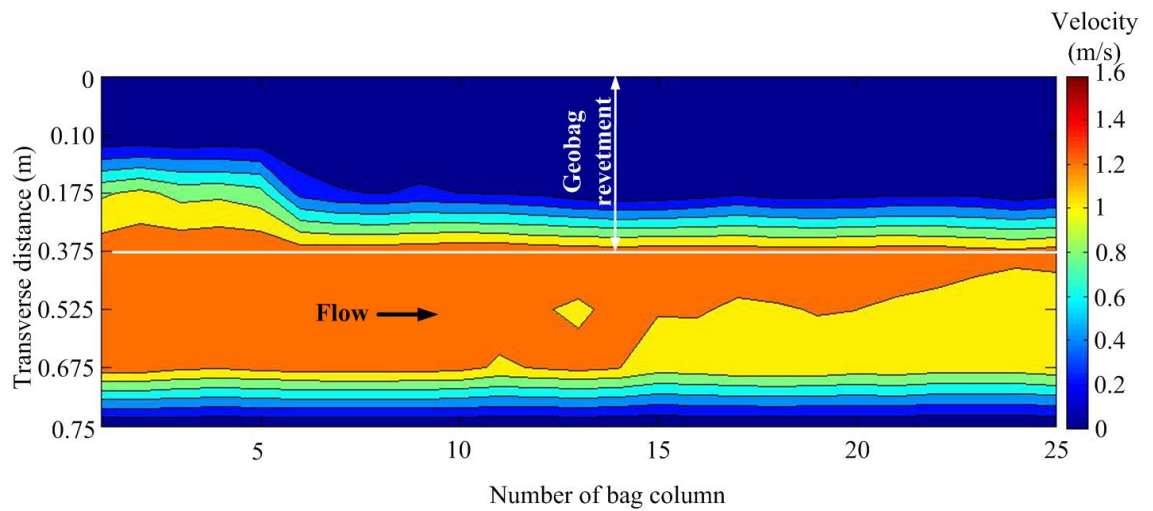
Appendix B: ADV measured velocity



Mean water level = 0.071 m (equal to 54.4% of the total revetment height)
Mean flow = 0.037 m³/s

Note: Transverse distance axis is not in scale

Figure B5: ADV measured flume velocity profile (Condition B)

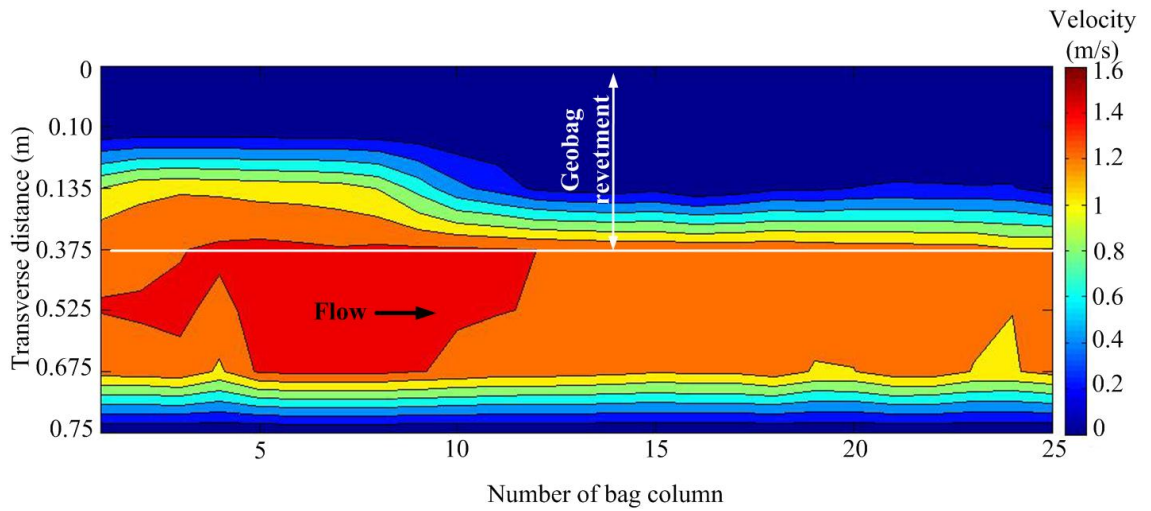


Mean water level = 0.088 m (equal to 67.7% of the total revetment height)
Mean flow = 0.049 m³/s

Note: Transverse distance axis is not in scale

Figure B6: ADV measured flume velocity profile (Condition C)

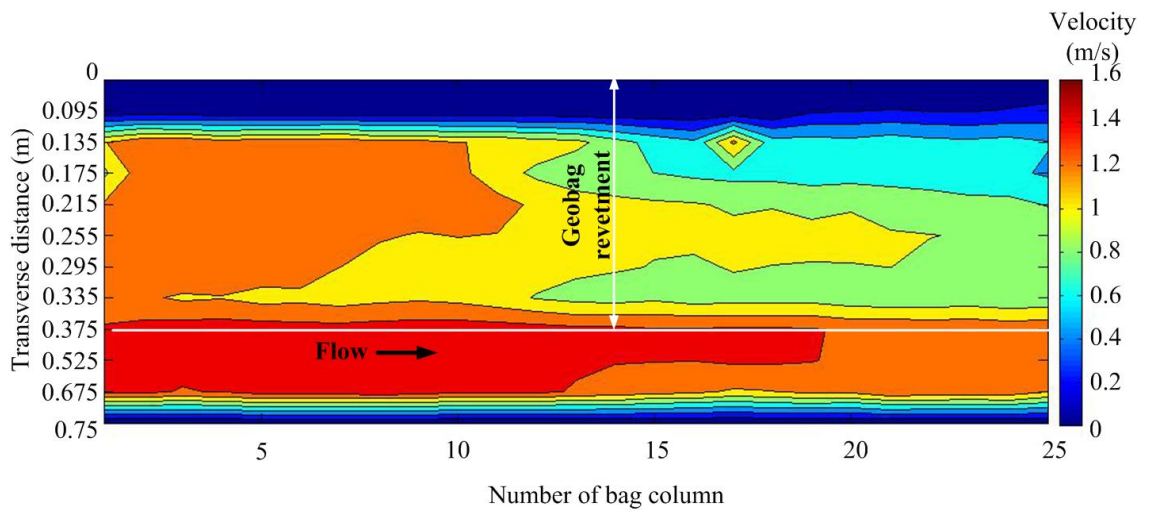
Appendix B: ADV measured velocity



Mean water level = 0.103 m (equal to 79% of the total revetment height)
 Mean flow = 0.062 m³/s

Note: Transverse distance axis is not in scale

Figure B7: ADV measured flume velocity profile (Condition C)



Mean water level = 0.124 m (equal to 95.5% of the total revetment height)
 Mean flow = 0.079 m³/s

Note: Transverse distance axis is not in scale

Figure B8: ADV measured flume velocity profile (Condition D)

Appendix C

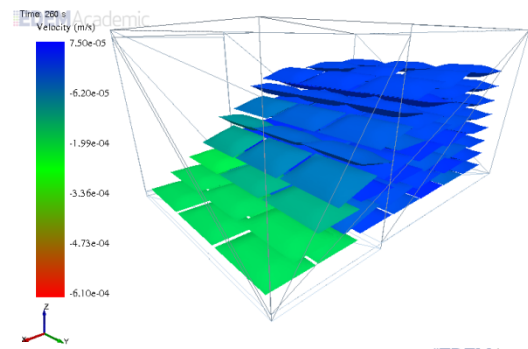
Comparison of dry geobag tests in Laboratory and EDEM[®] representations

Appendix C: EDEM predicted dry geobag performance

Scour depth = 0.01 m



Laboratory



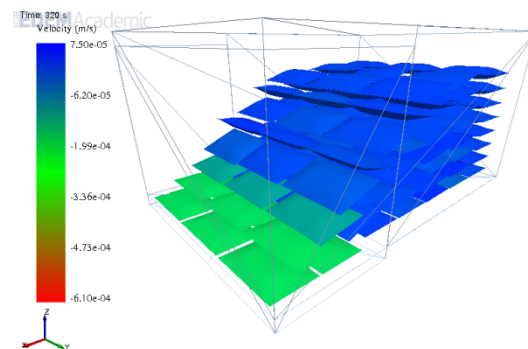
EDEM Academic

EDEM[®] representation

Scour depth = 0.02 m



Laboratory



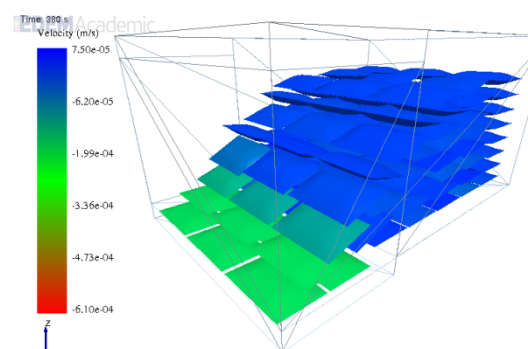
EDEM Academic

EDEM[®] representation

Scour depth = 0.03 m



Laboratory



EDEM Academic

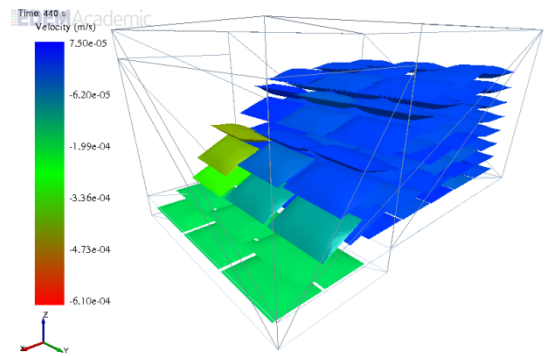
EDEM[®] representation

Appendix C: EDEM predicted dry geobag performance

Scour depth = 0.04 m



Laboratory



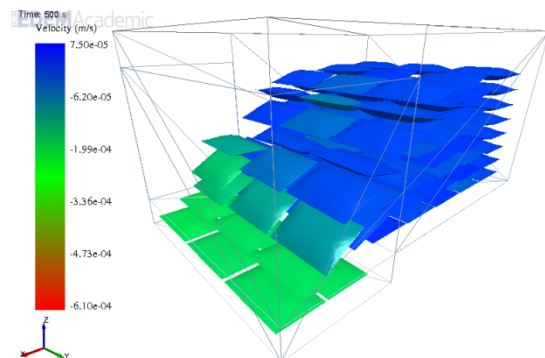
EDEM Academic

EDEM[®] representation

Scour depth = 0.05 m



Laboratory



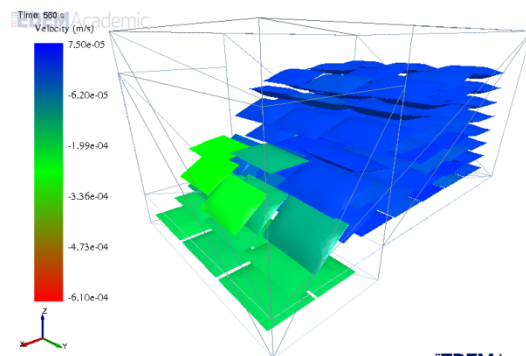
EDEM Academic

EDEM[®] representation

Scour depth = 0.06 m



Laboratory



EDEM Academic

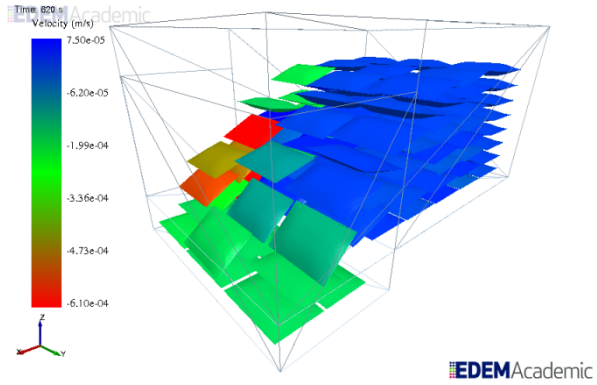
EDEM[®] representation

Appendix C: EDEM predicted dry geobag performance

Scour depth = 0.07 m



Laboratory

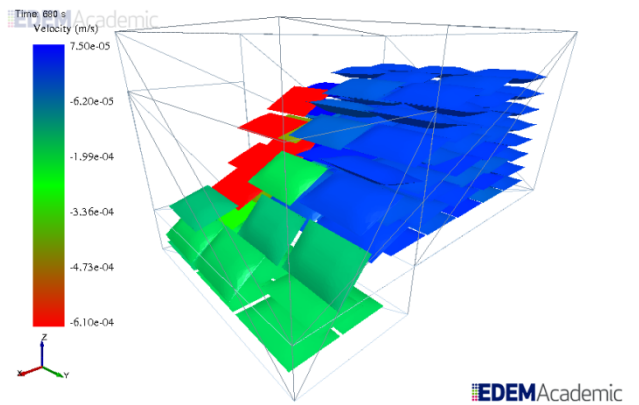


EDEM[®] representation

Scour depth = 0.08 m



Laboratory



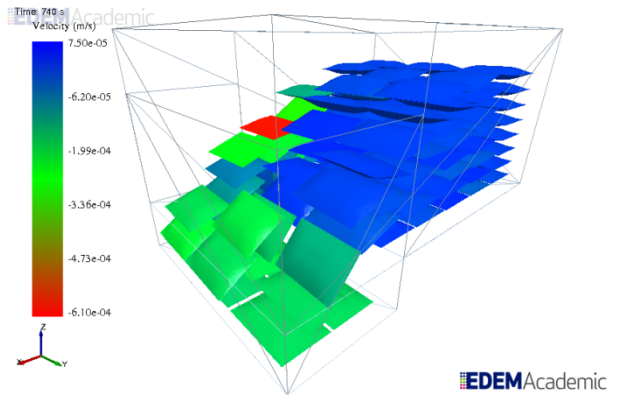
EDEM[®] representation

Appendix C: EDEM predicted dry geobag performance

Scour depth = 0.09 m



Laboratory

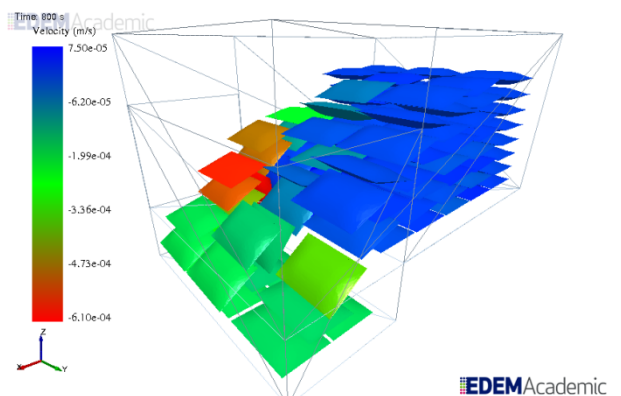


EDEM[®] representation

Scour depth = 0.10 m



Laboratory



EDEM[®] representation